Final Technical Report

Date of Submission:	February 5, 2016
Federal Agency/ Organization Element:	DOE/EERE/Office of Advanced Manufacturing Program (AMO)
Award Number:	DE-EE0005750
Project Title:	Bioelectrochemical Integration of Waste Heat Recovery, Waste-to-Energy Conversion, and Waste-to-Chemical Conversion with Industrial Gas and Chemical Manufacturing Processes
Project Period:	September 1, 2012 – August 31, 2015
Recipient Organization:	Air Products and Chemicals, Inc. 7201 Hamilton Blvd Allentown, PA 18195-1501
DUNS Number:	00-300-1070
Principal Investigator:	Dr. James Mac Dougall 610-481-7240 macdouje@airproducts.com
Business Contact:	Mr. Gregory Daub 610-481-1201 daubgh@airproducts.com
Partners:	The Pennsylvania State University
DOE Technology Manager:	Dr. Robert Gemmer 202-586-5885 bob.gemmer@ee.doe.gov
DOE Project Officer/Manager:	Dr. Gibson Asuquo 720-356-1433 gibson.asuquo@go.doe.gov
DOE Project Monitor:	Mr. Chad Sapp 720-356-1302 chad.sapp@go.doe.gov
DOE Contract Specialist:	Mr. Carlo DiFranco 720-356-1316 carlo.difranco@go.doe.gov

Acknowledgement

This material is based upon work supported by the Department of Energy under Award Number DE-EE0005750. The team wishes to recognize the outstanding efforts of John Cirucci, who championed this program from concept through successful conclusion.

Document Availability

Reports are available free via the U.S. Department of Energy (DOE) Information Bridge Website: http://www.osti.gov/bridge

Reports are available to DOE employees, DOE contractors, Energy Technology Data Exchange (ETDE) representatives, and Informational Nuclear Information System (INIS) representatives from the following source:

Office of Scientific and Technical Information
P.O. Box 62
Oak Ridge, TN 37831
Tel: (865) 576-8401
FAX: (865) 576-5728
E-mail: reports@osti.gov
Website: http://www.osti.gov/contract.html

Table of Contents

List of Acronyms

AC	acetate medium (buffered)
AEM	anion exchange membrane
AmB	ammonium bicarbonate
BES	bioelectrochemical systems
BOD	biochemical oxygen demand
CE	coulombic efficiency
CEM	cation exchange membrane
COD	chemical oxygen demand
GC	gas chromatography
HC	high concentration
IEM	ion exchange membrane
LC	low concentration
MEC	microbial electrolysis cell
MFC	microbial fuel cell
MHRC	microbial reverse electrodialysis fuel cell or electrolysis cell with heat integration
MHREC	microbial reverse electrodialysis electrolysis cell with heat integration
MHRFC	microbial reverse electrodialysis fuel cell with heat integration
MRC	microbial reverse electrodialysis fuel cell or electrolysis cell
MREC	microbial reverse electrodialysis electrolysis cell
MRFC	microbial reverse electrodialysis fuel cell
OCV	open circuit voltage
RED	reverse electrodialysis
sCOD	soluble chemical oxygen demand
WHR	waste heat recovery
WW	wastewater, domestic

List of Figures

List of Tables

1. Executive Summary

The purpose of this study was to demonstrate that waste heat and organics in wastewater can be converted to useful energy or products. With support from DOE, the project sought to reduce greenhouse gas (GHG) impacts and convert waste products into useful energy or hydrogen through the use of microbial fuel cells. This project successfully demonstrated the technical feasibility of this concept and elucidated opportunities to improve the various components that were brought together in this multifaceted program.

This study was to be carried out of over three budget periods, with a Go/No Go decision point at the end of each stage. The initial work required verification that the needed waste heat and effluents were available and amenable for treatment to produce energy or hydrogen. Wastewater effluent samples collected from select Air Products manufacturing plants were pre-screened for suitable high chemical oxygen demand (COD) and low-grade waste heat. A select portion of these effluent samples was tested by project partner Pennsylvania State University (Penn State) for treatability. Results from these tests suggest that a number of the streams provided sufficient COD to be used in microbial fuel cells for energy or hydrogen production.

In addition, this project produced an inventory of low-grade industrial waste heat at various Air Products manufacturing sites. This low-grade waste heat can be an important heat source for thermal regeneration of the organic Rankine cycle. This inventory provides the basis for further study of a broader sector of U.S. chemical (or other) manufacturers to survey low-grade waste heat available across the industry. The database which could be produced would allow further research into potential applications and provide opportunities to use this energy source to enhance energy utilization and efficiency broadly across U.S. manufacturing industries. As part of Budget Period 1, a basic process model was developed to allow global optimization of the three basic process modules: Microbial Fuel Cell, Reverse Electrodialysis (RED), and Thermal Regeneration/Waste Heat Recovery. During this period, Air Products also began to build economic models for the overall process, so that an economic viability analysis could be performed using the data obtained from the Penn State laboratory studies.

In Budget Period 2, detailed studies were conducted regarding integration of the MRC, RED and thermal regeneration processes. Through these studies it became apparent that the RED process was limited by the ion exchange membrane performance. The project plans were altered to put more effort into understanding the behavior of commercial ion exchange membranes with the ammonium bicarbonate system. Additionally, in Budget Period 2 a financial analysis was developed to understand the sensitivities around the various components of the overall system. Through this study, it was determined that there was a low probability of achieving the desired power and cost targets based on the current state of development and integration of these technologies.

These findings led to a “No Go” decision after Budget Period 2, thereby terminating the project. However, significant opportunities were identified to improve several of the areas studied. Increased efficiency of the MRC, lower ion exchange membrane cost and superior performance of the waste heat recovery system will provide the benefits needed to move this

technology toward commercialization. Improvements required to make this integrated technology commercially viable could come in the form of either membrane efficiency or energy efficiency.

2. Introduction

The overall objective of this project was to develop a novel configuration of a bioelectro-chemical system that can be integrated into current industrial chemical manufacturing processes to convert organics in wastewater and low-grade waste heat into useful energy and chemical products. The intent was for Air Products to collaborate with the Pennsylvania State University (Penn State) to develop this technology from current Technical Readiness Level (TRL) 3, proof-of-concept status, through TRL 6, prototype status. The goal of this project was to enable further development of this technology so that it can be applied across a wide variety of U.S. manufacturing segments.

The program provided the novel integration of three existing technologies into one complete system which recovers waste heat, uses a microbial electrolysis cell to convert waste material to produce electricity, and uses a reverse electrodialysis stack to provide electrical current in one configuration or hydrogen in another. This integrated system has the potential to provide both electricity and clean water.

Microbial fuel cells catalyze the oxidation of wastewater at low temperature to provide dual benefits of efficient wastewater treatment and electric power generation. A recent technological advance developed at Penn State couples reverse electrodialysis with a microbial fuel cell to synergistically amplify voltage and power output. Reverse electrodialysis requires the driving force of a salinity difference between high- and low-concentration salt streams, typically seawater and fresh water. In a novel process configuration, low-grade waste heat (60°C) from an industrial process is used to perform regeneration of high- and low-concentration salt streams in a closed salt loop. Hence, the energy content of both low-grade waste heat and waste effluent is efficiently converted to electric power. In a further novel configuration, the cell cathode can be operated anaerobically so that high-purity hydrogen gas can be produced at the cathode. This technology – microbial reverse electrodialysis integrated with waste heat recovery – represents a revolutionary combination of highly efficient, breakthrough biological processes with novel process cycle configurations. Compared to incumbent waste heat recovery processes, this technology can operate with lower-grade waste heat that is otherwise unsalvageable. Compared to incumbent wastewater treatment processes, it is much more efficient and has a higher yield and a smaller footprint. Further, waste heat recovery and wastewater treatment are combined for output greater than the sum of the parts. This revolutionary development could dramatically reduce energy consumption and manufacturing costs for a broad range of U.S. industrial processes and represents a dramatic departure from current practices. It can be applied to both new and existing manufacturing facilities. This technology has the potential to generate more than 10 billion kWh per year of zero-carbon, distributed electricity, provide $700-900 million per year of cost savings to U.S. manufacturing and make a substantial contribution to DOE-ITP's efforts to reduce energy use by half.

Microbial fuel cells. A microbial fuel cell (MFC) is a type of bioelectrochemical system (BES) in which organic matter is directly converted to electricity by certain bacteria abundant in the environment and also naturally present in domestic wastewaters.[1] These bacteria, called *exoelectrogens*,2 oxidize organic matter in the wastewater (treating the wastewater) and release electrons to an electrode (the anode) where they flow through a circuit to the counter electrode (cathode), producing electrical current and treated water (Figure *i*). The electrons are released from the cathode to the terminal electron acceptor (oxygen). An MFC produces carbon-neutral electricity while concurrently treating wastewater. [2-5]

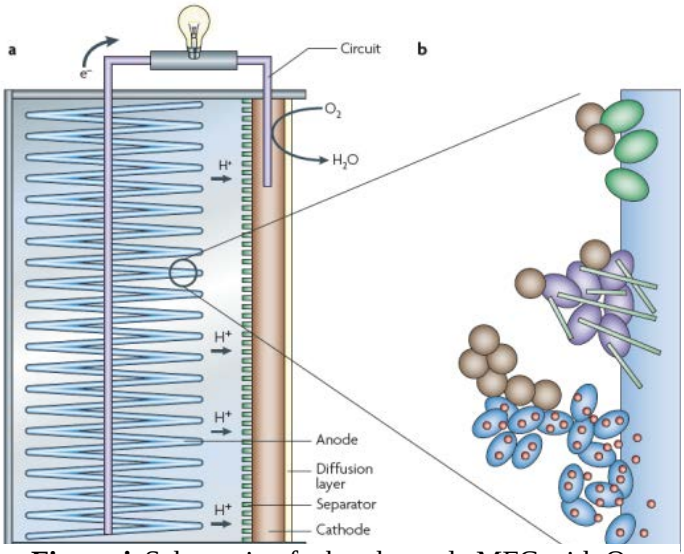

Figure *i*. Schematic of a brush anode MFC with O_2 cathode. Expanded view shows electrons transferred to the anode by nanowires, self-produced mediators, and direct contact.[1]

Research at Penn State, sponsored in part by Air Products, has focused on reducing MFC costs by eliminating the need for precious metals in the electrodes[6,7] and developing low-cost materials that increase power generation. High-surface-area electrodes are needed for the bacteria, and these materials must be electrically conductive and inexpensive. Many materials have been examined including carbon cloth, paper, foam, felt, reticulated vitreous carbon, and others.[1-8] The highest power densities have been achieved using graphite fiber brush anodes.[9] These electrodes are made by winding thin graphite fibers into a metal core, a manufacturing technology used to make bottle brushes. Flat electrode materials are less effective than brush anodes in generating high power densities.[10-13] Graphite fiber brush anodes have high surface areas (>10,000 m^2/m^3) and porosities (>95%)9. Because the anode is very effective, the air cathode usually limits power production. Oxygen leakage through the cathode can also reduce coulombic efficiencies (current recovery from the substrate). Air-cathode MFCs can contain separators between the electrodes to avoid electrode contact and prevent short circuiting, and to reduce oxygen transfer, although these can contribute to the undesirable evolution of pH gradients.[14-19]

Microbial electrolysis cells. A microbial electrolysis cell (MEC) is a type of modified MFC that can be used to convert electrical current produced by bacteria on the anode into hydrogen (H_2) at the cathode. In an MFC, current generation is thermodynamically favorable, and typically ~0.5 V is produced with oxygen as the electron acceptor at the cathode. The anode potential is around –0.3 V, with a cathode potential in an MFC of ~0.2 V [0.5 V + (–0.3 V)].[20-21]

In an MEC, however, the production of H_2 at the cathode requires the addition of energy to the system; the anode potential is still 0.3 V, but the potential needed for H_2 evolution is 0.411 V (corrected to pH=7). Thus, one must theoretically add at least 0.11 V to the MEC circuit in order to generate H_2 at the cathode.

The main advances in MECs have centered on minimizing applied voltages, avoiding use of precious metals, and increasing H_2 production rates. MECs usually use a Pt catalyst on the cathode to reduce electrical overpotential for H_2 evolution. A low overpotential is important because this reduces the extra amount of voltage (beyond the theoretical value) that is required to produce H_2. The overpotential directly relates to the electrical efficiency of an MEC and therefore the operational costs. A number of alternative materials to Pt have been examined, including stainless steel (SS), nickel alloys, and metal oxides.[22-25] SS and nickel alloys have proven to be effective among known materials, but these materials result in high overpotentials and therefore higher operating costs than Pt. Recently Penn State has shown that molybdenum disulfide (MoS_2) has a lower overpotential than SS, and that this material can achieve H_2 production rates similar to those produced with Pt on the cathodes.

The energy efficiencies in MECs can be evaluated in terms of electrical energy input alone, or based on both the electrical energy and substrate. For example, it was shown that an MEC producing 1.1 m^3 of H_2 per d per m^3 of reactor volume ($m^3\,H_2\,d^{-1}\,m^{-3}$) at an applied voltage of 0.6 V had an an energy efficiency of 288% (based solely on electricity applied), and 82% based on both electrical energy and the substrate (acetic acid, based on its heat of combustion) with a Pt catalyst. Improvements in the system architecture nearly doubled the H_2 production (2.0 $m^3\,H_2\,d^{-1}\,m^{-3}$), although the energy efficiencies were similar (254% relative to electrical energy, and 80% relative to both electrical energy and substrate).2[6] In an MEC with a high surface area SS cathode (810 m^2/m^3), the gas production rate was 1.7 ± 0.1 $m^3\,H_2\,d^{-1}\,m^{-3}$ at an applied voltage of 0.6 V,[27] with an energy efficiency relative to the electrical energy of 221%. These results demonstrate that energy efficiencies of these systems can be very high. However, electrical energy input is still needed in a conventional MEC.

Microbial reverse electrodialysis cells. To avoid using a source of electrical power in an MEC, or alternatively to increase the power production from an MFC, a reverse electrodialysis (RED) stack can be incorporated into a BES.[28,29] The RED stack generates power from a salinity-driven electromotive force, for example between salty sea water and fresh river water,[30] or other salt solutions. These microbial reverse electrodialysis systems (MRCs) can be used to produce electrical power or H_2. A RED-supported MFC is called a microbial reverse electrodialysis fuel cell (MRFC), a schematic of which is shown in Figure *ii*, where the two cell-paired RED stack is located in an MFC reactor between its anode and air cathode. In the RED system, cation- and anion-exchange membranes are alternatively placed between high- and low-salt-concentration cells. The concentration difference across the ion-exchange membrane drives the ionic transport in the system, generating an electromotive force[31] according to:

$$\Delta\varphi = \left(t_{\text{counter}} - t_{\text{co}}\right)\frac{RT}{z_{\text{counter}}F}\ln\left(\frac{f_{\text{counter,high}}c_{\text{counter,high}}}{f_{\text{counter,low}}c_{\text{counter,low}}}\right)$$

where $\Delta\varphi$ is the electromotive force driven by the concentration difference, *t* the transport number defined as the fractional contribution of the ionic flux to the current density in the membrane, *R* the gas constant, *T* the absolute temperature, *z* the ionic charge, *f* the activity coefficient, and *c* the ionic concentration. The subscripts *high* and *low* refer to the salt concentration cells; *counter* and *co* denote the counter- and co-ions to the membrane, respectively. Note that the counter- and co-ions are selected or excluded by the ion-exchange membrane. For instance, with a cation-exchange membrane, positively-charged sodium or ammonium ions are counter-ions, while negatively-charged chloride or bicarbonate ions are co-ions, and vice versa with an anion-exchange membrane.

The open circuit potential of this MRC reactor, with 0.6 M and 0.03 M NaCl solutions in the high- and low-concentration cells, is theoretically 0.3 V (assumed conditions of 25°C; transport number of the counter-ion 0.95, with activity coefficients determined by the Extended Debye-Huckel model). Assuming that the anode open circuit potential is –0.3 V (vs. normal hydrogen electrode, NHE) and the air cathode open-circuit potential is 0.4 V (vs. NHE),1 the total open-circuit potential of the MRC reactor is 1.0 V. This is a much higher potential than that produced solely by the MFC (~0.5 V). In addition, without the favorable reactions at the two electrodes, a RED system alone cannot produce this voltage. In a RED stack without organic matter at the anode, no useful power is generated until approximately 25 membrane pairs are used (sufficient to allow for the water splitting reaction and typical electrode overpotentials).

A RED stack can also be incorporated into an MEC, creating a microbial reverse electrodialysis electrolysis cell (MREC). At 25°C and neutral pH, a potential of –0.414 V (vs. NHE) is required to start producing H_2 at the cathode, while the anode potential cannot be more negative than –0.3 (vs. NHE) under normal conditions. Thus, in conventional MECs, external potential energy (usually greater than 0.25 V) is provided to drive H_2 evolution at the cathode.[1] However, the MREC does not require external potential energy, because the sum of the anode potential and salinity-driven electromotive force can drive H_2 evolution at the cathode with an appropriate number of cell pairs and concentration difference.

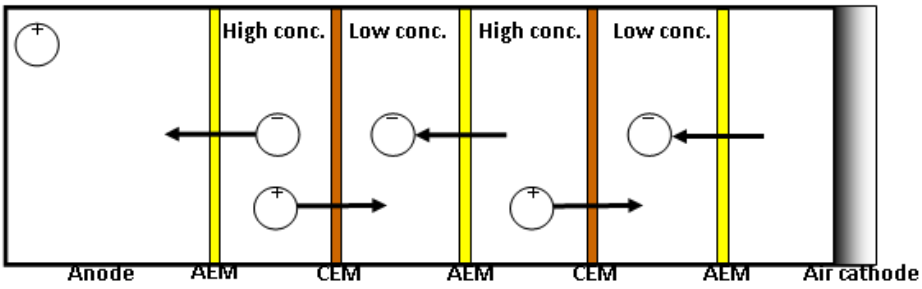

Figure *ii*. Two cell-paired MRC reactor (integration of a RED stack in a MFC). AEM and CEM are abbreviations of anion- and cation-exchange membranes, respectively.

3. Background

Many U.S. manufacturing facilities generate unrecovered, low-grade waste heat and also generate or are located near organic-content waste effluents. Bioelectrochemical systems, such

as microbial fuel cells (MFC) and microbial electrolysis cells (MEC), provide a means to convert these effluents into electric power and useful chemical products. The system to be developed in this project will further improve the production of electric power or hydrogen through the integration of low-grade waste heat.

The technological significance of MHRC in the reduction of industrial energy use is as a replacement for aerobic and anaerobic digestion for the treatment of industrial wastewater effluent streams. MEC and its technological cousin MFC represent a revolutionary technology that can transform this largely energy-negative industry into a green energy producer. It is a rapidly-evolving field, and the technology is rapidly improving. As shown in Figure *iii*, between 1998 and 2007 the power density obtainable from MFC's increased by about six orders of magnitude. Bioelectrochemical systems (BESs) now exhibit substantially higher energy efficiency and chemical conversion rates than incumbent biological and thermochemical processes for effluent energy recovery.[32,33] With incumbent technology, the percentage of energy transformed from substrate into H_2 is theoretically 33%, and practically only about 17% for dark fermentation. MEC breaks this paradigm and has already reached 98% substrate to H_2 conversion rates.[32]

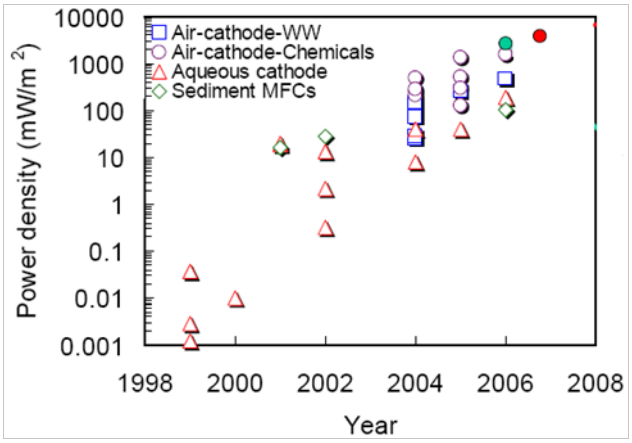

Figure *iii*. Improvement in MFC power density over time.

The integration of RED with MEC and MFC is a very recent and exciting technological innovation. It has already been established that integration of RED with MEC completely eliminates the need for an external power source in order to overcome the thermodynamic barrier and overpotential required to produce H_2.[34] For the power case employing MFC, RED integration has been shown to synergistically increase the performance relative to the individual systems.[35] In this study, it was shown that the energy efficiency of an MFC system operating independently was less than 7.2%, and the efficiency of the RED system was 14 – 35%. However, integration of the systems yielded 42% energy efficiency. Energy efficiency was measured by the method of Kim and Logan.[35]

RED integration with MFC/MEC has been demonstrated. The integration of a closed loop ammonium bicarbonate salt regeneration system via waste heat recovery is a novel idea for driving the RED system, which has yet to be demonstrated. However, Penn State has theoretically verified from first principle thermodynamic modeling. Thus is has been firmly established that the complete integration scheme provides a means for H_2 or electric power

production from waste effluent and waste heat without any parasitic power load other than what is required for fluid handling within the system. (Note: practical H_2 supply would also require additional energy for compression, purification and handling, depending upon the specific end-use application.)

This project was conducted by Air Products and Chemicals, Inc., as the primary recipient, and Penn State as the sub-recipient. With operations in over 40 countries and annual revenues of $10 billion, Air Products is a leading supplier of industrial gases and related equipment, as well as specialty chemicals, and has built leading positions in key growth markets such as semiconductor materials, refinery H_2, natural gas liquefaction, and advanced coatings and adhesives. For over 75 years, Air Products has developed expertise in the safe and reliable supply of industrial gases to a diverse customer base in the manufacturing, service and process industries. In the United States, Air Products operates 132 manufacturing facilities, which were surveyed for the best substrate samples for use in this project.

Air Products is recognized as a leading innovator in the markets in which it participates. The corporation currently maintains a portfolio of 927 granted U.S. patents which are in force, as well as 375 pending U.S. patents. The vast majority of these have corresponding patents in force or pending in numerous other counties where they have commercial or strategic value. The corporation maintains internal statistics regarding the percentage of revenues that are derived from new products introduced within the preceding five years, and routinely this value exceeds 5% of sales. Thus, Air Products successfully introduces innovative new products year after year in order to maintain its leadership positions in the markets it serves.

Over the years, Air Products has shown that it has the capabilities necessary to develop and then commercialize new technologies such as MHRC, including: 1) advanced materials and new equipment development; 2) process cycle design and engineering development and testing; 3) engineering project management; and 4) commercial business development. Through its Energy and Equipment division, Air Products has developed and commercialized numerous specialized equipment offerings that are utilized throughout the global industrial gas industry, including liquefied natural gas (LNG) heat exchangers, cryogenic air separation plants, on-site oxygen, nitrogen and H_2 generators, membrane separators and systems, oxy-fuel burners, food freezers, and gas cabinets and delivery systems. Air Products has access to the facilities and the marketing and commercialization experience to determine the technical and economic feasibility of MHRC in a real-world, industrial setting.

As the world's largest producer of H_2, Air Products is uniquely positioned to evaluate and eventually commercialize MHREC. Air Products supplies many of the world's largest refineries with their H_2 needs through its HyCO business unit. Air Products also commercially operates numerous smaller-volume H_2 plants through its Generated Gases business unit, and is thus well positioned to commercialize production on a scale commensurate with what would be produced through MHREC installations. This H_2 is used in chemicals, foods, glass, steel, electronics and other industry segments for hydrogenation, hydrotreating, reductive atmospheric control, catalyst regeneration or in-plant forklift fueling.

In addition to its bulk, liquid, and pipeline distribution systems, Air Products, through its Hydrogen Energy Systems business area, is the leading industrial gas company developing the H_2 economy. Since 1993, Air Products has built and operated more than 120 H_2 fueling stations in 19 countries, and currently completes over 300,000 H2 refuelings per year. Recent examples include supplying and fueling H_2 buses in London and in Beijing for the 2010 Olympic Games, as well as fueling Boeing's unmanned Phantom Eye airborne system demonstrator. Air Products also holds a powerful patent estate that enables the safe refueling of vehicles, which helps to protect Air Products' preeminent position in this developing market.

As a leading industrial gas supplier, Air Products operates in an extremely energy-intensive industry. In fact, the cost of energy is the corporation's single largest expense category other than personnel. Air Products also has an Energy business area focused on developing new technologies such as oxy-fuel firing of power plants, ion transport membrane separation of oxygen, and carbon capture and sequestration technologies for the energy market. As a result, Air Products employs numerous professionals who thoroughly understand and track the energy industry. Therefore, Air Products is also highly qualified to evaluate and commercialize an MHRFC offering. Since Air Products is in an energy-intensive industry, the organization is highly motivated to develop this technology to improve both our energy efficiency and our competitiveness.

Air Products has collaborated with the DOE on numerous projects, including the Pure Air – DOE Clean Coal II project (completed in1992, and still in operation with a notable 99.47% availability record), the Port Arthur, TX, CCS Demonstration (2009 – present), Flue Gas Purification Utilizing SOx/NOx Reactions During Compression of CO_2 Derived from Oxyfuel Combustion (2009 – 2010), Advanced Acid Gas Separation Technology for the Utilization of Low Rank Coals (2011 – 2012), ITM Syngas and ITM Oxygen (since 1996, now concluded), Development of New Adsorption (PSA) Technology to Recover High Valued Products from Chemical Plant and Refinery Waste Streams (2000 – 2004), Liquid Phase Methanol (prior to 2000), the Hydrogen Energy Station (Molten Carbonate Fuel Cell) project with Orange County Municipal Authority (1999 – present), and Development of a Turnkey Commercial Hydrogen Fueling Station (2002 – 2008), which was a H_2 fueling station built and operated on the Penn State campus.

Air Products has a substantial in-house engineering organization including more than 1,000 U.S. employees involved in engineering design, operations engineering services and process technology support. For 75 years, Air Products has designed, constructed and operated its own process plant facilities. Air Products engineering capabilities, which will be used in project and future technology scale-up and commercialization, include Project Management, Process Plant Cost Estimation, Flowsheet Engineering, Process Modeling, Unit Operations Design (separations and reactions), Mechanical Design (vessels, piping, machinery), Electrical Engineering, Instrumentation and Controls, Plant Process Safety, Corrosion and Material Expertise, and Chemical and Gas Analysis (with resident partner, Intertek Analytical Sciences Americas).

Researchers at Penn State are internationally recognized for their work on different bioelectrochemical systems, particularly technologies for developing an energy-sustainable water infrastructure. Thus, the laboratories at Penn State are well-equipped for studies on electrochemical systems. The research was overseen by Professor Logan and his group, with the research conducted in the newly-constructed 1,800 ft^2 BioEnergy Laboratory, part of the 9,800 ft^2 Kappe Environmental Engineering Laboratories on the University Park campus supervised by laboratory manager Mr. David Faulds. These laboratories include general research lab areas, dedicated microscopy and dark rooms, multiple temperature control rooms, and general-use rooms for instrumentation and preparations. Major equipment available for this project includes: single-channel (Gamry Scientific) and several multi-channel potentiostats; multimeters and computers for data acquisition; microscopes equipped for phase contrast, epifluorescence, and DIC techniques with digital image capture and analysis capabilities; anaerobic glove boxes for culture work; laminar flow hoods for sterile culture transfers; respirometers for gas production measurement in batch or continuous flow bioreactors; bioreactors with pH and reactor flow control; gas chromatographs for gas and volatile acids measurements; ion chromatographs for measuring cations and anions in water samples; UV-vis spectrophotometers; and a Total Organic Carbon/Total Nitrogen analyzer. Other equipment available include three particle counters, a high-pressure liquid chromatograph, a scintillation counter, an atomic absorption spectrophotometer (for metals analysis), and various centrifuges, ovens, balances, freezers, and other typical laboratory equipment.

4. Results and Discussion

a. Evaluation of Facility Waste Heat Recovery and Effluent Treatment

Waste heat characterization and waste effluent characterizations were initially completed for two specialty chemical facilities, two air separation plants and a membrane manufacturing facility. Following this initial study, a template for air separation plant waste heat sources was created to facilitate compilation of data in a standardized format for additional plants, with a focus on utilization of waste heat generated from air compression. Additional details of the study are located in Appendix A, including summary data for the 132 U.S. manufacturing facilities surveyed. Representative samples from the study were subjected to treatability analyses in cooperation with project partner Penn State. These results are summarized below.

b. Effluent Treatability Analyses

Six samples from four different Air Products industrial facilities were tested in miniature microbial electrolysis cells (mini MECs) to determine organic treatment performance and current generation characteristics. Based on this initial screening, a site was selected for further study in larger cube MEC reactors (cube MECs) to analyze gas production, current generation and organic treatment. In the secondary phase of the study, tests were conducted on three samples from different locations within the wastewater treatment operations at the potential site.

Mini MECs and Cube MECs

Mini MECs consisted of a 5 mL borosilicate serum bottle (Wheaton, Millville, NJ, USA) sealed with a butyl rubber stopper and aluminum crimp cap (Call and Logan, 2011; Figure 1a). Anodes were made of 1.0cm×1.5cm×0.32cm, Grade GM-10 graphite blocks (GraphiteStore.com, Inc., Buffalo Grove, IL, USA) connected to 0.032-gauge titanium wire current collectors (Malin Co., Brookpark, OH, USA) that extended through the rubber stopper. Cathodes were made of 50×50 Type 304 stainless steel mesh (McMaster-Carr, Elmhurst, IL, USA) cut to the same projected area as the anodes, and connected to 0.032- gauge stainless steel wire current collectors (Malin Co., Brookpark, OH, USA). Mini MEC liquid reactor volume was 5 mL. Empty reactors were autoclaved and sparged with an 80%:20% N_2:CO_2 mixed gas to ensure sterile, anaerobic conditions prior to use. Anodic biofilms were enriched by operating mini MEC reactors with primary clarifier effluent from the Penn State wastewater treatment plant, with new samples collected every 1-2 weeks. Mini MECs were acclimated until reproducible current peaks occurred, which took at least two weeks for all reactors. Acclimated reactors were then switched to industrial effluent samples. Generally, the substrate was changed when current dropped below 0.02 mA in at least two of the three reactors in a set. After effluent was removed and replaced with fresh substrate, the headspace was sparged with the same gas mixture for two minutes.

Cube MECs were made from 4-cm long by 3-cm diameter cylindrical polycarbonate chambers (Lexan, 32 mL liquid volume) with a 1.6-cm diameter by 7-cm tall glass tube glued to the reactor top to provide gas headspace (Call and Logan, 2008; Figure 1b). A carbon fiber brush (2.5-cm diameter by 2.5-cm length, Panex 35 polyacrylonitrile fiber; Zoltek, St. Louis, MO, USA) with a twisted-core, titanium wire current collector served as the anode. Brushes were heat treated at 450°C for 30 minutes before use to remove contaminants and create more favorable surface conditions for electrically active microbes (Feng et al., 2010). Cathodes were made of stainless steel mesh (Type 304, 50 × 50 mesh size; McMaster-Carr, Elmhurst, IL, USA) cut into 2 cm diameter discs with a total projected surface area of 12 cm^2, with 7 cm^2 exposed to the solution. A 0.5 mg/cm^2 platinum catalyst layer (10% (w/w) Pt on carbon black, Vulcan XC-72; Fuel Cell Store, College Station, TX, USA) was applied to the anode-facing side of the cathodes using Nafion as a binder (5% solution (w/w), 33.33 µL/cm^2; Sigma Aldrich, St. Louis, MO, USA). Gas bags (0.1 L capacity, Cali-5 bond, Calibrated Instruments Inc., Hawthorne, NY, USA) were connected to the headspace with plastic tubing and needles to collect additional gas and maintain atmospheric pressure in the headspace. Anodes were enriched by operating in microbial fuel cells (MFCs) with an air-diffusing cathode fed domestic wastewater prior to use in cube MECs. MFCs were connected to a 1000Ω external load and operated until repeatable current peaks were observed. Acclimated anodes were then transferred into cube MEC reactors and switched to industrial effluent substrate. Substrate in cube MECs was generally replaced when current dropped below 0.2 mA. After substrate replacement, headspaces were sparged with nitrogen gas for 20 minutes; gas bags were sparged by performing three cycles of filling the bags with nitrogen and vacuuming them empty.

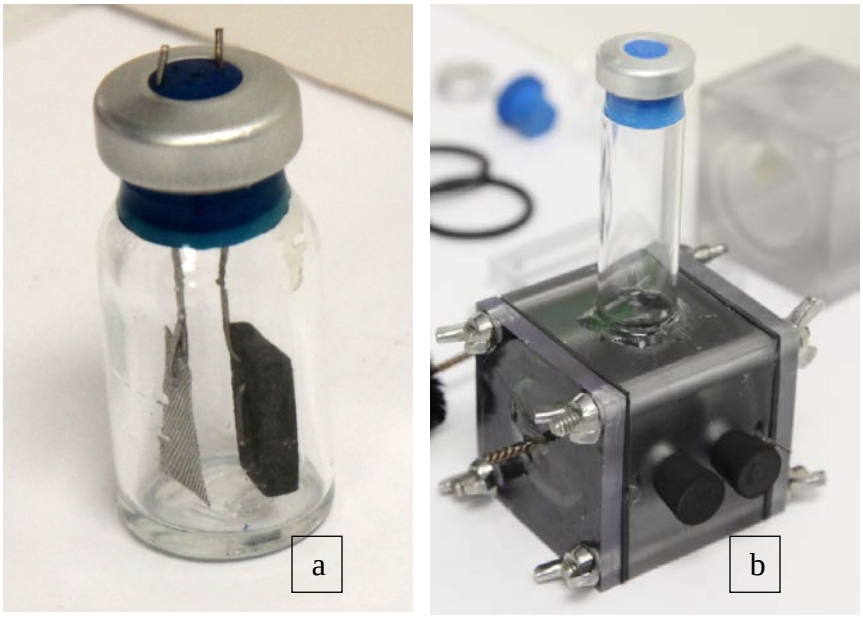

Figure 1. Photographs of mini (a) and cube MEC (b) reactors.

Reactors were operated in triplicate for mini MECs and in duplicate for cube MECs. The reactors were connected to a programmable DC power supply (model 3645A; Circuit 128 Specialists, Inc) with an applied potential of 0.7 V for mini MECs and 0.9 V for cube MECs. A multimeter (Kiethley Instruments, model 2700) connected to a computer was used to record voltage measurements across a 10 Ω resistor placed in series between the positive terminal of the power supply and anode of each reactor. Current was calculated from voltage measurements according to Ohm's Law. Influent and effluent COD were measured using a standardized chromic acid colorimetric method (Hach Co., Loveland, CO, USA). Biochemical oxygen demand (BOD) was measured using a 3-day headspace BOD test (Logan and Patnaik, 1997). A gas chromatograph (GC, Model 310; SRI Instruments, Torrance, CA, USA) with Ar as a carrier gas and a 6-foot molecular sieve-packed 5A column was used to measure cube MEC gas concentrations of H_2, CH_4, and N_2 after batch cycles. A GC with a He carrier gas and a 6-foot PoraPak™ Q column was used to measure CO_2 concentrations. Gas composition was determined by taking duplicate 0.2 mL samples from the cube reactor headspace and gas bag with an airtight syringe (0.5 mL Gastight® syringe, Hamilton Co., Reno, NV, USA) and injecting into each GC (total of 4 shots per sampling). Gas quantity was determined using the known headspace volume (10 mL) and the gas bag method, which uses a known volume of an inert tracer gas to induce a measurable change in the gas composition. Gas bag composition was initially measured, then 10 mL of ultra-high-purity nitrogen gas was added and the composition measured again. The initial bag volume was calculated as previously described (Ambler and Logan, 2011).

MEC performance was evaluated based on current generation, removal organics, and the efficiency of the conversion of organics into current and biogas. Appendix Equations A-1

through A-10 show the calculations for total charge collected over each batch cycle, average current, coulombic efficiency, the amount of energy added through the external power supply, treatment energy, energy efficiency, cathodic gas recovery, and overall hydrogen recovery.

Initial Treatability Assessments in Mini MECs:

Six samples (A1, B1, B2, C1, D1, and E1) from four Air Products facilities were collected and shipped overnight on ice to Penn State, where they were stored at 4°C until they were tested in mini MEC reactors. Samples B1 and B2 were collected from the same facility and at the same location within the treatment system, but at different times. Sample B2 was collected after a weekly operation that produces significantly higher COD than do normal operating conditions. Samples C1 and D1 were also collected from the same facility, but from different locations within the treatment operations: C1 was a process effluent, and D1 was the same process effluent combined with on-site sanitary waste. The initial pH, conductivity and COD for these samples are given in Appendix Table A1.

Prior to experiments in mini MECs, samples A1, B1 and B2 were neutralized to pH ~7.3 since low pH is known to inhibit electrically active microbes (He et al., 2008). Samples C1 and D1 were used as received and were not adjusted. Sample E1 was diluted with tap water to ~1000 mg/L COD due to the substantial initial COD load. In the diluted condition, E1 had a pH of 7.9 and solution conductivity of 0.38 mS/cm. After testing the 1000 mg/L COD dilution, a more concentrated sample diluted to a 1:100 ratio was also tested. The 1:100 diluted E1 had a COD concentration of 5440±210 mg/L. To provide a comparison for the Air Products industrial samples, domestic wastewater (WW) and a buffered acetate medium (AC) were also tested in MECs. WW was collected from the outlet of the primary clarifier at the Penn State wastewater treatment plant. AC was generated by dissolving 1 g/L of sodium acetate in 50 mM phosphate buffer solution, with trace vitamins and minerals added. The initial pH, conductivity and COD for domestic wastewater and buffered acetate medium are given in Appendix Table A2.

COD removal varied considerably between samples, with effluent concentrations ranging from 55 to 1260 mg/L COD (Figures 2a and 2b). COD removal from A1 was relatively modest, 34±2% on average (Figure 2c), leaving >1100 mg/L COD in the effluent. Approximately 70% of COD was removed from the B1 and B2 samples (Figure 2c). Sample C1 had the lowest influent COD concentration and the lowest COD removal, with only 22±13% removed on average (Figure 2c). D1, which was the process effluent combined with sanitary effluent, produced stable and repeatable cycles with a COD removal of 78±6% (Figure 2c). Sample E1 diluted to ~1000 mg/L COD also produced stable cycles, with 81±2% of COD removed on average (Figure 2c). The more concentrated E1 sample produced a significant drop in current generation and apparent damage to the anode, indicating that some wastewater components were toxic to the anodic biofilm at higher concentrations. Most of the samples performed favorably when compared to WW, but COD removal was not as high with the industrial samples as with AC.

Coulombic efficiency (CE) also varied between samples (Figure 2d). A1 was 89±7%, which was very similar to WW. B1 and B2 had the lowest CE of the samples tested, and both C1 and

D1 exceeded 100%. C1 was exceptionally high at >500%, which may have been caused by microbial degradation of the graphite electrode. E1 was near 80%, which was also similar to the CE of the WW sample. In general, low CE indicates that a significant portion of the COD removal was not due to anode-respiring microbes; it could be due to the presence of alternate electron acceptors and microbial activity away from the anode. A CE >100% typically indicates that hydrogen produced at the cathode is being used as an electron donor by anode-respiring microbes, effectively allowing electrons to "cycle" through the cell multiple times. Since hydrogen cycling increases current without oxidizing COD, the CE can exceed 100%. Optimally, the CE should be close to but >100%, as with the AC sample.

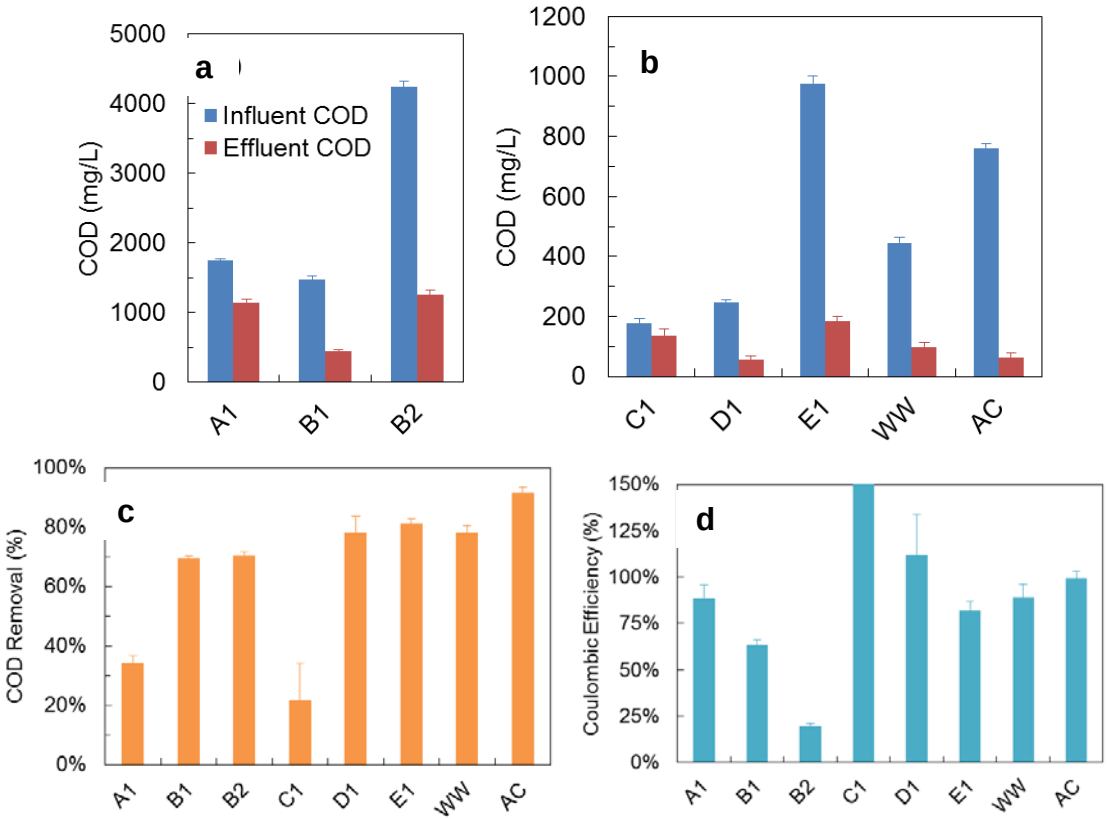

Figure 2. (a and b) Influent and effluent COD concentration, (c) percent COD removal for each sample in mini MECs, and (d) Coulombic efficiency (CE) for each sample in mini MECs. The CE for sample C1 was 558±682%, which greatly exceeded other samples, so it is not directly shown on the plot.

Current density, normalized to the projected cathode area and averaged over the time for 90% of the charge to accumulated, ranged from 0.25-2 A/m^2 with the industrial samples (Figure 3a). The highest current densities were observed with B1 and B2, which were both near 1.7 A/m^2. A1, C1 and D1 had relatively low average current densities of <0.5 A/m^2. Average current density provides a good indication of the sustained current, whereas peak current does not provide any information about the current over the whole cycle. This allows samples with different current profiles to be more easily compared.

Total charge recovered in mini MECs with A1, B1, B2 and E1 was 30-40 coulombs, which was close to the 42±1 coulombs recovered with AC (Figure 3b). C1 and D1 produced <15 coulombs, which was likely due to the low organic concentrations in these samples. Despite the significant difference in COD concentration between B1 and B2, the total recovered coulombs were very similar.

The average time for 90% charge accumulation was generally 1.5-3 days for all industrial samples except A1, which had a t_{90} of 5.3±0.8 days (Figure 3c). Most of the t_{90} times were similar to the WW sample (2.3±0.3 days) but longer than the AC sample, which is known to be rapidly degraded by electrically active microbes. Of the industrial samples, B1 and B2 had the lowest t_{90} at 1.7 days.

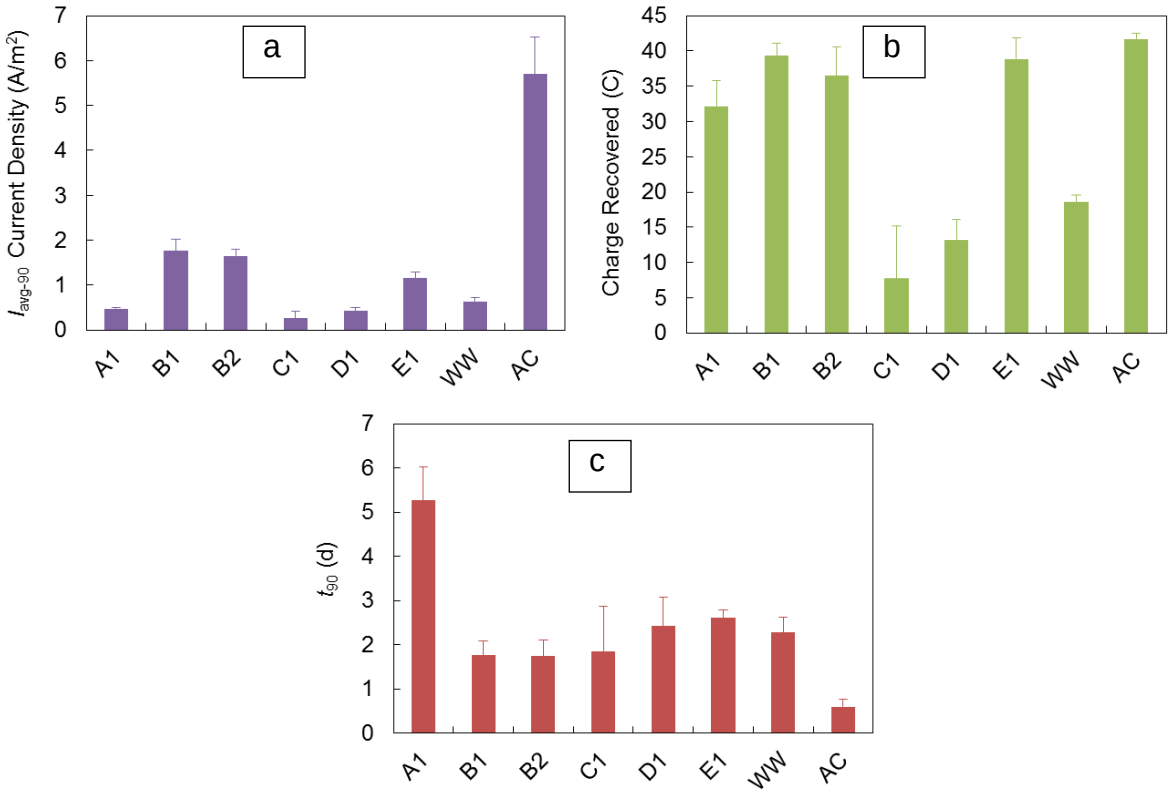

Figure 3. (a) Average current density calculated over the time to 90% charge accumulation (I_{avg-90}), (b) average total charge recovered (Q_{total}) in mini MECs for each sample, and (c) average time for 90% charge accumulation (t_{90}) for each sample.

Based on the results of the initial mini MEC screening, B1 and B2 showed the greatest potential for energy recovery and treatment in MECs with ~70% COD removal and total charge recovery near that of AC. They also had the fastest reaction time of the samples tested, as exhibited by the t_{90} time. A1 performed reasonably well, with CE near 90% and total charge recovery >30 coulombs per cycle. However, cycle length was substantially longer than for other samples, and COD treatment was also relatively low (<35% COD removal. C1 performed very inconsistently and most likely is too dilute to serve as a substrate in MECs. While D1 had

stable performance, total charge recovery and average current were lower than WW. E1 also had stable performance, but required significant dilution and showed potential toxic effects on the anodic biofilm when the concentration was increased.

Secondary Treatability Assessments in Cube MECs

Further sampling from Site B was conducted because samples B1 and B2 showed promising performance in the initial mini MEC assessment. Three more samples (B3, B4, and B5) were collected from different locations within the treatment operations at the same plant. B3 was collected upstream of the treatment operations before all the effluents are combined. B4 was drawn just prior to neutralization, which occurs before wastewater treatment after all effluent streams have been combined. B5 was collected just after wastewater neutralization. The samples were shipped to Penn State and stored at 4°C prior to performance analysis in both mini and cube MECs. Initial pH, conductivity and COD for these samples are given in Appendix Table A3.

B3 and B4 were neutralized with 0.3 M NaOH to pH 7.3 prior to tests in MECs. When initially added to mini and cube MECs, B4 had the highest COD load and produced inconsistent current and long cycle times. Around day 40 of reactor operation, B4 was diluted in a NaCl solution to 1450±40 mg/L of COD in an effort to reduce cycle time while maintaining solution conductivity. An NaCl solution was prepared to match the conductivity of the full-strength B4 sample, then mixed in a 3:1 ratio with B4. This shortened the cycle time and improved current generation.

Influent COD and $HBOD_3$ concentrations of the samples as used in MECs ranged between 450-4500 mg/L of COD and 230-790 mg/L of $HBOD_3$ (Appendix Figure A1). Of the five samples tested (B3, B4, B5, WW, and AC), the three industrial wastewater samples (B3, B4, and B5) had the highest influent COD concentrations, all exceeding 1400 mg/L. The $HBOD_3$/COD ratio provided insight into the aerobic biological degradability of the organic material in each sample, since it gives the fraction of COD that can be readily degraded by aerobic microbes. B3 and B5 had $HBOD_3$/COD ratios <0.2, meaning a significant portion of the COD was not readily degradable under aerobic conditions within three days. AC, which is a model substrate, had a $HBOD_3$/COD ratio of 0.7. At 0.5, B4 had the highest $HBOD_3$/COD ratio of the industrial wastewaters analyzed in this study.

A total of 66-86% of COD in B3, B4 and B5 was treated in mini and cube MECs (Figure 4A). This was similar to MECs fed WW, which removed 76-78% of COD, but not quite as good as AC-fed reactors, which removed over 90%. Effluent COD concentrations were still significant for the B samples, with 360-780 mg/L of COD remaining in the MEC effluent (Figure 4B). This indicates that further treatment would likely be necessary after treating wastewater with an MEC, but a substantial reduction in COD is possible. MECs were operated in open-circuit mode to determine the background COD removal in the absence of current generation (Figure 4C). Samples B3 and B5 had significant open-circuit reductions in COD, indicating that much of the COD removal observed in closed-circuit mode may not be attributed to organic oxidation by the electrically active microbes on the anode. Relatively little COD was

removed in B4-fed MECs during open-circuit cycles. Based on the process and treatment operations at the Site B facility, it is likely that the B3 and B5 samples contained a significant concentration of methanol which was not present in the B4 sample. This contributed to the observed difference in open-circuit COD removal.

Coulombic efficiency (CE), the fraction of COD that is converted into current, also varied and was relatively low for MECs fed the B3 and B5 samples at ~40% and ~20% (Figure 4D). Based on the open-circuit COD removal in the B3 and B5 MECs, there was a large fraction of COD that was removed but not converted into current, as reflected in the low CEs. B4 had a CE that exceeded 100%, suggesting that microbial hydrogen oxidation at the anode was contributing to the measured current density. Oxidation of hydrogen evolved at the cathode by electrically active microbes on the anode, also known as hydrogen cycling, is an issue in single-chamber MECs since there is no separation between the anode and cathode (Lee and Rittmann, 2010).

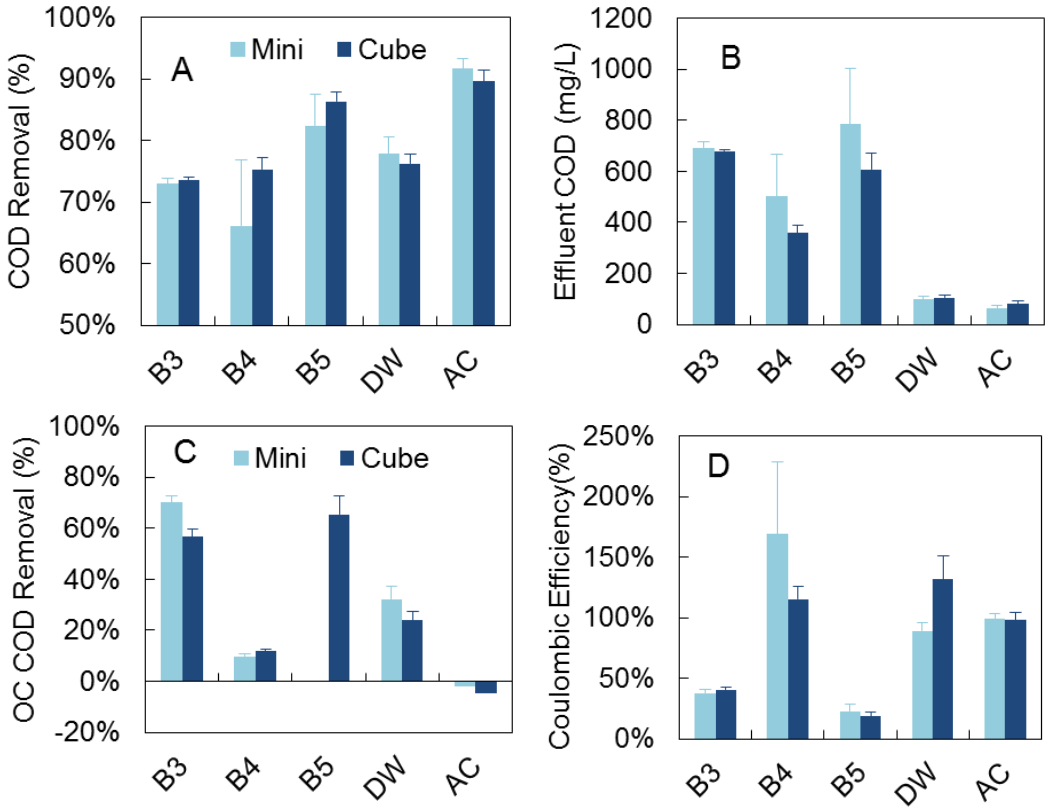

Figure 4. (A) COD removal, (B) effluent COD concentration, (C) COD removal measured during open-circuit operation with no current generation, and (D) Coulombic efficiency for mini and cube MECs fed each sample. Results were averaged over multiple cycles.

Current density, averaged over the time to 90% charge accumulation ($I_{avg\text{-}90}$), varied between samples but was greater in the MECs fed Site B effluents than in the WW-fed reactors (Figure 5A). $I_{avg\text{-}90}$ was generally higher in cube MECs than mini MECs, which was likely due to the slightly higher applied potential and the catalyst layer present on the cube MEC cathodes

that was not applied to the mini MECs. $I_{avg\text{-}90}$ was much higher with the ideal AC sample, a reflection of the short cycle time with a sharp current peak and rapid decrease that are not typical with real wastewater samples. The total coulombs recovered with the B3 and B5 samples were similar to AC (Figure 5B). B4-fed MECs showed the highest total coulombs recovered, but this was likely influenced by hydrogen oxidation at the anode.

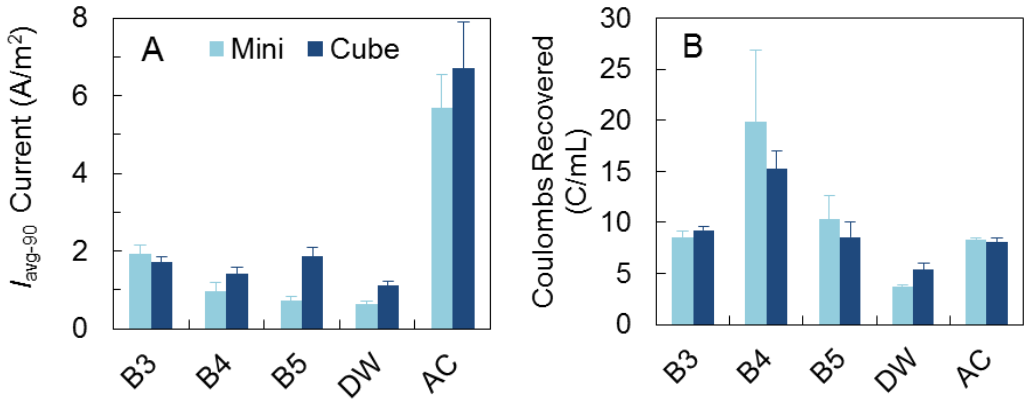

Figure 5. (A) Current density averaged over the time for 90% charge accumulation (t_{90}), and (B) total coulombs recovered (per mL of reactor liquid volume) over multiple cycles with mini and cube MECs.

Treatment energy, based on the additional energy added to the MEC through the power supply, was low for B3 and B5 because of the low CE and large COD reduction not associated with current generation (Figure 6). B4 had the highest treatment energy, but this was also influenced by hydrogen oxidation. This treatment energy calculation also does not account for any energy gained through hydrogen or gas production.

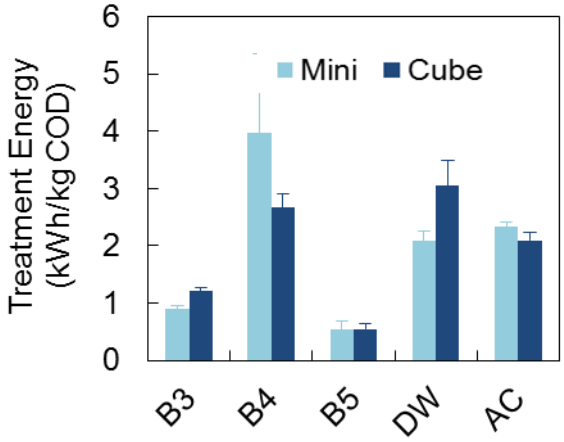

Figure 6. Average energy required for organic treatment based on COD removal and the additional energy added through the external power supply.

The volume of hydrogen recovered in B4-fed cube MECs was highest among the Site B samples tested, and similar to the hydrogen volume recovered with AC-fed MECs (Figure 7A). Methane was also present in all Site B samples but was most significant in the B5-fed reactors. Gas recovery after open-circuit cycles indicated that nearly all of the methane observed in the

B3 and B5 MECs was not related to current generation and was likely a result of methanogens converting the methanol present in the samples into methane (Figure 7B). Hydrogen was also measured in both the B3 and B5 samples during normal closed-circuit operation, but the volume was less than in the B4-fed MECs.

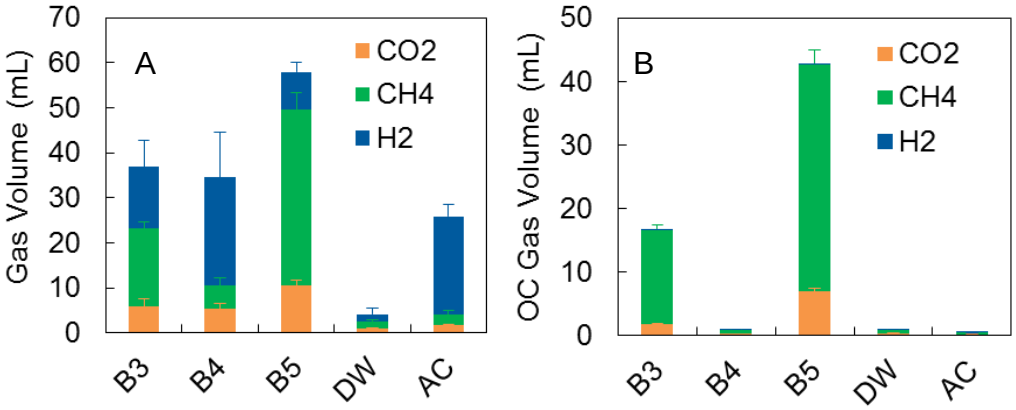

Figure 7. (A) Recovered gas composition and volume for each sample during normal closed-circuit operation and (B) gas recovered during open-circuit operation in the absence of current generation.

Overall energy efficiency – based on recovery of only hydrogen or combined hydrogen and methane using the heat of combustion to determine energy content – showed that all Site B samples generated more energy in the recovered gas than was consumed by adding energy through the power supply (Figure 8A). When only hydrogen was considered, efficiencies were <100% for all but the AC sample. Since these were single-chamber MECs, however, it is possible that hydrogen was converted into methane by methanogens. While the cathodic and overall recovery of hydrogen varied between samples, it was <40% for all B samples – indicating that a significant portion of current was not recovered as hydrogen (Figure 8B). Single-chamber systems are not optimally suited for high hydrogen recovery rates; a system with a separated anode and cathode chamber would produce higher conversion efficiencies.

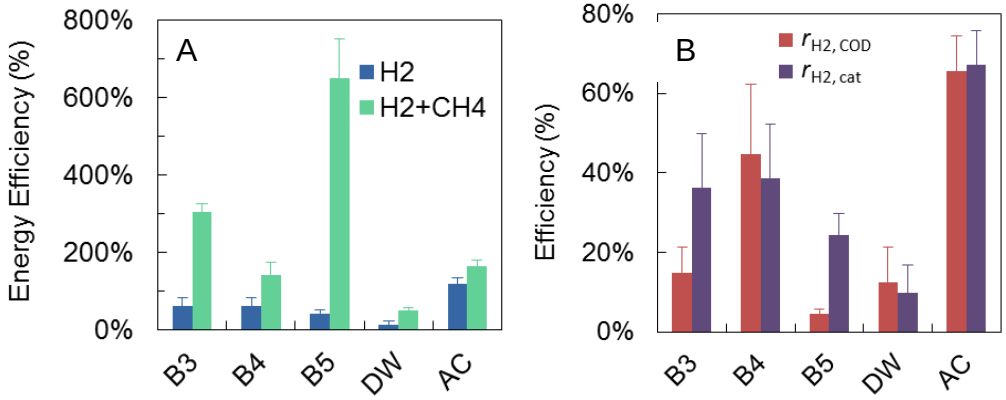

Figure 8. (A) Energy efficiency for cube MECs, with each sample based on the energy content of the gas recovered and the energy added through the external power supply. Efficiency was calculated using only recovered hydrogen and combined hydrogen and methane, using the heat of combustion to calculate the energy contained in the gas. (B) cathodic ($r_{H2,cat}$) and overall ($r_{H2,COD}$) recovery of hydrogen based on COD and current.

Hydrogen was generated with all three samples in MECs, with 66-86% of COD and >90% of BOD removed in MECs, which compared well to a domestic wastewater sample. Average current density for the industrial wastewater samples from the potential site was also greater than for the domestic wastewater sample. All three samples were found to be suitable substrates in MECs and could be viable candidates for a larger-scale MEC treatment system.

c. Process Unit Operation Configuration and Optimization

Although significant progress was made to understand individual unit operations, which are discussed below, efforts to optimize the overall process were delayed due to emphasis on the work to improve the ion exchange membranes. Had the project moved forward, additional efforts to more fully integrate the individual unit operations could have resulted in improvements for the overall efficiency of the process. This would need to take place should the program be restarted in the future due to changes in overall economic environment, or the improvements discussed in the various technologies involved.

d. Reverse Electrodialysis Cell Experimental Analyses

The objective of this task was to optimize the performance of a reverse electrodialysis (RED) stack in terms of flow rates, solution concentrations, and compositions. The pumping energy consumption, an important part of costs for RED operation, is a function of the liquid flow rates. The goal was to determine the lowest flow rate at which power output of the RED cell still was relatively unchanged. The flow rates of high-concentration (HC) and low-concentration (LC) solutions were investigated separately, as it was thought that lower flow rates could be used for HC solutions because LC solutions had higher solution resistances due to their lower conductivities. The waste heat energy needed to regenerate solutions is significantly affected by solution concentrations and compositions. Thus, lower concentrations of the HC solutions and higher concentrations of the LC solutions were preferred to minimize waste heat energy consumption. Based on these tests, the goal was to identify the optimum concentrations for HC and LC solutions considering waste heat energy consumption and power output of the RED cell. Ammonium bicarbonate (NH_4HCO_3, or AmB) is more easily to be regenerated compared to common sodium chloride (NaCl), but the performance difference of the RED cell with these salts is unknown. Therefore, comparisons were also made of RED cell performance using AmB versus NaCl solutions.

RED system and performance tests

The RED system was set up as shown in Figure 9. A RED cell composed of 10 cell pairs (ED 64002-020) was purchased from PCCell GmbH in Heusweiler, Germany. This unit consists of an anode chamber, a cathode chamber and a membrane stack between them. Both the anode and the cathode were titanium mesh coated with platinum and iridium (Ti/Pt-Ir) with a projected area of 64 cm^2 (8 cm × 8 cm). The membrane stack was assembled with 11 standard PC-SK cation exchange membranes (CEMs) and 10 standard PC-SA anion exchange membranes (AEMs). The active membrane area was 64 cm^2 (8 cm × 8 cm) per membrane, for a total active

membrane area of 0.13 m^2. The thickness of each cell pair was 0.5 mm. Three Masterflex® L/S pumps were used to pump HC solution, LC solution and electrolytes through the RED cell. A 35 g/L NaCl solution (100 mL) was recycled through both the anode and the cathode chambers at 100 mL min^{-1} to avoid large pH changes in the anolyte or catholyte. The HC and LC solutions flowed separately through the HC and LC channels of the stack in a single-pass mode at specific flow rates.

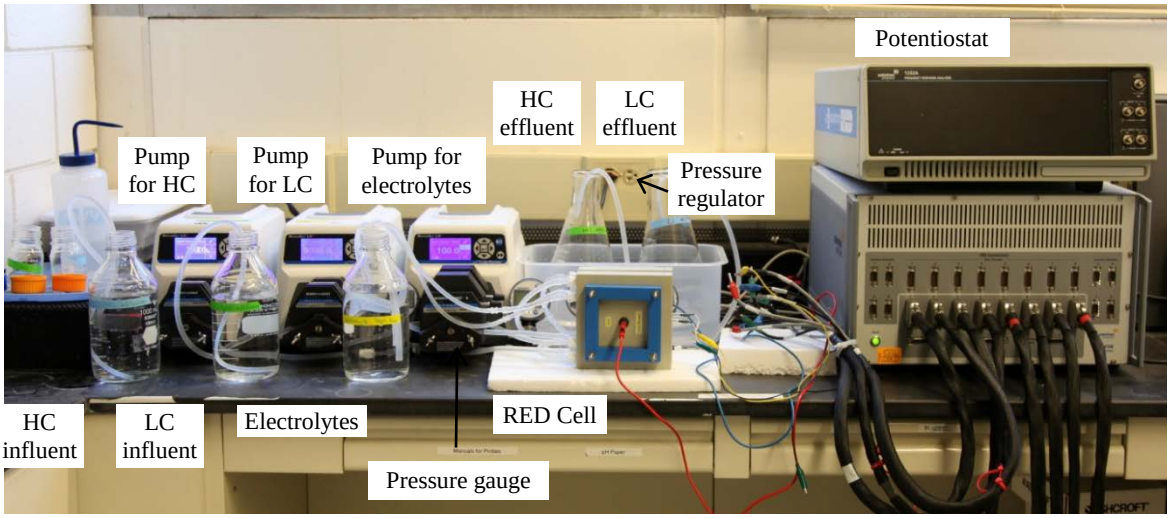

Figure 9. Photo of the reverse-electrodialysis (RED) cell system.

Four digital pressure gauges (DG25, Ashcroft Inc., Stratford, CT) were installed at the inlets and outlets of the HC and LC channels to monitor pressures. Two simple pressure regulators (Hoffman open jaw screw compressor clamp, Humboldt Scientific Inc., Raleigh, NC) were added at each of the outlets of the HC and LC channels to adjust the pressures in the RED cell HC and LC chambers. Hydrodynamic power losses (P_{hydro}, in W) when HC and LC solutions flowed through the stack at different rates were calculated based on the pressure drops measured by pressure gauges according to Veerman et al. (2009 & 2010):

$$P_{hydro} = Q_{HC}\Delta P_{HC} + Q_{LC}\Delta P_{LC} \quad [1]$$

where Q_{HC} and Q_{LC} are the flow rates of HC and LC solutions (m^3/s), and ΔP_{HC} and ΔP_{LC} are the pressure drops of the HC and LC channels (Pa).

A potentiostat (model 1470E, Solatron Analytical, Hampshire, England) was used to conduct polarization tests to evaluate RED cell performance. Current was scanned from zero to the maximum current (when the voltage of the membrane stack became reversed) at a rate of 0.2 mA s^{-1}. Ag/AgCl reference electrodes (BASi, West Lafayette, IN) were placed on either side of the membrane stack in the anolyte and catholyte to record the stack voltage during each sweep. At least three polarization curves were recorded under each condition. The power density of the membrane stack, excluding electrode overpotentials, was calculated per Hatzell et al. (2014):

$$P_{stack} = \frac{U_{stack} \cdot I_{stack}}{A_{mem}} \quad [2]$$

where P_{stack} is the power density of the membrane stack (W/m^2 membrane), U_{stack} is the voltage of the membrane stack (V), I_{stack} is the scanned current (A), and A_{mem} is the total active membrane area of the stack (m^2).

Optimum flow rates

Initially, HC and LC solutions were kept at the same flow rates, which were then simultaneously changed from 140 mL/min to 2 mL/min. Through polarization tests, the open circuit voltage, maximum current, maximum power density, and the conductivity of the effluents were obtained for the RED stack at different flow rates (Appendix A, Figure A2). The following three regions were identified:

(I) Diffusion layer resistance-dominating region (70~140 mL/min): The open-circuit voltages did not change much. This indicated that there was a similar electromotive force because the HC and LC solution conductivities changed only a little, while the maximum current and power density decreased with the flow rates. This was attributed to the increasing diffusion layer resistance at lower flow rates.

(II) Electromotive force and ohmic resistance-dominating region (30~70 mL/min): The solution concentration in LC channels increased with the decrease in flow rates. As a result, the electromotive force decreased a little (as shown by the decreasing open circuit voltage) while the ohmic resistance in LC channels decreased (as shown by the increasing maximum current). Due to the trade-off between the electromotive force and ohmic resistance, the maximum power densities were similar in this region.

(III) Electromotive force-dominating region (2~30 mL/min): The electromotive force greatly decreased (as shown by the decrease of open circuit voltage) due to the large decrease of HC concentration and increase of LC concentration at lower flow rates. Therefore, the maximum power density significantly declined in this region.

Hydrodynamic power loss was calculated according to Equation 1 based on the measured pressure drops (Figure 10A). The electric power output of the RED stack was calculated based on the maximum power density and total active membrane area (Figure 10B). The pressure drops of HC and LC channels decreased linearly with the flow rates. As a result, the hydrodynamic power loss (pumping energy) decreased with the flow rates (Figure 10B). Therefore, the net power output of the RED stack can be obtained by subtracting the hydrodynamic power loss from the electric power (Figure 10B). The maximum net power output was achieved when the flow rate of the HC and LC solutions was 20~50 mL/min.

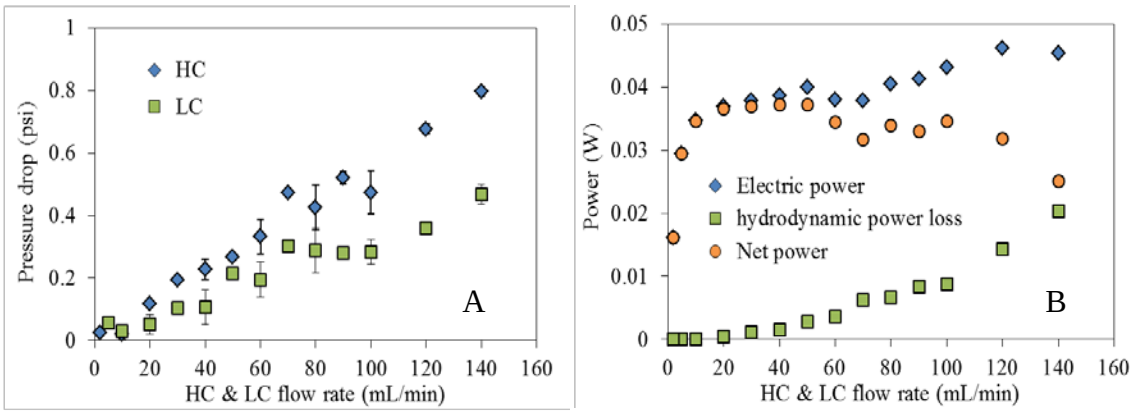

Figure 10. (A) Pressure drops of HC and LC channels, and (B) electric power, hydrodynamic power loss, and net power of the RED stack when the flow rates of HC and LC solutions simultaneously decreased from 140 mL/min to 2 mL/min.

In order to investigate if different flow rates can be used for HC and LC solutions, the LC solution flow rate was decreased from 50 mL/min to 2 mL/min, while the HC solution flow rate was fixed at 50 mL/min. The trends in the open-circuit voltage, maximum current, maximum power density, and effluent conductivity as function of the LC solution flow rate (Appendices, Figure A3) were quite similar to those when the HC and LC solution flow rates were changed simultaneously. This showed that RED stack performance was mainly determined by the flow conditions of the LC solution. The hydrodynamic power losses at different LC solution flow rates were also calculated according to Equation 1 based on the measured pressure drops (Figure 11A), with the net power output of the RED stack again obtained by subtracting the hydrodynamic power loss from electric power (Figure 11B). The maximum net power output was obtained when the LC solution flow rate was 20~50 mL/min. Considering that a lot of energy is used to pump the LC solution from the reservoir to the RED stack, the lowest flow rate of 20 mL/min would be the optimum LC solution flow rate to save part of the energy needed for pumping.

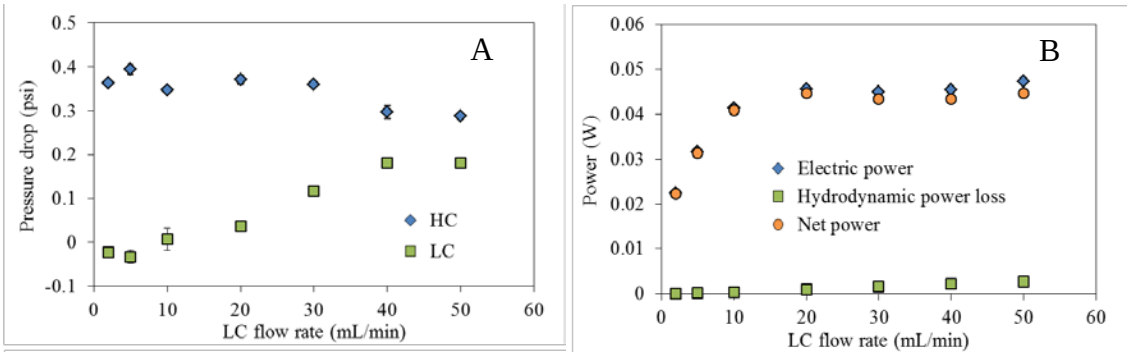

Figure 11. (A) Pressure drops of HC and LC channels. (B) Electric power, hydrodynamic power loss, and net power of the RED stack when the LC solution flow rate was decreased from 50 mL/min to 2 mL/min and the HC solution flow rate was held at 50 mL/min.

To obtain the optimum flow rate of HC solution, the flow rate of the HC solution was decreased from 50 mL/min to 2 mL/min while keeping the LC solution flow rate at 50 mL/min. The open-circuit voltage was relatively constant over the investigated range of flow rates (Appendices, Figure A4). The maximum current, maximum power density, and the conductivity of HC effluent did not begin to change until the flow rate of HC solution decreased to 10 mL/min (Appendices, Figure A4). The hydrodynamic power losses at different HC solution flow rates were calculated using Equation 1 and the measured pressure drops (Figure 12A); net power output was obtained by subtracting the hydrodynamic power loss from electric power (Figure 12B). The maximum net power output was obtained when the flow rate of HC solution was 10~30 mL/min. Considering the energy needs for pumping the HC solution from the reservoir to the RED stack, the lowest flow rate of 10 mL/min would be the optimum flow rate for HC solution.

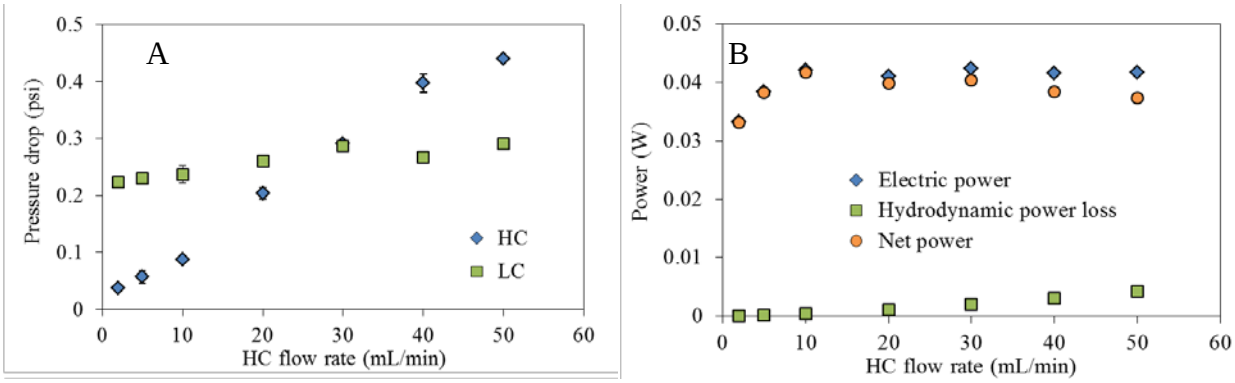

Figure 12. (A) Pressure drops of HC and LC channels. (B) Electric power, hydrodynamic power loss, and net power of the RED stack when the HC solution flow rate was decreased from 50 mL/min to 2 mL/min and the LC solution flow rate was held at 50 mL/min.

The performance of the RED stack was investigated under conditions called HC10/LC20, using the optimum HC and LC flow rates (10 and 20 mL/min respectively). This was compared to the RED stack performance at HC50/LC50 (both HC and LC solutions at 50 mL/min). Although the open-circuit voltage at lower flow rates (1.58 V) was a bit lower than at higher flow rates (1.70 V), the maximum power density was similar for these two cases (0.28 W/m^2-membrane) due to decreasing internal resistance at lower flow rates (Figure 13). Moreover, the hydrodynamic power loss when the HC and LC solutions were flowing through the RED stack was much lower at HC10/LC20 (0.4 mW) than it was at HC50/LC50 (4 mW).

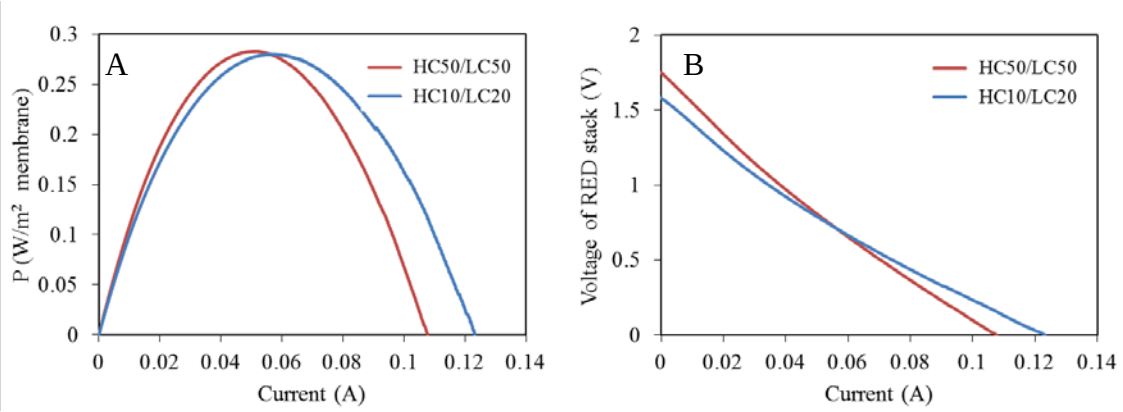

Figure 13. (A) Power density curves and (B) polarization curves of the RED stack when the flow rates of both HC and LC solutions were 50 mL/min (HC50/LC50) and the flow rate of HC solution was 10 mL/min with the flow rate of 20 mL/min for LC solution (HC10/LC 20).

Optimum solution concentrations

Different NaCl concentrations (0.6 M, 1.2 M, 1.8 M, 2.4 M, 3 M, 3.6 M, 4.2 M, 4.8 M, and 5.4 M saturated) in HC solutions were examined at a flow rate of 10 mL/min, while the NaCl concentration in the LC solution was fixed at 0.006 M with a flow rate of 20 mL/min. As HC concentration increased, the open circuit voltage was nearly constant (Figure 14A), while the maximum current (Figure 14B) and the maximum power density (Figure 14C) increased up to 3.6 M and then became stable above 3.6 M. Both HC and LC effluent conductivity increased with HC concentration (Figure 14D), indicating that the change of HC concentration would also affect the solution concentration in the LC channel. The improved performance of the RED stack at higher HC concentrations was mainly due to the increased salinity ratio. The optimum HC concentration was 3.6 M. Under this condition, open-circuit voltage was 1.56 V, maximum current was 274 mA, maximum power density was 0.78 W/m^2-membrane, and HC and LC effluent conductivities were 185 mS/cm and 16 mS/cm respectively. Pressure drop (0.3 psi) and hydrodynamic loss (1 mW) did not appear to be affected by HC concentration (Appendices, Figure A5).

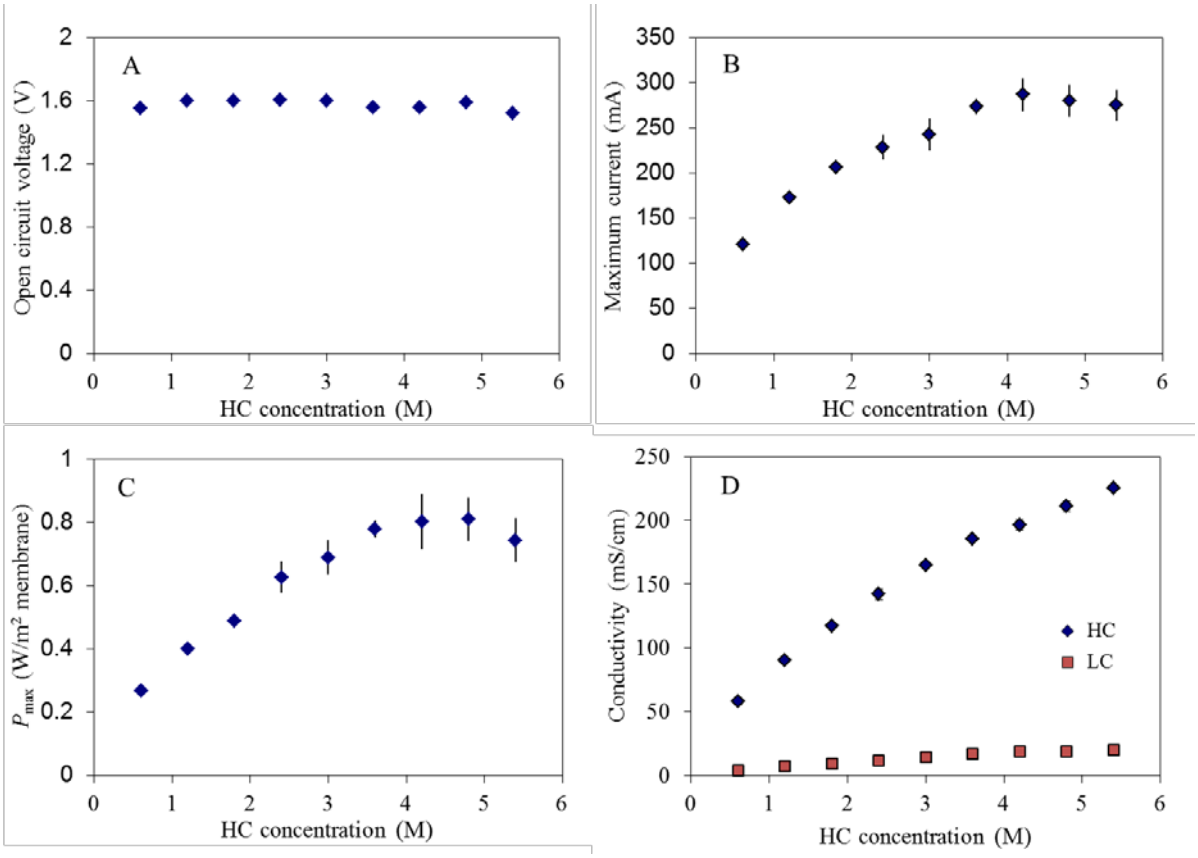

Figure 14. (A) Open-circuit voltage, (B) maximum current, (C) maximum power density, and (D) effluent conductivity when HC concentration increased from 0.6 M to 5.4 M (saturated) NaCl at a flow rate of 10 mL/min. LC solution was 0.006 M NaCl at a flow rate of 20 mL/min.

Different NaCl concentrations (0-3 M NaCl) in LC solutions were examined at a flow rate of 20 mL/min, while the NaCl concentration in the HC solution was fixed at 3.6 M with a flow rate of 10 mL/min. As LC concentration increased, the open-circuit voltage decreased (Figure 15A and 15B) due to the lower salinity ratio. However, the maximum power density was nearly constant at 0.6~0.7 W/m^2-membrane with LC concentrations below 0.14 M, then greatly decreased at LC concentrations above 0.14 M (Figure 15C and 15D). The stable power density below 0.14 M was thought to be due to the trade-off between the decreased salinity ratio and ohmic resistance with increased LC concentration (Dlugolecki et al., 2010). This reasoning was confirmed by the increasing maximum current (Figure 15E and 15F) and the LC effluent conductivity (Figure 15G and 15H). When LC concentration was >0.14 M, the role of salinity ratio (<25) would be more important than ohmic resistance. Thus, the power density of the RED stack greatly declined. The optimum LC concentration was found to be 0.14 M. Under this condition, open-circuit voltage was 1.08 V, maximum current was 302 mA, maximum power density was 0.62 W/m^2-membrane, and of HC and LC effluent conductivities were 189 mS/cm and 29.5 mS/cm respectively. The pressure drop (0.3 psi) and hydrodynamic loss (1 mW) also didn't change with increasing LC concentration (Appendices, Figures A6 and A7).

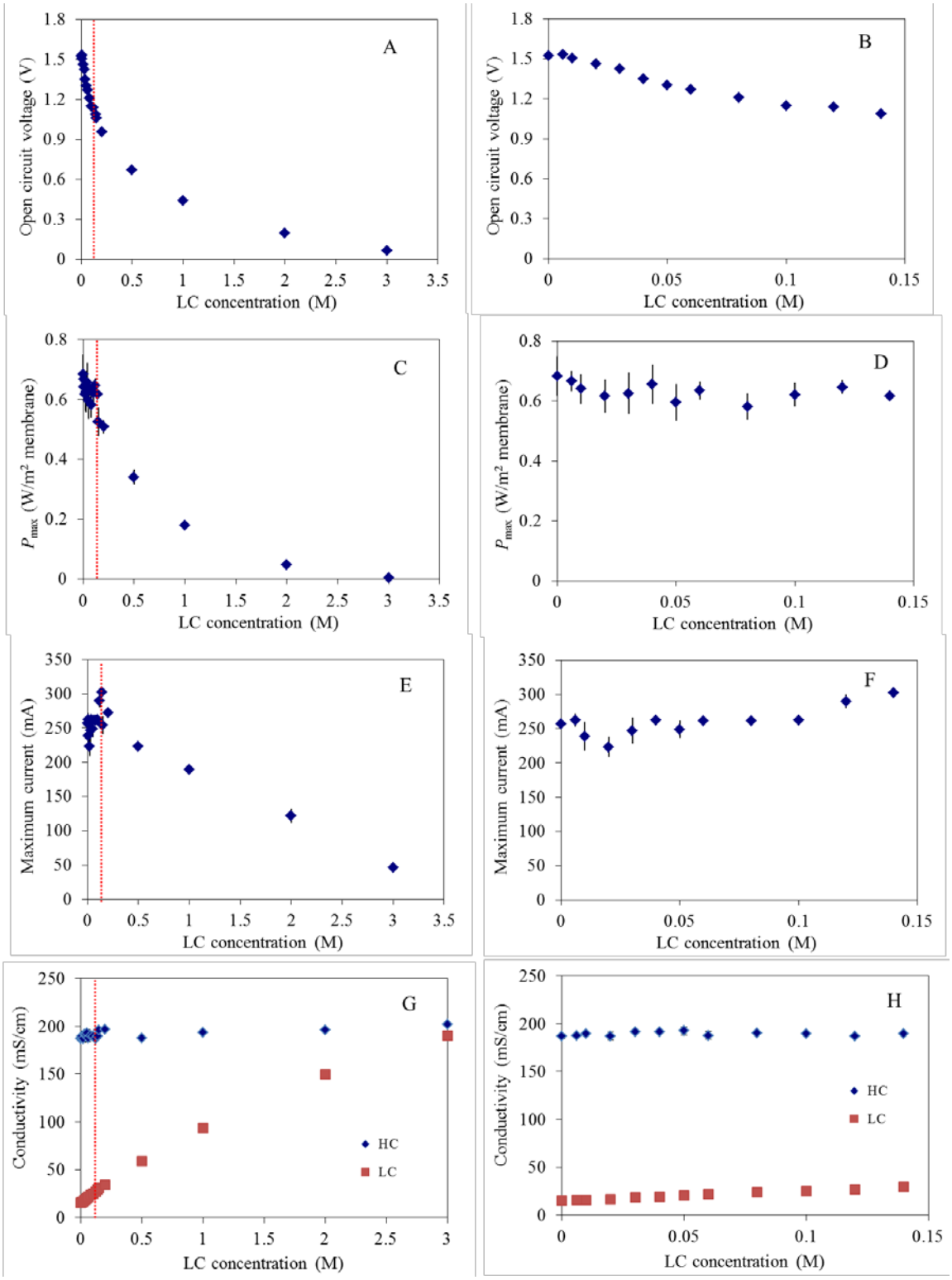

Figure 15. Open-circuit voltage for a wide (A) and a narrow (B) range, maximum current for a wide (C) and a narrow (D) range, maximum power density for a wide (E) and a narrow (F) range, and effluent conductivity for a wide (G) and a narrow (H) range when LC concentration increased from 0 M to 3 M NaCl at a flow rate of 20 mL/min. HC solution was 3.6 M NaCl at a flow rate of 10 mL/min.

Comparison of NaCl and AmB (NH_4HCO_3) solutions

The performance of the RED stack with different salts (NaCl vs. AmB) was examined at either the same molar concentrations or at the same solution conductivities with adjusted molar concentrations. Tests were conducted using two pairs of HC and LC concentrations (HC0.6M/LC0.006M and HC1.5M/LC0.015M) and two pairs of HC and LC conductivities (HC54 mS cm^{-1}/LC0.72 mS cm^{-1} and HC95 mS cm^{-1}/LC1.62 mS cm^{-1}). The corresponding concentrations and conductivities are given in Appendices Table A4.

The results demonstrated that RED stack performance was lower using the same concentration of AmB solution compared to NaCl solution (Figure 16A). This is due in part to the lower permselectivities of the membranes with AmB compared to NaCl (Geise, Cassaday et al., 2014). However, the main difference was due to the different conductivities of the solutions, which impacted solution and therefore stack resistance. The maximum power densities of the RED stack were similar for the NaCl and AmB solutions when their conductivities were adjusted to be the same (Figure 16B). Therefore, the results and conclusions for the NaCl solution should also apply to the AmB solution under the same conductivity conditions.

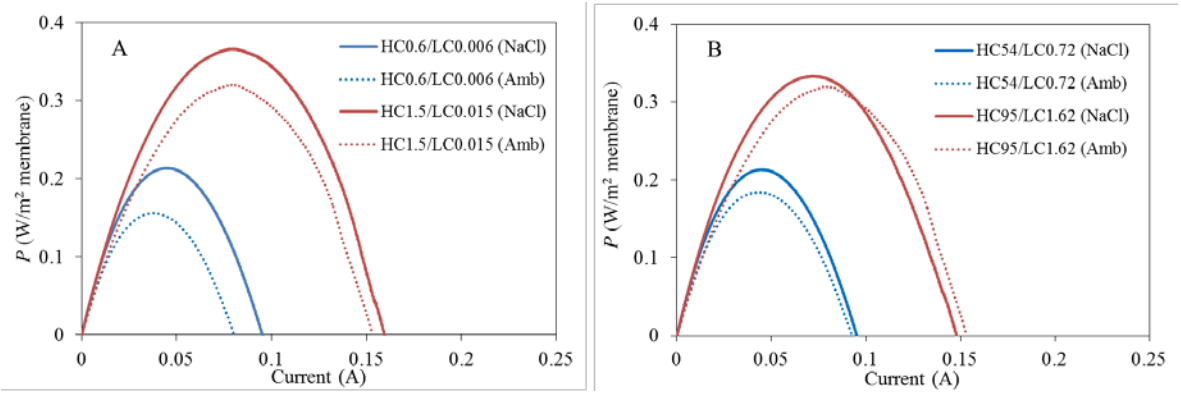

Figure 16. Polarization curves of the RED stack with (A) the same concentration NaCl and AmB solutions (HC0.6M/LC0.006M or HC1.5M/LC0.015M), and (B) the same conductivity NaCl and AmB solutions (HC54 mS cm^{-1}/LC0.72 mS cm^{-1} or HC95 mS cm^{-1}/LC1.62 mS cm^{-1}).

e. Ion Exchange Membrane Development

The objective of this task was to characterize the ex-situ fundamental ionic resistance and permselectivity of ion exchange membranes (IEMs) used in the RED process separately from the RED stack in small-scale test cells. The power of a RED stack is inversely proportional to the membrane resistance and directly proportional to the square of permselectivity, so developing a membrane with low resistance and high permselectivity is critical for an efficient RED device. Sodium chloride is a baseline salt used for characterizing membranes, while AmB is relevant to the development of a closed-loop waste heat reclamation unit with RED. The ionic resistance of two commercial AEMs and two commercial CEMs (from Selemion and PCCell respectively) was determined in these two salts of interest at concentrations ranging from 0.1 M to 1.0 M. Permselectivity was determined in these two salts, as well as the complementary salts

ammonium chloride and sodium bicarbonate to develop a relation between ion type and concentration and permselectivity. The information collected in this task was used to guide membrane choice and design for RED, and also to provide input parameters for RED Computational Model development (Section f).

Resistance measurement of ion exchange membranes

The resistance of commercially available IEMs was measured as a function of concentration in both sodium chloride and AmB solutions (Figure 17).

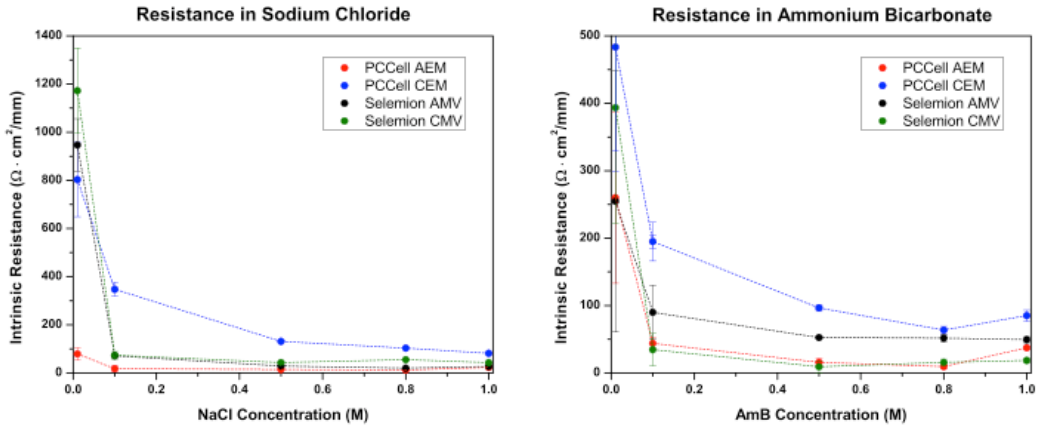

Figure 17. Resistance of PCCell and Selemion membranes in sodium chloride and AmB solutions as a function of concentration.

The measurement cell and experimental technique are described in previous work (Geise, Curtis, et al., 2014). Overall, the membrane resistance values in sodium chloride at low concentration are greater than the membrane resistances in AmB. The lower resistance of membranes in AmB is a promising aspect of membrane performance for AmB-driven reverse electrodialysis stacks. The fundamentals of how electrolytes in solution influence membrane resistance will be used to design low-resistance membranes (Geise et al., 2013).

The measured membrane resistance was observed to be a function of current density (Figure 18). As the current density was increased, the slope of the potential versus current density curve increased and gave a difference in membrane area resistance of 140 Ω-cm2 between the low and high current density regions. [The data in Figure 20 are for low current density.] The change in resistance at high current density is a phenomenon termed “over-limiting current” and may influence the accounting of the membrane resistance from stack measurements.

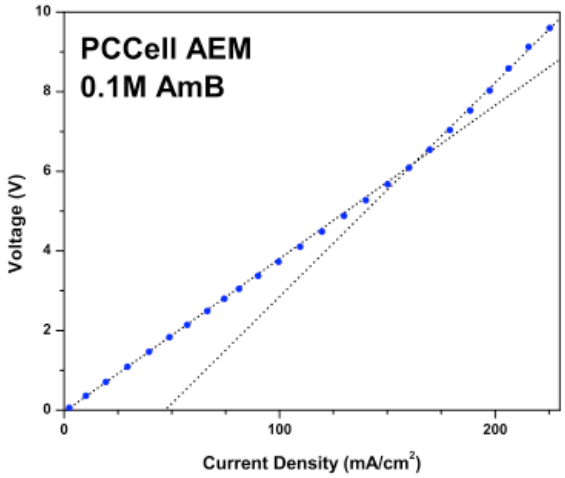

Figure 18. Voltage versus current density plot for calculating membrane resistance showing two different resistive slopes depending on current density.

These resistance measurements on commercial PCCell and Selemion membranes set the baseline for assessing new IEMs and membrane concepts to increase RED stack performance. This membrane resistance data and initial estimates of other membrane properties were used as input into an electrodialysis stack model based on the data acquired in PCCell stacks (see Section f, Reverse Electrodialysis Computational Model). This information was used to refine the electrodialysis stack model. In addition, these ex-situ resistance values measured under controlled conditions were compared to the membrane resistance values measured in a PCCell stack to understand how individual membrane measurements correspond to stack measurements.

Permselectivity measurements of ion exchange membranes

The permselectivity of commercial membranes was evaluated in sodium chloride (NaCl), ammonium chloride (NH_4Cl), sodium bicarbonate ($NaHCO_3$), and AmB (NH_4HCO_3) electrolytes. While the goal was to measure and understand the permselectivity of commercial membranes in AmB, several different salts were used to examine the anion- and cation-specific effects on membrane permselectivity. Permselectivity was measured with the membrane of interest placed between stirred compartments containing 0.5 M and 0.1 M solutions (Figure 19). The potential difference between the compartments was measured using double junction Ag/AgCl reference electrodes. The reference electrode offset was subtracted from the measured potential to give the membrane potential, E_m. Under ideal conditions where all of the transport parameters of the ionic species are known, the membrane potential can be converted into a permselectivity value between 0 (perfectly non-selective) and 1 (perfectly selective). This report presents the "apparent permselectivity" due to some assumptions that had to be made concerning the properties of carbamate and other minor species in solution (Geise, Cassady et al., 2014).

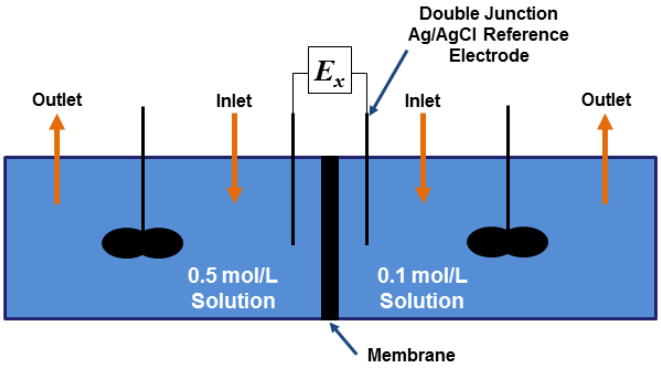

Figure 19. Cell setup for membrane potential measurements between 0.5 M and 0.1 M solutions.

Figure 20 shows that the apparent permselectivity of Selemion CMV and PCCell PC-SK membranes (commercial CEMs) declined in AmB compared to sodium chloride. In examining the apparent permselectivity of the other salts, both the ammonium cation and the bicarbonate anion decrease the apparent permselectivity of the CEMs. This is hypothesized to result from the charge density and polarizability of these monovalent ions that influence their exclusion (permselectivity) from the membrane. These ion-specific effects have been detailed in a published journal paper (Geise, Cassady et al., 2014). The data in Figure 20 show that values reported for commercial membranes in NaCl do not accurately reflect the values obtained in AmB. This decrease in permselectivity (and corresponding membrane potential) in AmB compared to sodium chloride will lower the obtained stack voltage in an AmB-based system. These experiments highlight the need to measure the permselectivity of the electrolytes of interest for the given process.

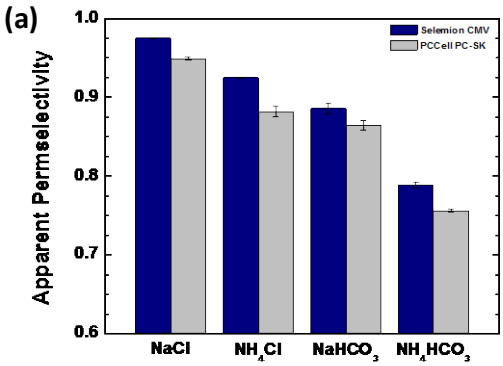

(b)

Selemion CMV

	Na^+	NH_4^+
Cl^-	0.975 ± 0.001	0.925 ± 0.001
HCO_3^-	0.886 ± 0.007	0.789 ± 0.004

PCCell PC-SK

	Na^+	NH_4^+
Cl^-	0.949 ± 0.002	0.882 ± 0.007
HCO_3^-	0.864 ± 0.006	0.756 ± 0.002

Figure 20. (a) Apparent permselectivity and (b) ion-specific effects using different salts for Selemion CMV and PCCell PC-SK membranes.

In the case of CEMs, the apparent permselectivity could be reasonably estimated because all ion solution parameters of the cations (the permselective transport species in CEMs) were known. However, for AEMs, the AmB speciation drastically influenced the calculation of the theoretical membrane potential and thus the apparent permselectivity. The carbamate anion was problematic in this case, since the dilute solution mobility of this species is not known. Figure

21 compares the permselectivity and membrane potential for Selemion AMV and PCCell AEM for the different anion/cations pairs. For NaCl and NH_4Cl, the permselectivity could be computed directly. However, for $NaHCO_3$ and AmB, only the membrane potentials are shown.

(a) Selemion AMV

	Na^+	NH_4^+
Cl^-	**0.908** ± 0.001	**0.96** ± 0.03
HCO_3^-	**33.8** ± 0.1 mV	**35.6** ± 0.3 mV

(b) PCCell AEM

	Na^+	NH_4^+
Cl^-	**0.82** ± 0.04	**0.89** ± 0.03
HCO_3^-	**28.4** ± 3.2 mV	**25** ± 3 mV

Figure 21. Apparent permselectivity and membrane potential values as a function of anion/cation salt pair for (a) Selemion AMV and (b) PCCell AEM.

The data in Figure 21 show that the permselectivity and membrane potential values for AEMs are on par with the CEMs measurements for the different salt pairs. Thus, while some loss in permselectivity is noted for AmB compared to sodium chloride, there is nothing catastrophic about the membrane values in AmB. This drop in permselectivity with AmB appears to be manageable in the stack.

Overall, this task provided clear insight into the differences between Is in NaCl and AmB, which is important for setting a baseline for future membrane development. Due to the short (9-month) duration of the membrane tasks, no novel materials were developed – but new groundwork has been laid for characterizing IEMs in unconventional salts. These types of insights will be useful for a variety of water treatment and energy recovery processes in the future.

f. Reverse Electrodialysis Computational Model

The RED stack, a critical component of the MHRFC/MHREC process, makes use of the concentration gradient between the HC and LC streams of the chosen electrolytic fluid (AmB) to generate electricity that powers the MFC/MEC components of the MHRFC/MHREC. The RED stack is composed of a stack of cell pairs of AEMs and CEMs. Between each membrane pair are fluid chambers supported with polymeric woven spacers.

Ionic transport (diffusion, convective flow, polarization) through the HC fluid chamber, AEMs, LC fluid chambers, and CEMs are the key parameters of concern at the cell pair level. At stack level, the key parameters include external electrical load, pumping pressure loss, and output power density optimization. Therefore, to better capture the complicated process at both levels, a multi-scale modeling approach has been adopted which 1) incorporates cell pair-level physics and stack-level behavior, and 2) can be integrated with operational components at other process levels. Once calibrated with experimental results, the model can be used to optimize the RED cell/stack design. In the future, this model will work with other units at the system level to optimize the overall process.

Experimental efforts proceeded to simultaneously provide calibration data for modeling efforts and optimize cell operation in a small scope. Because no regeneration system was in place for AmB, almost all lab work on the RED subsystem used sodium chloride (NaCl) as the

electrolyte. Therefore, the computational model was designed to account for such material differences by adjusting the corresponding fluid and membrane properties.

Model development

gPROMS®, an advanced mathematical software package, was used for cell pair and stack-level modeling. Information from previous studies by Veerman et al. (2011) and Tedesco et al. (2012, 2014) was used to set up the cell pair model. Details of the model development parameters are found in Appendix C.

A one-dimensional spatial distribution model was set up which discretized data along the cell length. Due to the salt mass transfer from the HC to LC chamber (and, to a lesser extent, water mass transfer from the LC to HC chamber), salt concentration varied along the cell length. While many material and membrane properties are highly concentration-dependent, it is important to consider the spatial distribution. AmB contains many species (NH_4^+, HCO_3^-, $NH_2CO_2^-$, CO_3^{2-}, OH^-, NH_3 etc) and is a more complicated solution than NaCl. At the concept stage, it was assumed that AmB dissociates to only NH_4^+ and HCO_3^- ions, since they made up most of the cations and >80% of the anions at equilibrium.

Cell pair model

Figure 22 shows a schematic drawing of a cell pair model. Each cell pair has a high-concentration chamber and a low-concentration chamber where HC and LC fluids flow concurrently. Chambers are separated by IEMs which selectively pass either anions (AEMs) or cations (CEMs). Permselectivity (α_{AEM} and α_{CEM} respectively) is an important membrane property reflecting such ionic selectivity. Estimated values of 0.8 and 0.8 were applied and are subject to further validation.

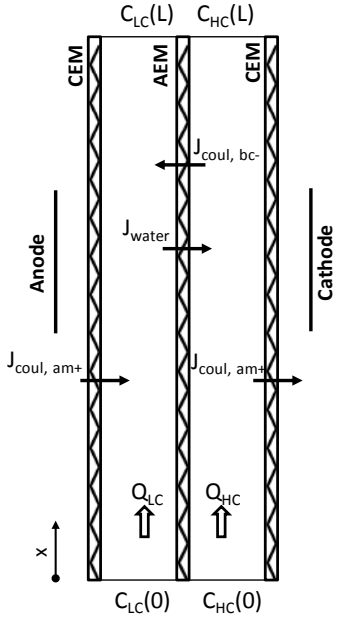

Figure 22. Schematic of cell pair model.

Mass balance within the HC and LC chambers gives the following:

$$\frac{dC_{HC}(x)}{dx} = -\frac{w}{Q_{HC}} J_{tot} + C_{HC}(x)\frac{w}{Q_{HC}} J'_{water} \quad [3]$$

$$\frac{dC_{LC}(x)}{dx} = \frac{w}{Q_{LC}} J_{tot} - C_{LC}(x)\frac{w}{Q_{LC}} J'_{water} \quad [4]$$

where C_{HC} and C_{LC} are concentrations of the corresponding chamber, w is the cell width, and x is a spatial variable along the cell length. Overall cell length is L. Q_{HC} and Q_{LC} are the volumetric feeding rates to the corresponding chamber (in unit of m^3/s). Under a concentration gradient, ions transfer through the appropriate IEM from the HC chamber to the LC chamber. J_{tot} is the total salt flux, which includes both co-ion and counter-ion flux (Equation 5). Co-ions carry the same charge as the IEM fixed charge; counter-ions carry the opposite charge. Therefore, counter-ion flow is the designed flow generating electricity, while co-ion flow also occurs since real membrane permselectivity is less than the ideal value of 1.0. Net counter-ion flux relates directly to the current density, as shown in the first term on the right side of Equation 5. Co-ions, bonded with the corresponding counter-ions, diffuse through IEMs without generating net current flow. The contribution of this flow is shown in the second term of Equation 5, where D_{AmB} is the diffusivity coefficient of AmB molecules through IEMs. There are two membranes per cell pair, and δ_m is the membrane thickness. Because AEMs and CEMs have the same thickness, they are combined with a factor of two in the second term of Equation 5.

$$J_{tot} = \frac{j(x)}{F} + 2\frac{D_{AmB}}{\delta_m}[C_{HC}(x) - C_{LC}(x)] \quad [5]$$

Besides ion transport, water molecules move from the LC to the HC chamber under electro-osmotic forces, in the opposite direction of electrolytic ions transport. This is J'_{water} in Equations 3 and 4, which also affects the salt concentration in each chamber along the flow direction. J'_{water} is defined as follows:

$$J'_{water} = -2RT\frac{P^H_{water}}{\delta_m}\left[C_{HC}(x) - C_{LC}(x)\right] \quad [6]$$

where P^H_{water} is the osmotic water permeability through IEMs. It should be noted that both D_{AmB} and P^H_{water} are also concentration-dependent. As a starting point, the modeling uses constant values, based on lab testing data of NaCl solutions conducted at Penn State. These values were derived assuming certain scalability between NaCl and AmB solutions. Parameter sensitivity is going to be evaluated; a more accurate parameter model may be required if sensitivity to these parameters is high.

Cell pair open circuit voltage follows the Nerst equation:

$$OCV_{cell}(x) = (\alpha_{CEM} + \alpha_{AEM})\frac{RT}{F}\ln(\frac{\gamma(C_{HC})C_{HC}(x)}{\gamma(C_{LC})C_{LC}(x)}) \quad [7]$$

where γ is the activity coefficient of the electrolyte. Due to the wide concentration range, activity coefficient was modeled using OLI data. The following is the regressed model for the AmB solution activity coefficient:

$$\log_{10}\gamma(C) = 1/(-\frac{2.0942}{\sqrt{C}} - 1.3976) \quad [8]$$

Cell pair electrical resistance is a summation of four components (HC chamber, AEM, LC chamber, CEM) connected in series:

$$\begin{aligned} R_{cell}(x) &= R_{HC} + R_{LC} + R_{AEM} + R_{CEM} \\ &= f\frac{\delta_{HC}}{\Lambda_{HC}(C)C_{HC}(x)} + f\frac{\delta_{LC}}{\Lambda_{LC}(C)C_{LC}(x)} + R_{AEM}(C(x)) + R_{CEM}(C(x)) \end{aligned} \quad [9]$$

The HC and LC chambers, which are open, are filled with a woven spacer. δ_{HC} and δ_{LC} are chamber thicknesses. *f* is a factor representing the extra resistance from the spacer due to its effects of shadowing the membrane and detouring its flow path. Λ is the electrical conductivity of the electrolyte solution. OLI data were used again to produce the following regressed model for AmB conductivity:

$$\begin{cases} \Lambda(C) = 10.52\text{C(x)}\text{\^{}}2 - 4.959\text{C(x)}\text{\^{}}1.5 + 0.8786\text{C(x)} - 0.07429\text{C(x)}\text{\^{}}0.5 + 0.01202 \\ \quad (when\ C(x) < 0.15 mol/m^3) \\ \Lambda(C) = 8.18e^{-4}\text{C(x)} - 3.137\text{e}^{-3}\text{C(x)}\text{\^{}}0.5 + 9.634\text{e}^{-3}\ (otherwise) \end{cases} \quad [10]$$

Membrane resistance is concentration-dependent. Penn State conducted tests on AmB solutions and PCcell membranes over a concentration range of 0.01~1 mol/m^3. Equation 11 shows the regressed correlations for AEMs and CEMs:

$$\begin{aligned} R_{AEM}(C) &= 9.0805C^{-0.409} \\ R_{CEM}(C) &= 3.5758C^{-0.562} \end{aligned} \quad [11]$$

Since inside each cell pair, IEMs contacts different concentrations of AmB solutions, Each Equation 11 is averaged over the range from C_{HC} to C_{LC} to give:

$$\begin{aligned} R_{AEM}(C) &= \frac{9.0805\left(C_{HC}^{(1-0.409)} - C_{LC}^{(1-0.409)}\right)}{(1-0.409)(C_{HC} - C_{LC})} \\ R_{CEM}(C) &= \frac{3.5758\left(C_{HC}^{(1-0.562)} - C_{LC}^{(1-0.562)}\right)}{(1-0.562)(C_{HC} - C_{LC})} \end{aligned} \quad [12]$$

Cell pair electrical resistance can be obtained by substituting Equations 8, 10, and 12 into Equation 9.

Stack modeling

A cell stack is made up of many cell pairs in series with electrode chambers at two ends. Therefore, open circuit voltage and resistance at stack level can be defined as:

$$OCV_{stack}(x) = \sum_{i=1}^{N} OCV_{cell}(x) \quad [13]$$

$$R_{stack}(x) = \sum_{i=1}^{N} R_{cell}(x) + R_{electrodes} \quad [14]$$

Current density is thus:

$$j(x) = \frac{OCV_{stack}(x)}{R_{stack}(x) + R_{external}} \quad [15]$$

Because cell pairs are connected in series, the current density connects the cell pair-level modeling with the stack-level modeling. Current efforts at Air Products are focusing on a stack with a small number of cell pairs. With this type of stack, it can be assumed that Q_{HC} and Q_{LC} at the cell pair level is an even fraction of the total feeding rates. However, in future scaled-up stacks with a larger number of cell pairs (e.g. >50 per stack), there would be a biased flow rate distribution across different cell pairs. That will require some adjustments on Q_{HC} and Q_{LC} settings.

A critical parameter in RED stack evaluation is power density, which is the power output per membrane area (in W/m^2). This is particularly important given that membrane cost is a major capital cost in RED stack construction. Power density is defined by:

$$P_d(x) = j(x)^2 R_{external} / (2N+1) \quad [16]$$

where N is the number of cell pairs per stack. The total number of membranes is 2N+1. To maximize power density, substitute Equation 15 into Equation 16 and do the derivative over $R_{external}$ [note that maximum power density occurs at $R_{external} = R_{stack}$ (x)]. The fact that R_{stack} varies over the cell length suggests that segmenting the electrodes can improve the power density. In fact, some researchers have already investigated this concept (Veerman thesis, 2010).

Another important parameter is the net power output. The cost for pumping solutions through the stack is represented by the pumping pressure drop P_{pump}. Net power P_{net}, as the name suggests, is the total electrical power output minus P_{pump}. In smaller stacks, pumping loss is mainly from HC and LC chambers and is relatively small. Manifold pressure loss becomes significant for bigger stacks with higher feeding rates.

Model summary

Input variables:

- Inlet concentration: $C_{LC}(0)$, $C_{HC}(0)$
- Inlet flow rate: Q_{LC}, Q_{HC}
- External resistance: $R_{external}$

Parameters:

- Membrane
  - Permselectivity: α_{AEM}, α_{CEM}
  - Membrane thickness: δ_{AEM}, δ_{CEM}
  - Salt diffusion constant: D_{AmBC}
  - Water osmotic permeability: P^{H}_{water}
  - Area resistance: $R_{AEM}(C)$, $R_{CEM}(C)$
- Cell
  - Compartment thickness: δ_{LC}, δ_{HC}
  - Spacer obstruction factor: f
  - Cell length: L
  - Cell width: w
- HC, LC fluids
  - Activity coefficients: $\gamma(C)$
  - Conductivity: $\Lambda(C)$

Output variables:

- Spatial dependent values
  - Concentrations: $C_{LC}(x)$, $C_{HC}(x)$
  - Stack resistance R(x)
  - current, voltage, power density: i (x), E(x), P(x)
- Single values
  - Concentrations: $C_{LC}(L)$, $C_{HC}(L)$
  - Mean current, voltage: i, E
  - Max power density: P_d

Software interface:

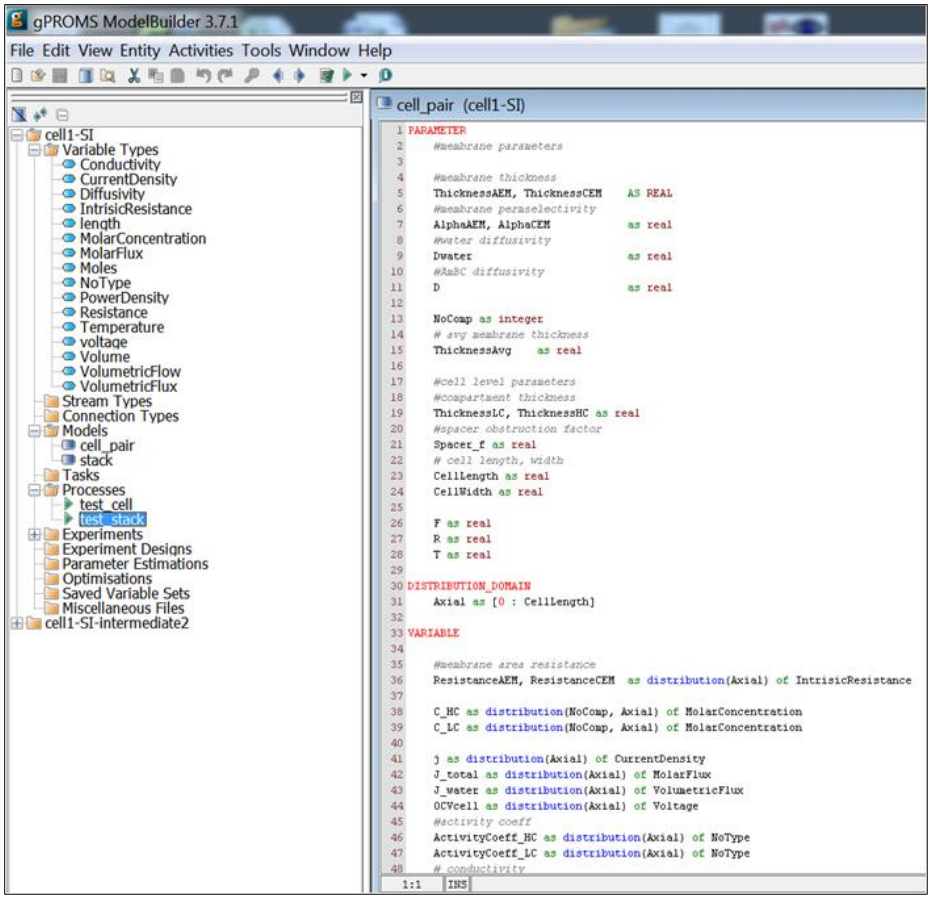

Example of model output with some input parameters typically used at Penn State:

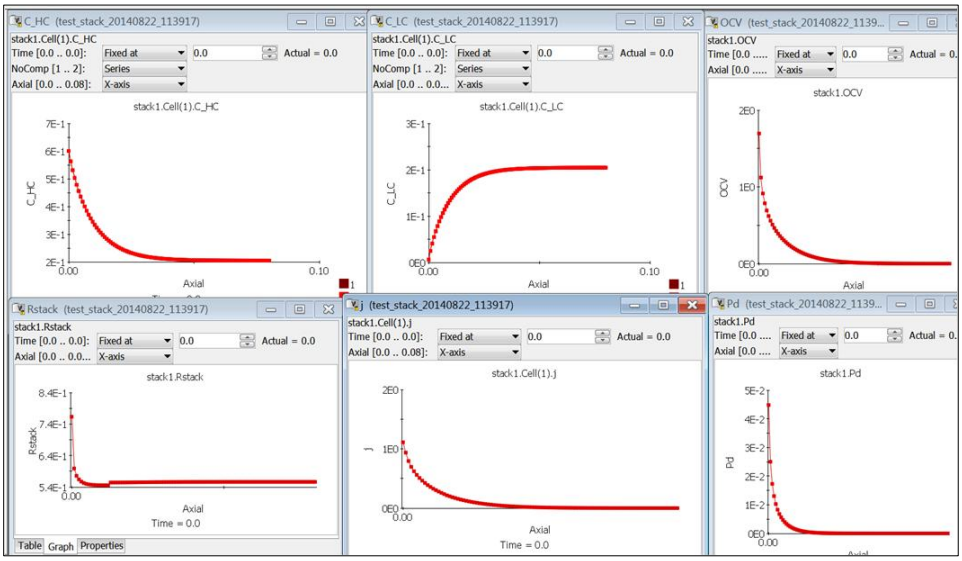

Parameter estimation

Before the model developed here can be used quantitatively, some model parameters need to be estimated using experimental data from Penn State, and a sensitivity study must be conducted on parameters D_{AmB} and P^{H}_{Water}. Spacer effect f can be obtained through parameter estimation. Two additional parameters which can benefit from parameter estimation are explained below.

In a RED cell, boundary layers form on the interfaces with each IEM. There is diffusion (vs. convective) flow through these layers in the bulk flow chamber, which creates a concentration gradient across a boundary layer. This means that the electrolyte concentration at the membrane interface is different from the bulk concentration. On the HC chamber side, membrane interfacial concentration is lower than the HC bulk concentration. On the LC chamber side, membrane interfacial concentration is higher than the LC bulk concentration. This is a polarization effect, which makes the cell open circuit voltage (OCV) smaller:

$$
\begin{aligned}
OCV_{cell}(x) &= P_1(\alpha_{CEM}+\alpha_{AEM})\frac{RT}{F}\ln\left(\frac{\gamma^{\text{int}}(C^{\text{int}}_{HC})C^{\text{int}}_{HC}(x)}{\gamma^{\text{int}}(C^{\text{int}}_{LC})C^{\text{int}}_{LC}(x)}\right) \\
&\approx P_1(\alpha_{CEM}+\alpha_{AEM})\frac{RT}{F}\ln\left(\frac{\gamma(C_{HC})C_{HC}(x)}{\gamma(C_{LC}+dC_{LC})(C_{LC}(x)+dC_{LC}(x))}\right) \\
&\approx P_1(\alpha_{CEM}+\alpha_{AEM})\frac{RT}{F}\ln\left(\frac{\gamma(C_{HC})C_{HC}(x)}{\gamma(C_{LC})C_{LC}(x)}\times P_2\right)
\end{aligned}
\qquad [17]
$$

This polarization effect has been found to be very small on the HC chamber side (Tedesco et al, 2014), which allows the correlation to be simplified – modeling parameter P_2 was introduced

to represent the polarization effect. Another modeling parameter, P_1, was also added to account for any permselectivity inaccuracy.

g. Process Economic Analysis

The experimental work and process model development performed under this project, as well as published prior art related to reverse electrodialysis and microbial fuel cells, provide a useful database of process parameters for the development of a detailed process economic evaluation. However, because there is not yet scale-up, first-time engineering or industrial operating experience with this technology, considerable uncertainty still exists. Principal areas of uncertainty include:

- Extent of future fundamental performance improvement
- Extent of future engineering cost optimization
- Performance changes with system scale-up
- Plant capacity factor, operating labor and maintenance costs
- Large-scale manufactured cost of ion exchange membranes
- Site-specific cost factors – utilities, infrastructure, land use

To create a meaningful analysis of the commercial viability of this technology amidst uncertainty, a detailed stochastic sensitivity analysis was created. Despite the uncertainty, sufficient data and subject matter expertise are available to quantify a probabilistic distribution for all key parameters. These were compiled to perform a Monte Carlo simulation using the Oracle® Crystal Ball add-in for Microsoft® Excel.

Table 1. Sensitivity variables for stochastic process economic analysis.

Parameter	**Costs and Financial Parameters**
cell and power system	membrane cost
power density, gross, per total membrane area	heat exchanger cost
cell efficiency, RED cell electric/actual Δsalinity	BOP cost factor - cell stack and power/membrane
HC concentration	installation factor - cell stack and power
LC concentration	BOP cost factor - regen system/exchanger
thermolyte extent of mixing	installation factor - regen system
cell pressure drop	capacity factor
efficiency, net AC/gross DC electricity conversion	maintenance cost factor
power contribution from WW oxidation	operating labor
efficiency, DCOD produced energy/ theoretical total energy	electricity price
energy produced per DCOD	WWT chemical and sludge disposal cost avoidance
aeration energy consumption avoidance per DCOD	plant lifetime
WHR and Thermolyte Regeneration System	
regen efficiency, Δsalinity/WH	
regen exchanger Uo	
regen loop pressure drop	

This model was applied to define probability distributions for various financial metrics: internal rate of return (IRR), net present value (NPV), payback period, overnight capital cost and levelized cost of energy (LCOE). Representative results for NPV at a 20% hurdle are depicted in Figure 23. The probability profile indicates a predicted median value of $-250,000 NPV. There is only 10% probability that the NPV will be positive. A comparable probability distribution was determined for the levelized cost of energy based on power output from the system, as shown in Figure 24. The predicted median LCOE is $0.61/kWh. There is only a 4% probability that a LCOE of less $0.16/kWh may be attained.

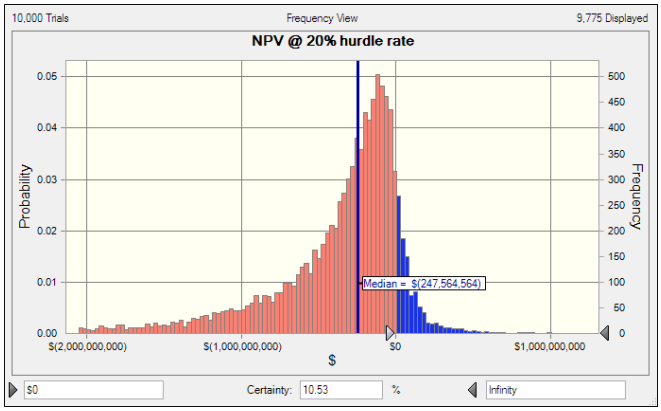

Figure 23. Probabilistic result distribution for net present value at a 20% hurdle rate.

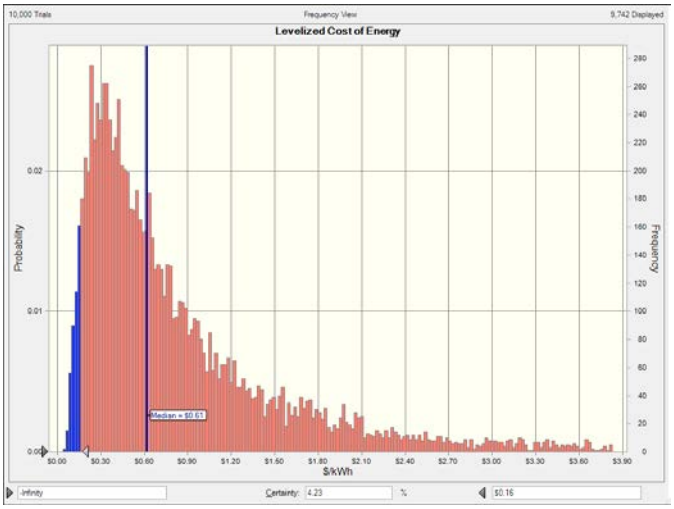

Figure 24. Probabilistic result distribution for levelized cost of energy.

These results are indicative of other financial results that indicate a low probability of financial attractiveness and, therefore, commercial viability. The predominant factors that would require significant improvement are those which relate to membrane, notably power density and membrane unit area cost. At favorable limits of other factors, membrane cost would need to be about $8 per m^2 or less to produce attractive financial results. This is greater than an order of magnitude lower than current cost for high-performance ion exchange membranes.

5. Benefits Assessment

As part of the program, Air Products conducted analyses in an attempt to quantify the potential energy, economic, environmental and market benefits for the U.S. manufacturing industry. Based on the assumptions outlined below, Air Products believes implementing this technology could potentially provide the following benefits:

- Yield on total COD basis adjusted from 34% to 29% based on treatability tests.
- 2.75x factor of surplus power or hydrogen from improved RED ion transfer performance (assumptions: 50% approach to thermolyte equilibrium, 50% efficiency; 0.14 kWh/m3 thermolyte parasitic pump energy requirement).
- Net effect = 235% increase in potential hydrogen or energy output.
- Net increase in U.S. energy savings of ~ $800+ million per year.

The implementation of MHRC has enormous potential to greatly increase energy efficiency and convert waste to energy or useful products. The combination of these effects, along with byproduct credits, could result in substantially lower manufacturing costs across a broad array of U.S. industry segments. There are approximately 3,000 U.S. manufacturing facilities in the chemical, food, pharmaceutical and refinery market segments for which MHRC technology can be considered based on wastewater COD content and availability of low-grade waste heat sources. Assuming 15% of these facilities are amenable to MHRFC technology for electric output and 95% average system availability, the U.S. electric power production from these facilities will be 25.4 billion kWh per year, which is more than 2% of industrial electricity use. MHRC would provide distributed generation of electricity at manufacturing facilities with end-user demand, thereby easing grid congestion, deferring transmission line investment, and aiding grid stability. Alternatively, these facilities could operate MHREC to produce 183,000 metric tons per year of H_2 for internal processes or as a transport fuel. This H_2 has an equivalent energy value of 22.4 TBtus per year. Although MHREC provides a lower equivalent energy output than MHRFC, H_2 is a high-value product which will be profitable for facilities that require in-situ H_2 for processing or can make use of H_2 as a transport fuel, e.g. for forklift operation. It must be noted that the H_2 produced from an MHRC would require clean up (to remove water) and compression to be used as a transportation fuel or in other industrial processes. These processes require additional energy and process steps which will add costs to the overall process.

The MHRC process uses waste biomass and waste heat for energy input and therefore does not produce any net carbon dioxide emissions. MHRFC or MHREC provides substantial offsets by avoided carbon dioxide emissions from electric power or H_2 production, respectively. The reduction in U.S. carbon dioxide emissions associated with MHRFC electric power production could be 6.4 million metric tons per year. The reduction in U.S. carbon dioxide emissions associated with MHREC H_2 production could be greater than 2,000,000 metric tons per year relative to pipeline supply H_2. Greater reduction is realized relative to delivered liquid or compressed H_2. Since MHRC is a biologically catalyzed, low-temperature process, little to no

SO_x or NO_x emissions are produced. There are accompanying benefits of >70% COD removal from wastewater, substantially mitigating wastewater treatment requirements in the form of capital and operating cost reduction and providing a 60% reduction in sludge disposal volume over the incumbent technologies.

A representative manufacturing facility (average basis EPA Permit Compliance Database, see Table 2) that employs MHRC could realize an operating cost savings of greater than $4 million/year from electric power production or $4.3 million/year from H_2 production. The total benefit to U.S. manufacturing, assuming 15% amenability in the target segments, is greater than $1.8 billion per year.

Table 2. MHRC energy, environmental and economic benefit for U.S. manufacturing.

	Chemical	Food	Pharma	Pulp & Paper	Refinery	TOTAL
No of plants in PCS Database[1]	1022	1366	76	249	241	**2954**
Average Wastewater Flow, MGD (permit limit)[1]	4.35	1.74	3.05	11.41	6.84	**27.38**
Typical COD level per segment (ppm)	1000	2500	3500	250	350	
Facility average Wastewater Flow (MGD)[2]	3.26	1.30	2.29	8.55	5.13	
Facility average COD (metric tons/d)	12.3	12.3	30.2	8.1	6.8	
U.S.total Wastewater Flow (MGD)	3335	1778	174	2130	1237	**8654**
U.S.total COD (metric tons/d)	12599	16798	2298	2012	1635	**35342**
MHRFC for Power Production						
Facility average power production potential (MW)[3,4]	7.1	7.1	17.4	4.6	3.9	
U.S. total power production potential (MW)[5]	1086	1448	198	173	141	**3046**
U.S. total power production potential (billion kWh/y)[6]	9.0	12.0	1.6	1.4	1.2	**25.4**
U.S. total power production potential (Tbtu/y)[4]	30.8	41.1	5.6	4.9	4.0	**86.5**
CO_2 reduction (metric tons per year)[7]	5,605,345	8,237,943	1,127,177	986,616	801,902	**16,758,983**
Value $ Billions per year[8]	0.646	0.861	0.118	0.103	0.084	**1.812**
MHREC for Hydrogen Manufacture						
Facility average H_2 production potential (metric tons/d)[9]	1.2	1.2	3.0	0.8	0.7	
U.S.total H_2 production potential (metric tons/d)[4]	188	251	34	30	24	**528**
U.S. total H_2 production potential (metric tons/y)	65325	87096	11917	10431	8478	**183247**
U.S. total H_2 production potential (Tbtu/y)[4,10]	8.0	10.6	1.5	1.3	1.0	**22.4**
CO_2 reduction (metric tons per year)[11]	776585	1035394	141670	124004	100788	**2178440**
Value $ Billions per year[12]	0.688	0.917	0.125	0.110	0.089	**1.929**

[1] EPA Permit Compliance System (PCS) Database, www.epa.gov/enviro/facts/pcs
[2] Assumption: actual wastewater flow at 75% of permit limit
[3] **29%** power yield and **2.75** waste heat amplification factor **based on RED improvement target**
[4] Assumption: 80% efficiency for DC-to-AC power conversion
[5] Assumption: 15% of facilities in these segments are amenable for MHRC technology
[6] Assumption: continuous operation with 95% availability. Air Products' own-operate onstream rates for other systems are often >99% availability
[7] Equiv CO_2 impact = 1.299 lb CO_2/kWh with U.S. electricity grid mix; SOURCE: EPA eGRID2010 Version 1.1 Year 2007 Summary Tables (May 2011).
[8] 2010 average industrial electricity price = $0.0679/kWh; SOURCE: U.S. EIA Nov 2011 Monthly Energy Review
[9] **29%** hydrogen yield and **2.75** waste heat amplification factor **based on RED improvement target**
[10] Assumption: apply hydrogen higher heating value @ 61000 btu/lb
[11] Equiv CO_2 impact = 11.888 kg CO_2/kg H_2; SOURCE: Spath, P. L. and Mann, M. K., Life Cycle Assessment of Hydrogen Production via Natural Gas Steam Reforming, NREL Technical Report 570-27637, Revised Feb 2001.
[12] Assumption: hydrogen pricing @ $5 per lb delivered.

Table 3. Summary of energy, environmental and economic benefit.

MHRFC for Power Production		
Initial commercialization year		2017
Market penetration by 2020	% of amenable market	2%
2020 U.S. Energy Savings	Tbtus/y	11.5
2020 U.S. Reduction in CO_2 Emissions	Mlb/y	1117
2020 U.S. Economic Benefit	$B/y	0.06
Full market penetration	% of amenable market	15%
Full U.S. Energy Savings	Tbtus/y	86.5
Full U.S. Reduction in CO_2 Emissions	Mlb/y	33518
Full U.S. Economic Benefit	$B/y	1.8
MHREC for Hydrogen Manufacture		
Initial commercialization year		2018
Market penetration by 2020	% of amenable market	0.5%
2020 U.S. Energy Savings	Tbtus/y	0.7
2020 U.S. Reduction in CO_2 Emissions	Mlb/y	145
2020 U.S. Economic Benefit	$B/y	0.064
Full market penetration	% of amenable market	15%
Full U.S. Energy Savings (basis: H_2 HHV)	Tbtus/y	22.4
Full U.S. Reduction in CO_2 Emissions	Mlb/y	4357
Full U.S. Economic Benefit	$B/y	1.93

6. Commercialization

Because a No Go decision was made at the end of Budget Period 2, there were no specific efforts made with regard to commercialization. The economic analysis presented above shows that prior to any first-time commercialization efforts, improvements would be needed in membrane cost per unit area and efficiency of the MHRC. Given the background work completed for the economic analysis, it should prove straightforward to determine the improvements necessary for moving this technology forward. Significant factors to address in any commercialization are the first-time engineering and construction costs, which will provide additional barriers to bringing this technology to market.

7. Accomplishments

Many significant technical accomplishments were achieved over the course of this research effort. The team demonstrated the overall viability of this approach to combine three technologies – microbial fuel cells, reverse electrodialysis and recovery of waste heat – into a process that can produce either electricity or H_2 and provide wastewater treatment. The study of low-grade waste heat and wastewater composition at many manufacturing sites across the U.S. could provide the basis for additional studies at other industrial manufacturing sites, which might enable creation of a database of low-grade waste heat and treatable streams amenable for further study. The methodology used to produce this data could be used as part of this additional study.

This program provided the opportunity to demonstrate the viability of MEC at several different scales using real-world samples of industrial waste streams. This comparison allowed the team to focus on certain classes of manufacturing sites that would have sufficient waste heat and effluent streams with significant amounts of COD. During the course of the investigation, it became known that improvements in MFC efficiency were needed. This study provided an understanding of the opportunity to make such improvements.

Significant progress was made in modeling various parts of the combined system from both economic and process perspectives. An important outcome of the economic modeling was the realization that significant improvements were needed in power density and membrane unit area cost. This outcome provides important direction for areas of additional study to make this technology both viable and cost-effective in the future. Excellent opportunities exist to better understand the behavior of commercial ion exchange membranes with ammonium bicarbonate systems.

8. Conclusions

This project successfully demonstrated that waste heat and organics in wastewater can be converted to useful energy or products and elucidated opportunities to improve the various components that were brought together in this multifaceted program. A survey of available low-grade waste heat and effluents was completed at a sampling of Air Products manufacturing plants in the United States. This low-grade waste heat can be an important heat source for thermal regeneration of the organic Rankine cycle. This inventory provides the basis for further study of a broader sector of U.S. chemical (or other) manufacturers to survey low-grade waste heat available across the industry.

Wastewater effluent samples collected from these manufacturing plants were pre-screened for suitable high chemical oxygen demand (COD) and low-grade waste heat. A select portion of these effluent samples was tested by project partner Penn State for treatability. Results from these tests suggest that a number of the streams provided sufficient COD to be used in microbial fuel cells for energy or hydrogen production. Based on the initial and secondary treatment assessment, there are multiple effluent sources at Site B that show potential for treatment in MECs or similar bio-electrochemical systems. Of the three samples tested in cube MECs, B4 showed the greatest hydrogen production but also had long cycles times and required dilution and neutralization prior to treatment. Sample B3 also showed reasonable hydrogen production, but also had a significant concentration of methane present in the recovered gas. This could be alleviated with a separate anode and cathode chamber, but methane production may persist at the anode if methanol is present. This was also observed with sample B5, but it did not require neutralization.

Detailed studies were conducted regarding potential integration of the MRC, RED and thermal regeneration processes. Regarding the Reverse Electrodialysis Cell Experimental Analyses, it was demonstrated that under the optimum flow rates (HC 10 mL/min and LC 20 mL/min) and concentrations (HC 3.6 M NaCl, 221 mS/cm and LC 0.14 M NaCl, 14 mS/cm), the open-circuit voltage of the RED stack was 1.08 V, the maximum current was 302 mA, and

the maximum power density was 0.62 W/m^2-membrane. The pressure drop was 0.3 psi and the hydrodynamic loss 1 mW. Improvement of RED stack performance would require enhanced properties of the IEMs.

A basic process model was developed to allow global optimization of the three basic process modules: Microbial Fuel Cell, Reverse Electrodialysis (RED), and Thermal Regeneration/Waste Heat Recovery. Air Products also built economic models for the overall process, and an economic viability analysis was performed using the data obtained from the Penn State laboratory studies. Additionally, a financial analysis was developed to understand the sensitivities around the various components of the overall system. Through this study, it was determined that there was a low probability of achieving the desired power and cost targets based on the current state of development and integration of these technologies.

One key lesson learned was that the project structure provided an effective mechanism to use learnings from each stage as the basis for the next steps. This multi-gated structure provided an excellent basis for a decision to terminate the program early due to understanding both the technical accomplishments and needs as well as the financial considerations. Stopping the project at this stage avoided significant expenses that were planned at the outset of the project (scale-up activities and a large demonstration unit) without full understanding of the achievable outputs of the technology. In addition, there was enough flexibility in the program team and DOE support to focus on improvements in ion exchange membrane properties, an unanticipated critical path area required for this development effort. Modifying the scope of work enabled further exploration of this area, which was determined to be both a limiting factor for commercial success and also a significant area of research for further development of this technology.

9. Recommendations

Based on the technical results to date and the information from the economic assessment using a detailed stochastic sensitivity analysis, in collaboration with the DOE the decision was made to suspend the project at the end of Budget Period 2. This program successfully demonstrated the initial expectations of technical viability for the integrated MHRC system. The combination of technologies demonstrated that the MHRC can recover and convert low-grade waste heat (<150°C) to electrical energy or hydrogen. This finding could be particularly useful for application in areas where power is costly and low-grade waste heat and appropriate waste streams are available.

Developments in reverse electrodialysis (RED) should be followed, especially the REAPower pilot project. These developments could show sufficient progress to prompt a reevaluation of the techno-economic analyses outlined in this work. The other area for potential study relates to advances in large-scale manufacture of low-cost ion exchange membrane material, which could enable technologies such as RED. Should significant advances in this area be achieved, the economics for the overall process could improve the probability of commercial viability of this combination of technologies. Commercial viability could certainly be enhanced through improvements in the power density of microbial fuel cells.

10. Literature Cited – Background & Introduction

1. Logan, B. E. *Microbial fuel cells*. (John Wiley & Sons, Inc., 2008).
2. Logan, B. E. & Regan, J. M. Microbial fuel cells—challenges and applications. *Environ. Sci. Technol.* **40**, 5172-5180.
3. Liu, H., Ramnarayanan, R. & Logan, B. E. Production of electricity during wastewater treatment using a single chamber microbial fuel cell. *Environ. Sci. Technol.* **38**, 2281-2285.
4. Logan, B. E. Extracting hydrogen and electricity from renewable resources. *Environ. Sci. Technol.* **38**, 160A-167A.
5. Logan, B. E. *et al.* Microbial fuel cells: methodology and technology. *Environ. Sci. Technol.* **40**, 5181-5192.
6. Cheng, S., Liu, H. & Logan, B. E. Power densities using different cathode catalysts (Pt and CoTMPP) and polymer binders (Nafion and PTFE) in single chamber microbial fuel cells. *Environ. Sci. Technol.* **40**, 364-369.
7. Zhao, F. *et al.* Application of pyrolysed iron (II) phthalocyanine and CoTMPP based oxygen reduction catalysts as cathode materials in microbial fuel cells. *Electrochem. Commun.* **7**, 1405-1410.
8. Logan, B. E. in *Bioelectrochemical systems: from extracellular electron transfer to biotechnological applications* eds K. Rabaey, L. Angenent, U. Schröder, & Jürg Keller) Ch. 9, 184-204 (IWA Publishing, 2010).
9. Logan, B. E., Cheng, S., Watson, V. & Estadt, G. Graphite fiber brush anodes for increased power production in air-cathode microbial fuel cells. *Environ. Sci. Technol.* **41**, 3341-3346.
10. Xie, X. *et al.* Three-dimensional carbon nanotube−textile anode for high-performance microbial fuel cells. *Nano Letters* **11**, 291-296.
11. Saito, T. *et al.* Effect of nitrogen addition on the performance of microbial fuel cell anodes. *Bioresour. Technol.* **102**, 395-398.
12. Zhu, N. *et al.* Improved performance of membrane free single-chamber air-cathode microbial fuel cells with nitric acid and ethylenediamine surface modified activated carbon fiber felt anodes. *Bioresour. Technol.* **102**, 422-426.
13. Fan, Y. *et al.* Nanoparticle decorated anodes for enhanced current generation in microbial electrochemical cells. *Biosensors and Bioelectronics* **26**, 1908-1912.
14. Rozendal, R. A., Hamelers, H. V. V. & Buisman, C. J. N. Effects of membrane cation transport on pH and microbial fuel cell performance. *Environ. Sci. Technol.* **40**, 5206-5211.
15. Rozendal, R. A., Sleutels, T. H. J. A., Hamelers, H. V. M. & Buisman, C. J. N. Effect of the type of ion exchange membrane on performance, ion transport, and pH in biocatalyzed electrolysis of wastewater. *Wat. Sci. Technol.* **57**, 1757-1762.
16. Kim, J. R., Cheng, S., Oh, S.-E. & Logan, B. E. Power generation using different cation, anion and ultrafiltration membranes in microbial fuel cells. *Environ. Sci. Technol.* **41**, 1004-1009.
17. Zhang, X., Cheng, S., Wang, X., Huang, X. & Logan, B. E. Separator characteristics for increasing performance of microbial fuel cells. *Environ. Sci. Technol.* **43**, 8456-8461.
18. Zhang, X., Cheng, S., Liang, P., Huang, X. & Logan, B. E. Scalable air cathode microbial fuel cells using glass fiber separators, plastic mesh supporters, and graphite fiber brush anodes. *Bioresour. Technol.* **102**, 372-375.
19. Watson, V. J., Saito, T., Hickner, M. A. & Logan, B. E. Polymer coatings as separator layers for microbial fuel cell cathodes. *J. Power Sources* **196**, 3009-3014.
20. Liu, H., Grot, S. & Logan, B. E. Electrochemically assisted microbial production of hydrogen from acetate. *Environ. Sci. Technol.* **39**, 4317-4320.
21. Logan, B. E. *et al.* Microbial electrolysis cells for high yield hydrogen gas production from organic matter. *Environ. Sci. Technol.* **42**, 8630-8640.
22. Selembo, P. A., Merrill, M. D. & Logan, B. E. The use of stainless steel and nickel alloys as low-cost cathodes in microbial electrolysis cells. *J. Power Sources* **190**, 271-278.

23. Selembo, P. A., Merrill, M. D. & Logan, B. E. Hydrogen production with nickel powder cathode catalysts in microbial electrolysis cells. *Int. J. Hydrogen Energy* **35**, 428-437.
24. Zhang, F., Saito, T., Cheng, S., Hickner, M. A. & Logan, B. E. Microbial fuel cells cathodes constructed from stainless steel mesh that use poly(dimethylsiloxane) diffusion layers. *Environ. Sci. Technol.* **44**, 1490-1495.
25. Zhang, Y., Merrill, M. D. & Logan, B. E. The use and optimization of stainless steel mesh cathodes in microbial electrolysis cells *Int. J. Hydrogen Energy* **35**, 12020-12028.
26. Call, D. & Logan, B. E. Hydrogen production in a single chamber microbial electrolysis cell (MEC) lacking a membrane. *Environ. Sci. Technol.* **42**, 3401-3406.
27. Call, D., Merrill, M. D. & Logan, B. E. High surface area stainless steel brushes as cathodes in microbial electrolysis cells (MECs). *Environ. Sci. Technol.* **43**, 2179-2183.
28. Kim, Y. & Logan, B. E. Hydrogen production from inexhaustible supplies of fresh and salt water using microbial reverse-electrodialysis electrolysis cells. *Proc. Natl. Acad. Sci. USA*, **108**, 16176-16181.
29. Kim, Y. & Logan, B. E. Microbial reverse electrodialysis cells for synergistically enhanced power production. *Environ. Sci. Technol.*, **45**, 5834–5839.
30. Weinstein, J. N. & Leitz, F. B. Electric power from differences in salinity: The dialytic battery. *Science* **191**, 557-559.
31. Bard, A. J. & Faulkner, L. R. *Electrochemical Methods: Fundamentals and Applications*. 2nd edn, (John Wiley & Sons, 2001).
32. Cheng, S. and B.E. Logan. High hydrogen production rate of microbial electrolysis cell (MEC) with reduced electrode spacing. *Biores. Technol.* **102,** 3571–3574.
33. Fan, Y., Hu, H. and Liu, H. Enhanced Coulombic efficiency and power density of air-cathode microbial fuel cells with an improved cell configuration. *Journal of Power Sources.* **171,** 348–354.
34. Kim, Y. & Logan, B. E. Hydrogen production from inexhaustible supplies of fresh and salt water using microbial reverse-electrodialysis electrolysis cells. *Proc. Natl. Acad. Sci. USA*, **108**, 16176-16181.
35. Kim, Y. & Logan, B. E. Microbial reverse electrodialysis cells for synergistically enhanced power production. *Environ. Sci. Technol.*, **45**, 5834–5839.

11. References

Ambler, J.R., Logan, B.E., 2011. “Evaluation of stainless steel cathodes and a bicarbonate buffer for hydrogen production in microbial electrolysis cells using a new method for measuring gas production.” *International Journal of Hydrogen Energy* 36, 160-166.

Call, D., Logan, B.E., 2008. “Hydrogen production in a single chamber microbial electrolysis cell lacking a membrane.” *Environmental Science & Technology* 42, 3401-3406.

Call, D.F., Logan, B.E., 2011. “A method for high throughput bioelectrochemical research based on small scale microbial electrolysis cells.” *Biosensors and Bioelectronics* 26, 4526-4531.

Dlugolecki, P., Ogonowski, P., Metz, S.J., Saakes, M., Nijmeijer, K., Wessling, M., 2010. “On the resistances of membrane, diffusion boundary layer and double layer in ion exchange membrane transport.” *Journal of Membrane Science* 349, 369-379.

Feng, Y., Yang, Q., Wang, X., Logan, B.E., 2010. “Treatment of carbon fiber brush anodes for improving power generation in air–cathode microbial fuel cells.” *Journal of Power Sources* 195, 1841-1844.

Geise, G.M., Cassady, H.J., Paul, D.R., Logan, B.E., Hickner, M.R., 2014. “Specific ion effects on membrane potential and the permselectivity of ion exchange membranes.” *Physical Chemistry Chemical Physics*, 16, 21673-21681.

Geise, G.M., Curtis, A. J., Hatzell, M. C., Hickner, M. A., Logan, B. E. 2014. “Salt Concentration Differences Alter Membrane Resistance in Reverse Electrodialysis Stacks,” *Environ. Sci. Technol. Lett.*, 1 (1), 36-39.

Geise, G. M., Hickner M. A., Logan, B. E. 2013. “Ionic resistance and permselectivity tradeoffs in anion exchange membranes,” *ACS Appl. Mater. Interfaces*, 5 (20), 10294–10301.

Hatzell, M.C., Ivanov, I., Cusick, R.D., Zhu, X.P., Logan, B.E., 2014. “Comparison of hydrogen production and electrical power generation for energy capture in closed-loop ammonium bicarbonate reverse electrodialysis systems.” *Physical Chemistry Chemical Physics* 16, 1632-1638.

He, Z., Huang, Y., Manohar, A.K., Mansfeld, F., 2008. “Effect of electrolyte pH on the rate of the anodic and cathodic reactions in an air-cathode microbial fuel cell.” *Bioelectrochemistry* 74, 78-82.

Lee, H.-S., Rittmann, B.E., 2010. “Significance of biological hydrogen oxidation in a continuous single-chamber microbial electrolysis cell.” *Environmental Science & Technology* 44, 948-954.

Logan, B.E., Patnaik, R., 1997. “A gas chromatographic-based headspace biochemical oxygen demand test.” *Water Environment Research* 69, 206-206.

Tedesco, M., Cipollina, A., Tamburini, A., Bogle, D., Micale, G., 2014 (in press). "A simulation tool for analysis and design of Reverse Electrodialysis using concentrated brines” *Chem. Eng. Res. Des.*

Tedesco, M., A. Cipollina, A., Tamburini, A., van Baak, W., Micale, G., 2012. "Modelling the Reverse ElectroDialysis process with seawater and concentrated brines," *Desalination and Water Treatment*, vol. 49, pp. 404-424.

Ullery, M.L. and B.E. Logan. 2014. “Comparison of complex effluent treatability in different bench scale microbial electrolysis cells.” *Bioresource Technology*, 170:530-537.

Ullery, M.L. 2014. “Screening and acclimation methods for accomplishing treatment and energy recovery from wastewater in microbial electrolysis cells.” (graduate student thesis).

Veerman, J., 2010. “Reverse electrodialysis: design and optimization by modeling and experimentation.” (thesis).

Veerman, J., Saakes, M., Metz, S.J., Harmsen, G.J., 2009. “Reverse electrodialysis: Performance of a stack with 50 cells on the mixing of sea and river water.” *Journal of Membrane Science* 327, 136-144.

Veerman, J., Saakes, M., Metz, S.J., Harmsen, G.J., 2010. “Electrical power from sea and river water by reverse electrodialysis: a first step from the laboratory to a real power plant.” *Environ. Sci. Technol.* 44, 9207-9212

Veerman, J., Saakes, M., Metz, S.J., Harmsen, G.J., 2011. "Reverse electrodialysis: A validated process model for design and optimization," *Chemical Engineering Journal*, vol. 166, pp. 256-268, 2011.

Zhu, X.P. and B.E. Logan. “Saving pumping energy by using different flow rates for high and low concentration solutions in reverse electrodialysis cells.” *Journal of Membrane Science* (in preparation).

Zhu, X.P. and B.E. Logan. “Influence of solution concentration and composition on the performance of reverse electrodialsysis cells.” *Journal of Membrane Science* (in preparation).

12. Appendices

A. Evaluation of Facility Waste Heat Recovery and Effluent Treatment

An initial part of this program was to collect data and samples from various United States based Air Products facilities to evaluate the potential for waste heat recovery (WHR), effluent treatment and energy yield. Air Products compiled amenability data from 132 U.S. manufacturing facilities which produce hydrogen, oxygen, nitrogen, argon, specialty chemicals, and electronic gases to assess which facilities are most amenable to incorporation of MHRC. Wastewater effluent data, as routinely measured and recorded by plant facilities, were compiled. These included volumetric flow, COD, BOD, pH and composition information where available. Waste heat discharge data for individual process sources were collected from instrument measurements, energy balance calculations and design case information. These included medium, flow rate, temperature, pressure, and proximity to a potential waste effluent substrate. Facility electrical energy consumption data and hydrogen consumption data, where applicable, were compiled.

Waste heat and waste effluent characterizations were completed for 31 major U.S. facilities including air separation plants, steam methane reformer hydrogen plants, partial oxidation hydrogen plants, specialty chemical facilities and a membrane manufacturing facility. This information could be combined with similar data from other industrial companies to get a broader dataset of amenable process waste heat and waste effluent available for recovery and use to generate useable energy.

Process waste heat data was evaluated to determine which subject facilities are suitable for integration into the MHRC system for energy recovery potential at various minimum temperature cut-offs. The total potential, recoverable waste heat from all point sources at the subject facilities is over 1 GW. As shown in Figure A-1, at successively increasing minimum outlet cut-off temperatures, the recoverable waste heat diminishes rapidly: 590 MW at 60°C, 314 MW at 100°C, and 68 MW at 150°C. Based on these data, 60-100°C, was the target range chosen for evaluation of MHRC as part of the process modeling analysis.

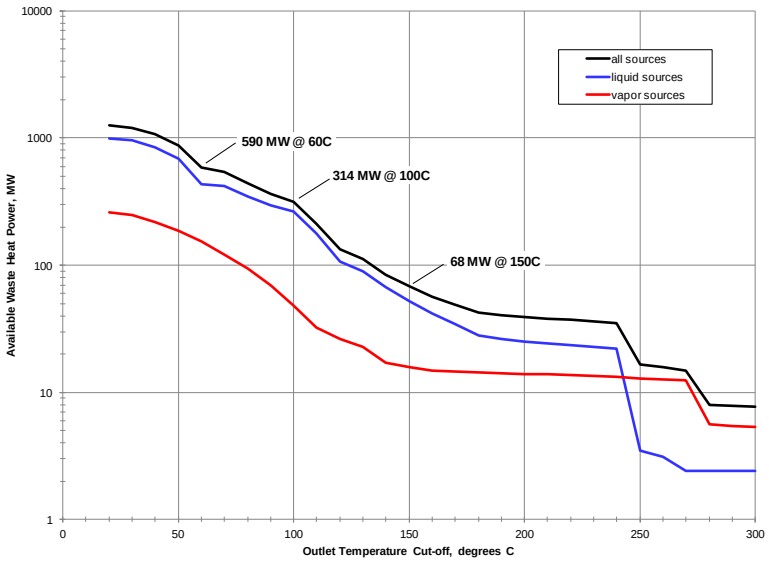

Figure A-1. Available waste heat power at major manufacturing facilities.

The data was also parsed by process stream phase, major fluid component, inlet temperature, power level and facility type. The individual waste heat source power level is a strong function of minimum outlet temperature cut-off, as can be seen in Figure A-2. Over the target temperature cut-off range of 60-100°C, the average individual waste source average power is 298 to 172 KW. This information provided guidance for estimate system scale that was applied in the equipment design and costing studies.

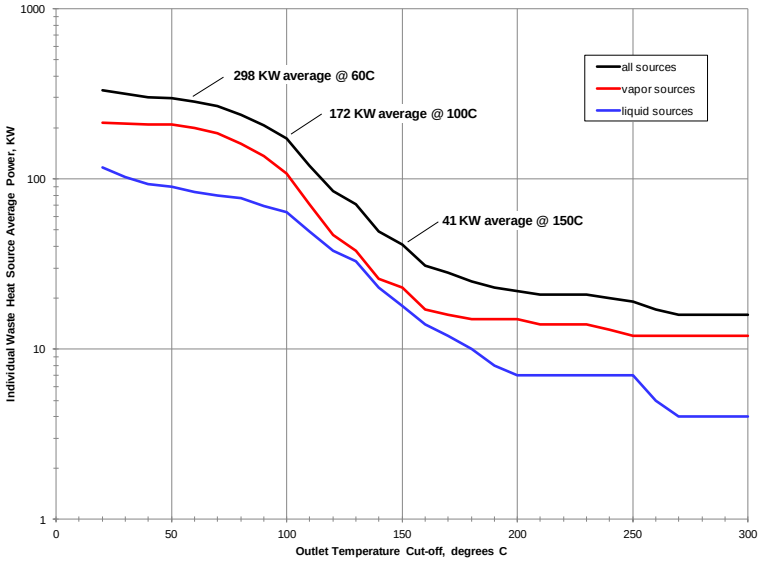

Figure A-2. Average power of individual waste heat sources at major manufacturing facilities.

B. Effluent Treatability Analyses

Total charge collected over each batch cycle was calculated using current measurements and integrating over the length of the cycle. Data measurements were collected every 10 minutes and a trapezoidal approximation was used to estimate total charge:

$$Q_{total} = \sum_{i=1}^{n} \frac{I_{i-1}+I_i}{2} \Delta t \qquad [B\text{-}1]$$

Where Q_{total} (C) = total charge recovered

I_i (A) = current measurement at a specific time interval

Δt (s) = time interval between current measurements (10 min)

Coulombic efficiency relates electrons measured as current to those removed from the organic substrate, measured as COD. There are 8 g of O_2 per mole of e^- in the oxygen reduction reaction, and using this conversion, coulombic efficiency can be calculated as follows:

$$CE = \frac{8Q_{total}}{Fv_{an}\Delta COD} \qquad [B\text{-}2]$$

Where CE (%) = coulombic efficiency

Q_{total} (C) = total charge recovered

F (C/mol e^-) = Faraday constant, 96485 C/mol e^-

v_{an} (L) = reactor liquid volume
ΔCOD (g/L) = difference between influent and effluent COD concentration

Average current is typically approximated by dividing the total charge accumulated over a cycle by the cycle length. This approach can underestimate current, since current generation can decrease exponentially at the end of the cycle, providing little additional current but increasing the cycle time. Averaging the current over the time for 90% of the total charge to accumulate provides a better representation of the current generation over the whole cycle:

$$I_{avg,90} = \frac{Q_{total}}{t_{90} A_{cat}} \quad [B\text{-}3]$$

Where $I_{avg,90}$ (A/m^2) = average current over the time for 90% charge accumulation
Q_{total} (C) = total charge recovered
t_{90} (s) = time to 90% charge accumulation

The amount of energy added through the external power supply is calculated based on the current, applied potential, and cycle length. A midpoint approximation was used to estimate the current for each time series. Data were collected every 10 minutes. Adjusting for the loss across the 10 Ω resistor, the added energy is given as:

$$W_E = \sum_{i=1}^{n} \left(\frac{I_{i-1}+I_i}{2}\right) E_{ap} \Delta t - \left(\frac{I_{i-1}+I_i}{2}\right)^2 R_{ex} \Delta t \quad [B\text{-}4]$$

Where W_E (Wh) = energy added through the power supply
I_i (A) = current measurement at a specific time interval
E_{ap} (V) = applied potential
Δt (h) = time interval between measurements (10 min)
R_{ex} (Ω) = external resistance (10 Ω)

Treatment energy is a measure of the amount of additional energy from the power supply normalized to the COD removal. This indicates the amount of energy required for COD treatment, but does not account for energy recovered as gas.

$$W_{EL} = \frac{W_E}{\Delta COD} \quad [B\text{-}5]$$

Where W_{EL} (kWh/kg COD) = treatment energy
W_E (kWh) = energy added through the power supply
ΔCOD (g/L) = difference between influent and effluent COD concentration

Energy efficiency relative to the electrical input is based on the amount of energy recovered in the hydrogen and methane compared to the energy added through the external power supply. The energy content of the gas is calculated based on the heat of combustion for hydrogen (ΔH_{H2} = 285.8 kJ/mol) and methane (ΔH_{CH4} = 891 kJ/mol). The energy efficiency can be based on just the hydrogen recovered, or the combined energy of the hydrogen and methane recovered.

$$\eta_{H2} = \frac{n_{H2} \Delta H_{H2}}{W_E} \quad [B\text{-}6]$$

Where η_{H2} (%) = energy efficiency of hydrogen recovered relative to the electrical input
n_{H2} (mol) = moles of hydrogen gas recovered
ΔH_{H2} (kJ/mol) = heat of combustion of hydrogen gas
W_E (kJ) = electrical energy added through the power supply

$$\eta_{H2+CH4} = \frac{n_{H2}\Delta H_{H2} + n_{CH4}\Delta H_{CH4}}{W_E} \quad \text{[B-7]}$$

Where η_{H2+CH4} (%) = energy efficiency of biogas recovered relative to the electrical input
n_{H2} (mol) = moles of hydrogen gas recovered
n_{CH4} (mol) = moles of methane gas recovered
ΔH_{H2} (kJ/mol) = heat of combustion of hydrogen gas
ΔH_{CH4} (kJ/mol) = heat of combustion of methane gas
W_E (kJ) = electrical energy added through the power supply

Cathodic gas recovery is the efficiency of current conversion into hydrogen and methane, based on the hydrogen evolution reaction ($2H^+ + 2e^- \rightarrow H_2$) and hydrogenotrophic methano-genesis ($CO_2 + 4H_2 \rightarrow CH_4 + 2H_2O$). The cathodic gas recovery can be based on recovered hydrogen alone, or on hydrogen and methane. In this calculation, measured methane is assumed to be generated by hydrogenotrophic methanogenesis and is converted to an equivalent hydrogen volume based on 4 mol of hydrogen per mol of methane.

$$r_{H2,cat} = \frac{2Fn_{H2}}{Q_{total}} \quad \text{[B-8]}$$

Where $r_{H2,cat}$ (%) = cathodic gas recovery for hydrogen
F (C/mol e^-) = Faraday constant, 96485 C/mol e^-
n_{H2} (mol) = moles of hydrogen gas recovered
Q_{total} (C) = total charge recovered

$$r_{H2+CH4,cat} = \frac{2F(n_{H2} + 4n_{CH4})}{Q_{total}} \quad \text{[B-9]}$$

Where $r_{H2+CH4,cat}$ (%) = cathodic gas recovery for hydrogen and methane
F (C/mol e^-) = Faraday constant, 96485 C/mol e^-
n_{H2} (mol) = moles of hydrogen gas recovered
n_{CH4} (mol) = moles of methane gas recovered
Q_{total} (C) = total charge recovered

The overall hydrogen recovery is the ratio of actual hydrogen and methane recovered to the maximum amount possible based on the conversion of COD into gas. Using coulombic efficiency and cathodic gas recovery, the overall gas recovery can be calculated.

$$r_{H2+CH4,COD} = CE * r_{H2+CH4,cat} \quad \text{[B-10]}$$

Where $r_{H2+CH4,COD}$ (%) = overall hydrogen and methane recovery
CE (%) = coulombic efficiency
$r_{H2+CH4,cat}$ (%) = cathodic gas recovery for hydrogen and methane

Table B-1. Summary of initial Air Products sample conditions.						
	A1	**B1**	**B2**	**C1**	**D1**	**E1**
Date Received	2/5/13	2/22/13	4/18/13	5/10/13	5/10/13	7/10/13
pH	5.4[1]	5.1[1]	5.1[1]	6.9	7.3	11.8
Conductivity (mS/cm)	0.54	0.61	0.48	1.53	2.71	20.15
TCOD (mg/L)	1700 ± 41	1570 ± 45	4870 ± 98	171 ± 2	257 ± 4	>500,000
HBOD (mg/L)	370 ± 14	513 ± 24	n/a	<20	54 ± 10	214 ± 7[2]

[1]Neutralized before use in MEC reactors.

[2]Measured after sample was diluted ~1000 mg/L COD in tap water

Table B-2 . Summary of comparative samples.		
	WW	**AC**
pH	8.2	7.0
Conductivity (mS/cm)	1.0	4.0
TCOD (mg/L)	457 ± 2	777 ± 12
HBOD (mg/L)	233 ± 5	566 ± 15

Table B-3. Summary of initial Air Products sample conditions used in secondary assessment.			
	B3	**B4**	**B5**
Date Received	4/25/13	8/22/13	8/28/13
pH	5.4[1]	4.9[1]	7.8
Conductivity (mS/cm)	0.73	1.9	1.7
TCOD (mg/L)	2585 ± 44	6750 ± 95	4700 ± 201
HBOD (mg/L)	490 ± 27	985 ± 38	443 ± 28

[1]Neutralized before use in MEC reactors.

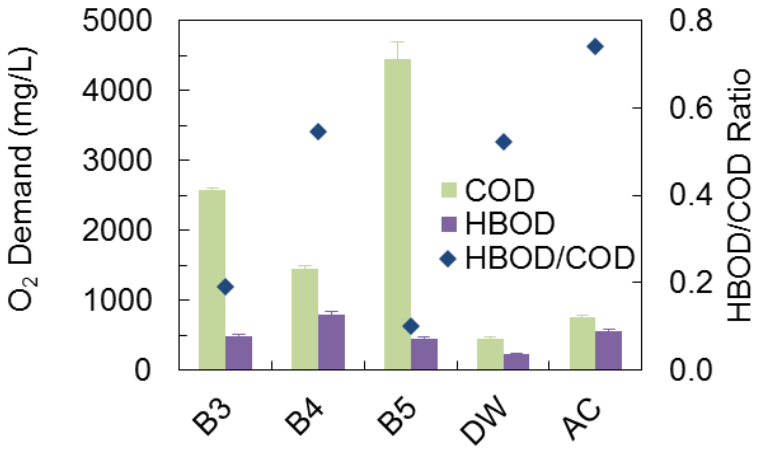

Figure B-1. Influent COD and $HBOD_3$ concentrations and COD/$HBOD_3$ ratio prior to MEC treatment, measured after pH adjustments to B3 and B4 and dilution of B4 sample.

C. Reverse Electrodialysis Computational Model

Variable type definition:

Name	Lower bound	Default value	Upper bound	Units
ActivityCoefficient	0.01	0.5	1.0	
Conductivity	4E-5	25.0	500.0	m2/ohm mol
CurrentDensity	0.0	1E-4	1E9	A/m2
Diffusivity	1E-20	1E-7	1.0	m2/s
IntrisicResistance	0.1	1.0	100.0	ohm m
length	0.0	0.1	1.0	m
MolarConcentration	0.005	1.0	5.0	kmol/m3
MolarFlux	-1E9	0.0	1E9	mol/m2s
Moles	0.0	1.0	1E9	kmol
NoType	-1E9	1.0	1E9	
PowerDensity	0.0	0.5	100.0	W/m2
Resistance	1E-6	0.1	100.0	ohm m2
Temperature	0.0	298.0	1E9	K
voltage	0.0	0.001	100000.0	V
Volume	0.0	1.0	1E9	m3
VolumetricFlow	0.0	0.5	1E9	m3/s
VolumetricFlux	-1E9	0.0	1E9	m3/m2s
Add new				

Cell model code:

```
PARAMETER
   #membrane parameters
   #membrane thickness
   ThicknessAEM, ThicknessCEM    AS REAL
   #membrane permselectivity
   AlphaAEM, AlphaCEM          as real
   #water diffusivity
   Dwater                      as real
   #AmBC diffusivity
   D                           as real
   NoComp as integer
   # avg membrane thickness
   ThicknessAvg    as real

   #cell level parameters
   #compartment thickness
   ThicknessLC, ThicknessHC as real
   #spacer obstruction factor
   Spacer_f as real
   # cell length, width
   CellLength as real
   CellWidth as real

   F as real
   R as real
   T as real

DISTRIBUTION_DOMAIN
   Axial as [0 : CellLength]

VARIABLE
   #membrane area resistance
   ResistanceAEM, ResistanceCEM  as distribution(Axial) of IntrisicResistance

   C_HC as distribution(NoComp, Axial) of MolarConcentration
   C_LC as distribution(NoComp, Axial) of MolarConcentration

   j as distribution(Axial) of CurrentDensity
   J_total_108x as distribution(Axial) of MolarFlux
   J_water_108x as distribution(Axial) of VolumetricFlux
   OCVcell as distribution(Axial) of Voltage
   #activity coeff
   ActivityCoeff_HC as distribution(Axial) of ActivityCoefficient
   ActivityCoeff_LC as distribution(Axial) of ActivityCoefficient
   # conductivity
```

```
   Conductivity_HC_103x as distribution(Axial) of Conductivity
   Conductivity_LC_103x as distribution(Axial) of Conductivity

   Rcell as Distribution(Axial) of Resistance
   CC_HC as distribution(Axial) of Resistance
   CC_LC as distribution(Axial) of Resistance

   Rref as Resistance
   QHC_108x, QLC_108x as VolumetricFlow

SET
   ThicknessAvg:=(ThicknessAEM + ThicknessCEM)/2;
   F :=96485; # C/mol
   R :=8.314;
   Axial :=[BFDM, 1, 100];

BOUNDARY
   C_HC(,0)=0.6; #Kmol/m3
   C_LC(,0)=0.006; #Kmol/m3

EQUATION
# Model equations
   FOR i := 1 TO NoComp DO
      FOR x := 0|+ TO CellLength DO
            partial (C_HC(i,x), Axial) =CellWidth/QHC_108x*(-J_total_108x(x)+C_HC(i,x)*J_water_108x(x));
            partial (C_LC(i,x), Axial) =CellWidth/QLC_108x*(J_total_108x(x)-C_LC(i,x)*J_water_108x(x));
      End
   FOR x := 0 TO CellLength DO
      J_total_108x(x) =j(x)/F*1e+8+2*D/ThicknessAvg*(C_HC(1,x)-C_LC(1,x))*1e+8;
      J_water_108x(x) =-2*Dwater/ThicknessAvg*(C_HC(1,x) -C_LC(1,x))*0.018/1000*1e+8;
      ActivityCoeff_HC(x) =10^((-2.0942*(C_HC(1,x))^(-0.5)-1.3976)^(-1));
      ActivityCoeff_LC(x) =10^((-2.0942*(C_LC(1,x))^(-0.5)-1.3976)^(-1));
      OCVcell(x)=(AlphaAEM+AlphaCEM)*R*T/F*LOG(ActivityCoeff_HC(x)*C_HC(1,x)/(ActivityCoeff_LC(x)*C_LC(1,x)));
      Conductivity_HC_103x(x) = 0.818*C_LC(1,x)-3.137*C_LC(1,x)^0.5+9.634;
      IF C_LC(1,x) < 0.15 THEN
         Conductivity_LC_103x(x) = 10.52e+3*C_LC(1,x)^2-4.959e+3*C_LC(1,x)^1.5+878.6*C_LC(1,x)-74.29*C_LC(1,x)^0.5+12.02;
      Else
         Conductivity_LC_103x(x) = 0.818*C_LC(1,x)-3.137*C_LC(1,x)^0.5+9.634;
      END
      ResistanceAEM(x)=9.0805*(C_HC(1,x)^(1-0.409)-C_LC(1,x)^(1-0.409))/(1-0.409)/(C_HC(1,x)-C_LC(1,x));
      ResistanceCEM(x)=3.5758*(C_HC(1,x)^(1-0.562)-C_LC(1,x)^(1-0.562))/(1-0.562)/(C_HC(1,x)-C_LC(1,x));
      Rcell(x)=CC_HC(x)+CC_LC(x)+ResistanceAEM(x)*ThicknessAEM+ResistanceCEM(x)*ThicknessCEM;
      CC_HC(x)*Conductivity_HC_103x(x)*C_HC(1,x)=Spacer_f*ThicknessHC;
      CC_LC(x)*Conductivity_LC_103x(x)*C_LC(1,x)=Spacer_f*ThicknessLC;
   End
   Rref =INTEGRAL (x:=0:CellLength; Rcell(x))/CellLength;
```

Stack model code:

```
PARAMETER
   NoPairs As INTEGER
   CellLength as real
DISTRIBUTION_DOMAIN
   Axial as [0 : CellLength]
UNIT
Cell AS ARRAY(NoPairs) of cell_pair
VARIABLE
   Rext As Resistance
   Rends As Resistance  #two electrode chamber R
   Rref AS Resistance #avg Rstack+Rends
   Rstack As DISTRIBUTION (Axial) of Resistance
   OCV AS DISTRIBUTION (Axial) of voltage
```

```
   j AS DISTRIBUTION (Axial) of CurrentDensity
   Pd AS DISTRIBUTION (Axial) of PowerDensity
   QHC, QLC as VolumetricFlow
SET
   Cell().CellLength :=CellLength;
   Axial :=[BFDM, 1, 100];
EQUATION
# Model equations
   Cell().QHC_108x = QHC/NoPairs*1e+8;
   Cell().QLC_108x = QLC/NoPairs*1e+8;
   FOR x := 0 TO CellLength DO
      Rstack(x)=SIGMA(Cell().Rcell(x))+Rends;
      OCV(x)=SIGMA(Cell().OCVcell(x));
   end
   Rref = SIGMA(Cell().Rref)+Rends;
#   j()=OCV()/(Rstack()+Rref); # Rext=avg value of Rinternal
   j()=OCV()/(Rstack()*2); # Rext=Rstack
#    Pd()=j()^2*Rext/NoPairs;
#    Pd()=j()^2*Rstack/((2*NoPairs+1)*Cell(1).CellLength *Cell(1).CellWidth); # Rext=Rstack
   Pd()=j()^2*Rstack/(2*NoPairs+1); # Rext=Rstack
   For i := 1 TO NoPairs Do
      Cell(i).j()=j();
   End
```

Stack process code:

```
UNIT
stack1 as stack

SET
   stack1.CellLength := 0.08; #m
   stack1.NoPairs := 10;
   for i :=1 TO stack1.NoPairs do
      within stack1.Cell(i) do
         T:=298;     #K
         CellWidth  := 0.08; #m
         ThicknessHC := 0.5*1e-3; #m
         ThicknessLC := 0.5*1e-3; #m
         ThicknessAEM := 0.13*1e-3; #m
         ThicknessCEM := 0.22*1e-3; #m
         AlphaAEM :=0.8; #assumed
         AlphaCEM :=0.8; #assumed
         NoComp :=2;
         Spacer_f :=2.5;
         D:=1e-11; # m2/s
         Dwater:=R*T*0.145*1e-14/3600*1000/0.018; #m2/s #0.145 unit of L.micrometer/m2 hr bar
      end
Assign
   within stack1 do
      QHC:=1.67e-7; #m3/s  10ml/min
      QLC:=3.33e-7; #m3/s  20ml/min
      Rext :=10; #ohm guessed
      Rends := 0.5; #ohm guessed
   end
SOLUTIONPARAMETERS
   DASolver := "DASOLV" [
      "InitialisationNLSolver" := "BDNLSOL" [
         "BlockSolver" := "SPARSE" [
            "ConvergenceTolerance" := 1E-010,
            "EffectiveZero" := 1E-010,
            "FDPerturbation" := 1.0E-10,
            "NStepReductions" := 20
```

D. Reverse Electrodialysis Cell Experimental Analyses

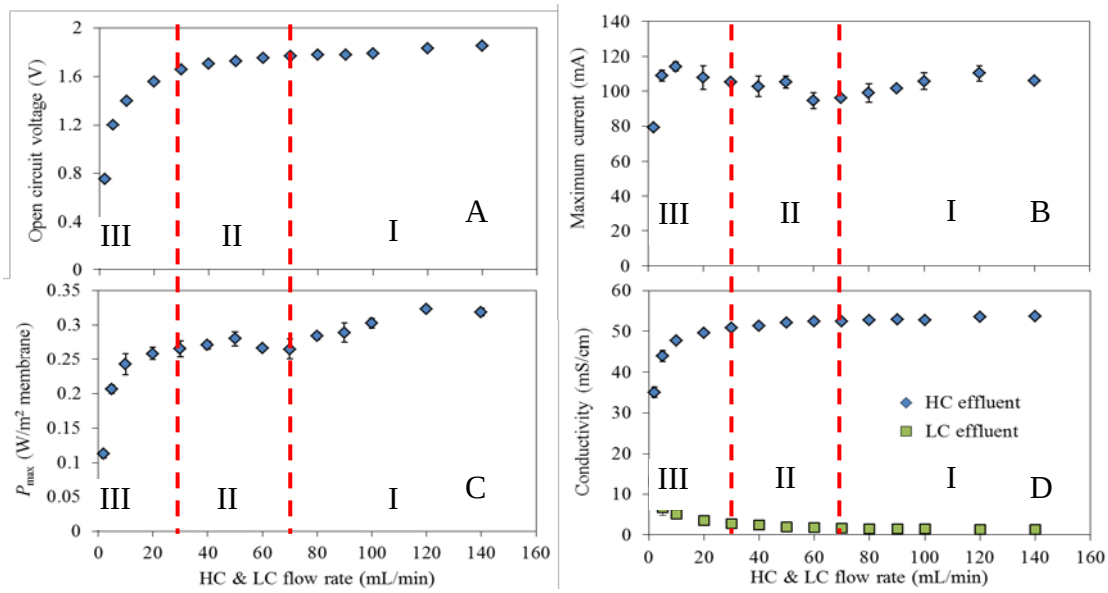

Figure D-1. (A) Open circuit voltage, (B) maximum current, (C) maximum power density, and (D) conductivity of HC and LC effluents when the flow rates of HC and LC solutions simultaneously decreased from 140 mL/min to 2 mL/min.

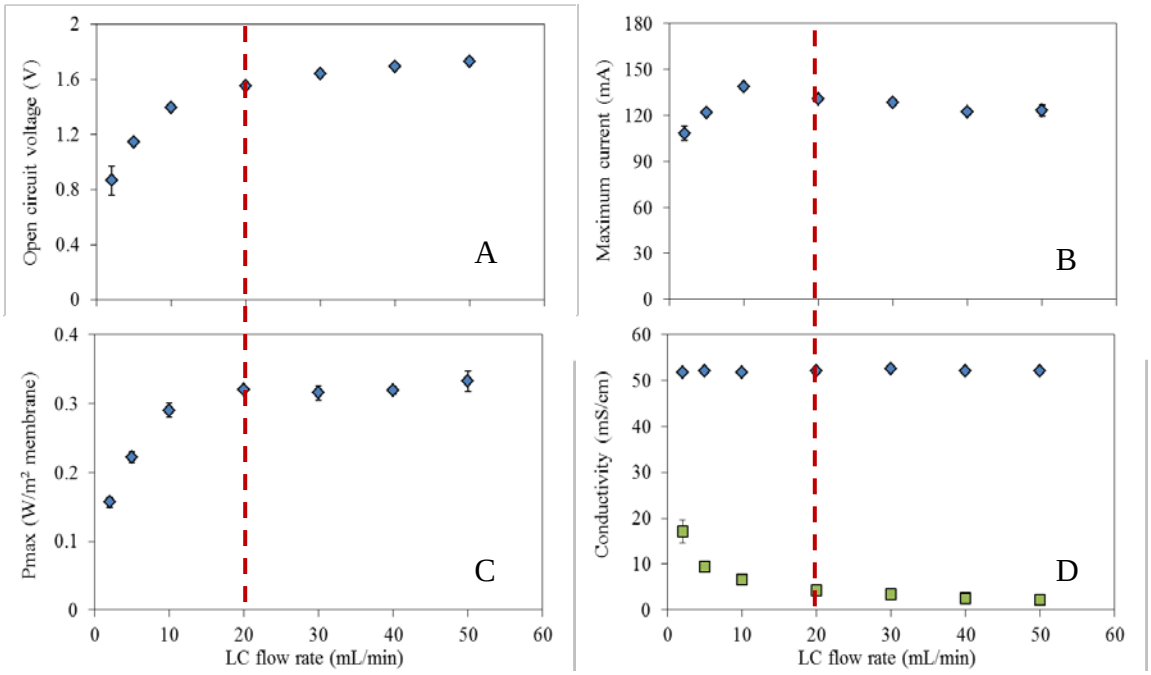

Figure D-2. (A) Open circuit voltage, (B) maximum current, (C) maximum power density, and (D) effluent conductivity when the flow rates of LC solution decreased from 50 mL/min to 2 mL/min and the flow rate of HC solution was 50 mL/min.

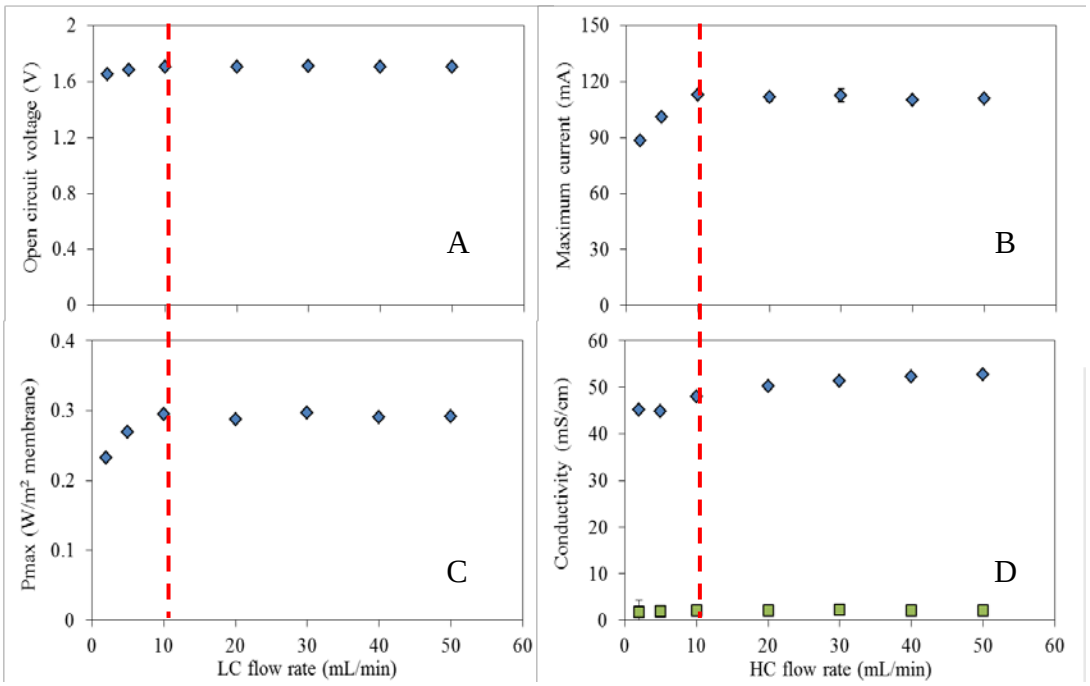

Figure D-3. (A) Open circuit voltage, (B) maximum current, (C) maximum power density, and (D) effluent conductivity when the flow rates of HC solution decreased from 50 mL/min to 2 mL/min and the flow rate of LC solution was 50 mL/min.

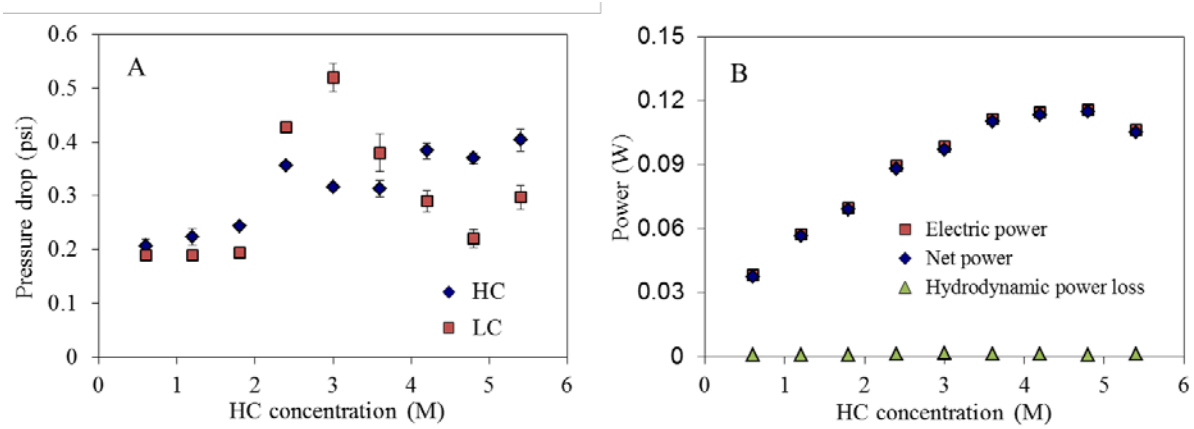

Figure D-4. (A) Pressure drops of HC and LC channels, and (B) electric power, hydrodynamic power loss, and net power of the RED stack when HC concentration increased from 0.6 M to 5.4 M (saturated) NaCl at a flow rate of 10 mL/min. LC solution was 0.006 M NaCl at a flow rate of 20 mL/min.

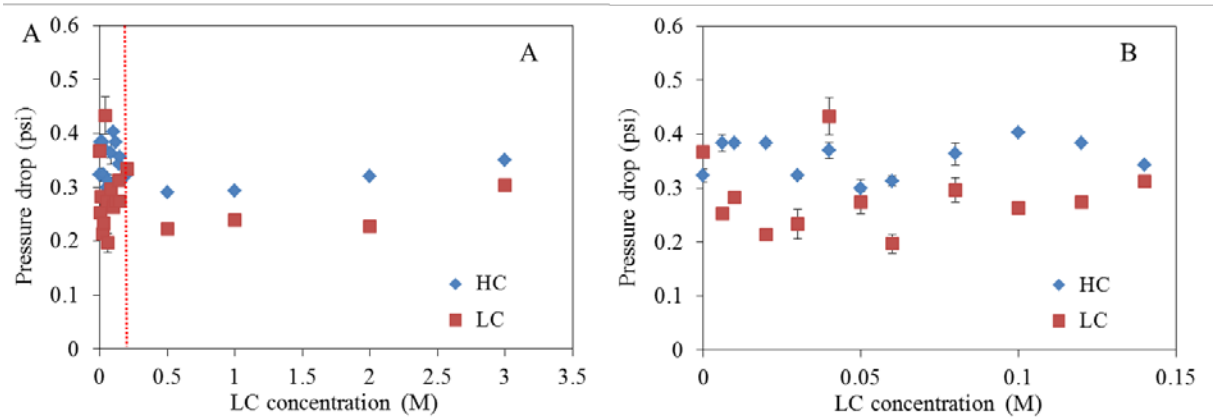

Figure D-5 Pressure drops of HC and LC channels for a wide (A) and narrow (B) range when LC concentration increased from 0 M to 3 M NaCl at a flow rate of 20 mL/min. HC solution was 3.6 M NaCl at a flow rate of 10 mL/min.

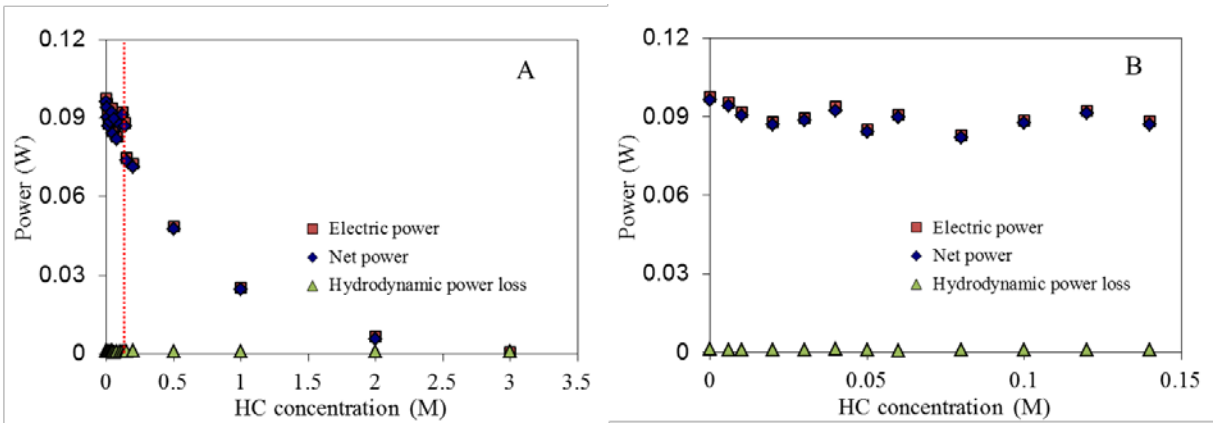

Figure D-6. Electric power, hydrodynamic power loss, and net power of the RED stack for a wide (A) and a narrow (B) range when LC concentration increased from 0 M to 3 M NaCl at a flow rate of 20 mL/min. HC solution was 3.6 M NaCl at a flow rate of 10 mL/min.

Table D-1. Concentration (*C*, in M) and conductivity (*S*, in mS cm^{-1}) of NaCl and AmB.

NaCl				**AmB (NH_4HCO_3)**			
HC		**LC**		**HC**		**LC**	
***C*/M**	***S*/mS cm^{-1}**	***C*/M**	***S*/mS cm^{-1}**	***C*/M**	**S/mS cm^{-1}**	***C*/M**	***S*/mS cm^{-1}**
0.6	54	0.006	0.72	0.6	45	0.006	0.8
0.6	54	0.006	0.72	0.74	54	0.005	0.72
1.13	95	0.013	1.62	1.5	95	0.015	1.62
1.5	119	0.015	1.85	1.5	95	0.015	1.62

E. Ion Exchange Membrane Development

Due to the decision to halt this program after Budget Period 2, there was no specific work carried out to develop new ion exchange membranes for this application. The groundwork completed during this study will facilitate future developments in this important area by providing a methodology to characterize new ion exchange membranes in unconventional salt systems. Future work in membrane development could enable the commercialization of this technology, as limitations with commercial materials contributed significantly to the unfavorable economics for moving this technology forward. It is anticipated that funding and research emphasis in this area could lead to the improvements in ionic resistance and permselectivity needed to provide the power and efficiency of RED devices.

F. Process Economic Analysis

As part of the Discovery Driven Planning approach to understand the economics of the integrated MHRC process, these views provide some additional insights into the factors that have the highest impact on cost as well as different payback scenarios.

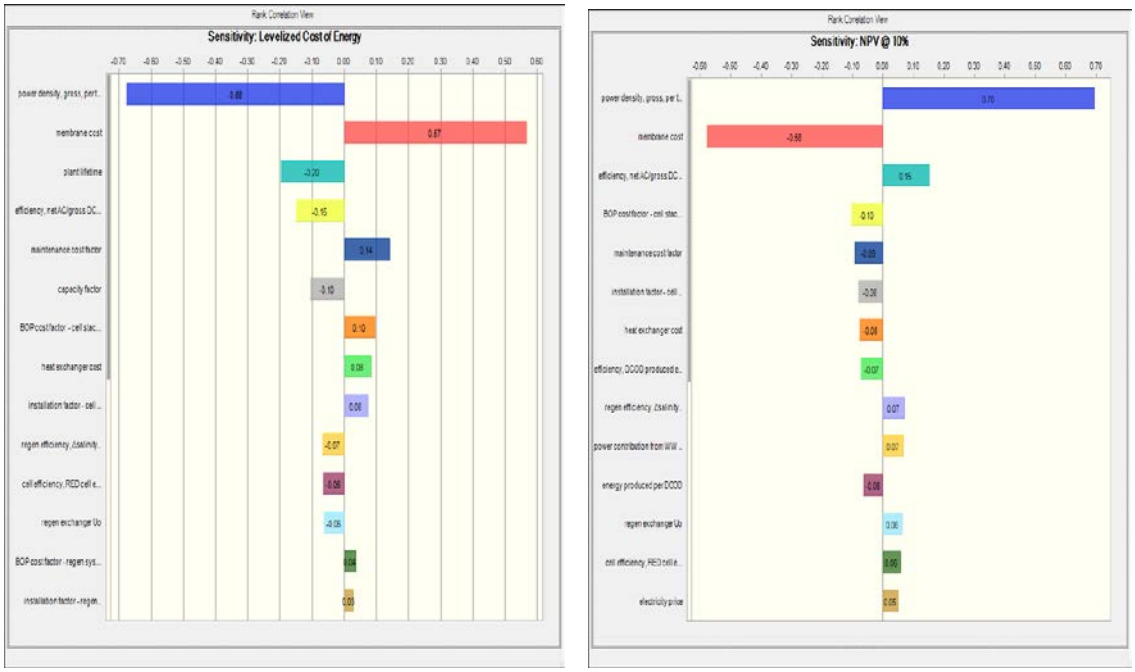

Figure F-1. Hurricane plots of the sensitivity analysis related to various process parameters.

As discussed earlier, power density and IEM cost have the largest impact on both levelized cost of energy and profitability (NPV) of any of the major factors considered in this analysis. This information underscores the need to improve these specific factors to enable this technology to be successfully brought to market.

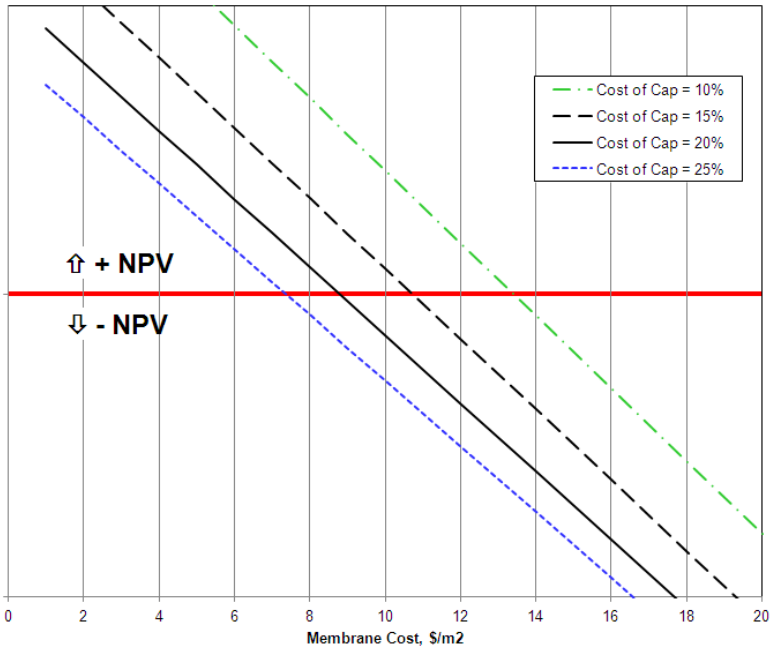

Figure F-2. Sensitivity of profitability (NPV) to membrane cost and capital cost percentage.

This analysis reinforces the need for improved ion exchange membranes to enable commercial success of this technology.

Basis: Net Rated Power Output	MW		10	
Parameter	unit	MIN	likeliest	MAX
Cell and Power System				
power density, gross, per total membrane area	W/m2	0.5	2	20
cell efficiency, RED cell electric/actual Δsalinity		10%	30%	60%
HC concentration	M	0.5	2	3
LC concentration	M	0.01	0.02	0.2
thermolyte extent of mixing		0.1	0.5	0.8
cell pressure drop	kPa	10	30	60
efficiency, net AC/gross DC electricity conversion	%	50%	80%	95%
power contribution from WW oxidation	%	5%	20%	50%
efficiency, DCOD produced energy/ theor total energy	%	2%	10%	30%
energy produced per DCOD	kWh/kg COD	0.5	1.0	3.0
aeration energy consumption avoidance per DCOD	kWh/kg COD	0.4	0.6	1.2
cell pairs			20	
cell projected area	m2		1	
membrane spacing	mm		1.0	
WHR and Thermolyte Regeneration System				
regen efficiency, Δsalinity/WH		1%	10%	20%
regen exchanger Uo	W/(m2-C)	6	568	1135
regen exchanger LMDT	C		10	
regen loop pressure drop	kPa	30	50	200
pump efficiency			75%	
Costs and Financial Parameters				
membrane cost	$/m2	10	30	200
heat exchanger cost	$/m2	1	10	100
BOP cost factor - cell stack and power/membrane		1.1	1.5	2
installation factor - cell stack and power		1.2	1.5	2
BOP cost factor - regen system/exchanger		1.5	3	6
installation factor - regen system		2	4	6
capacity factor		0.6	0.85	0.95
maintenance cost factor	annual	0.01	0.02	0.10
operating labor	$/y	$ 50,000	$ 100,000	$ 500,000
electricity price	$/kwh	0.06	0.10	0.16
plant lifetime	years	5	10	30
tax rate			25%	
finance rate (for Modified IRR)			5%	
reinvestment rate (for Modified IRR)			10%	
discount rate (for LCOE)			3%	

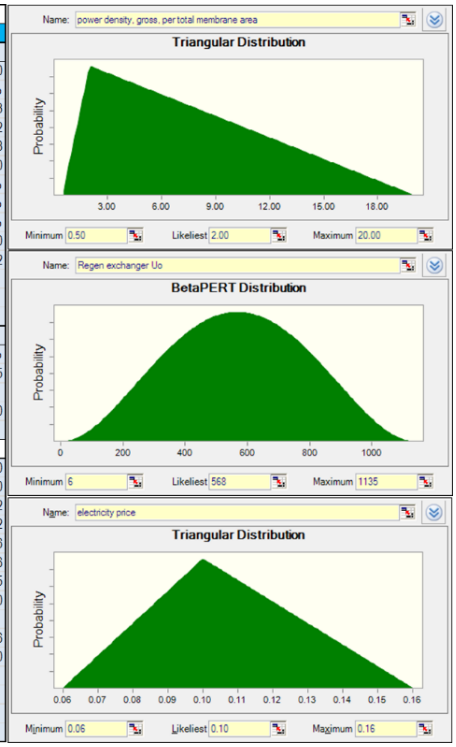

Figure F-3. Output from Oracle® Crystal Ball analysis.

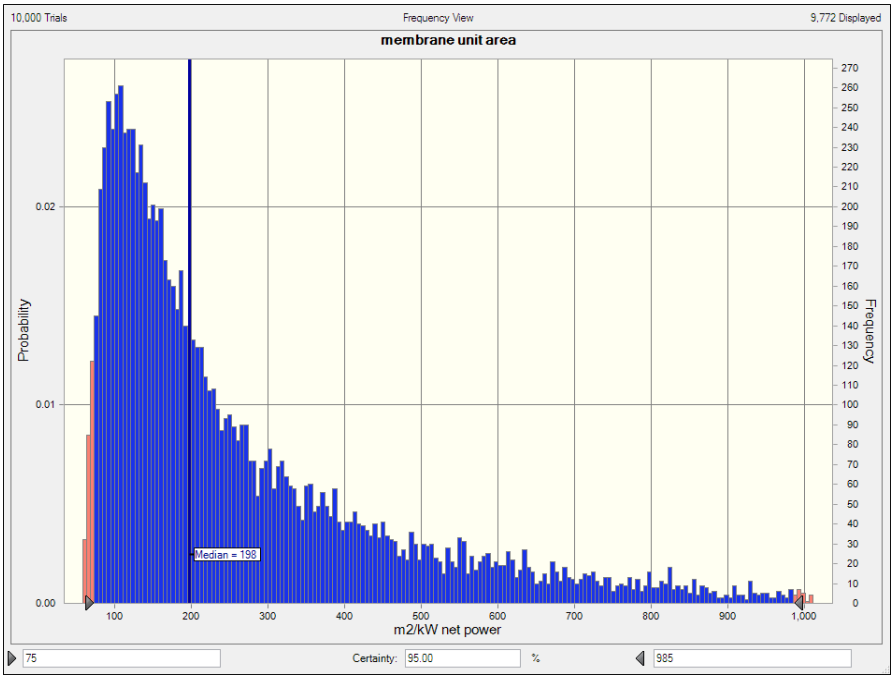

Figure F-4. Probability distribution for net power with membrane unit area.

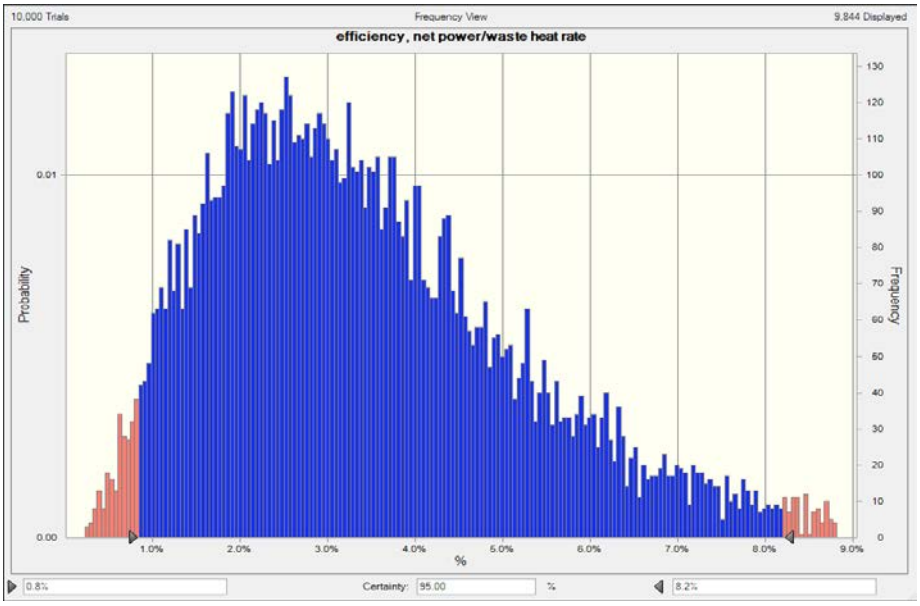

Figure F-5. Probability distribution for overall efficiency (net power/waste heat rate).

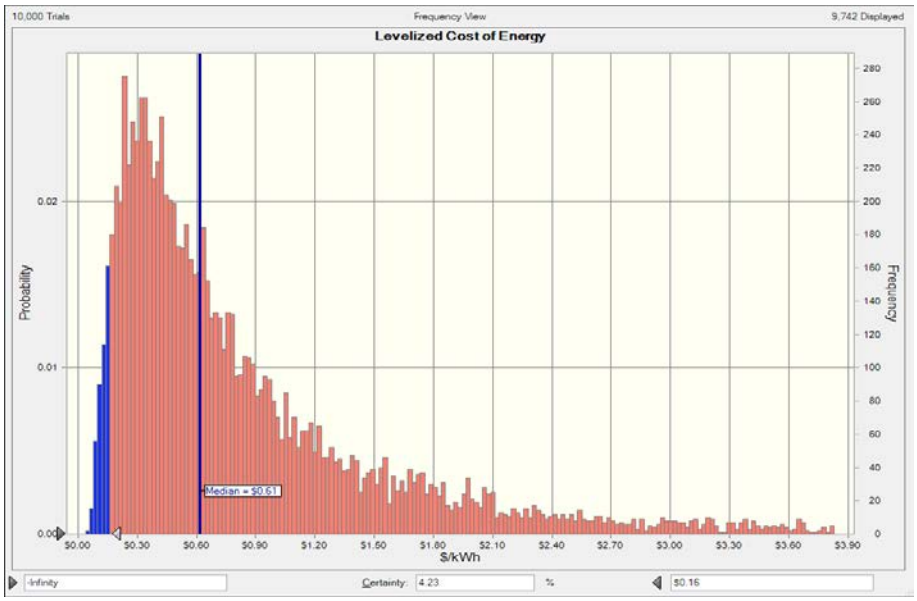

Figure F-6. Probability distribution for levelized cost of energy.

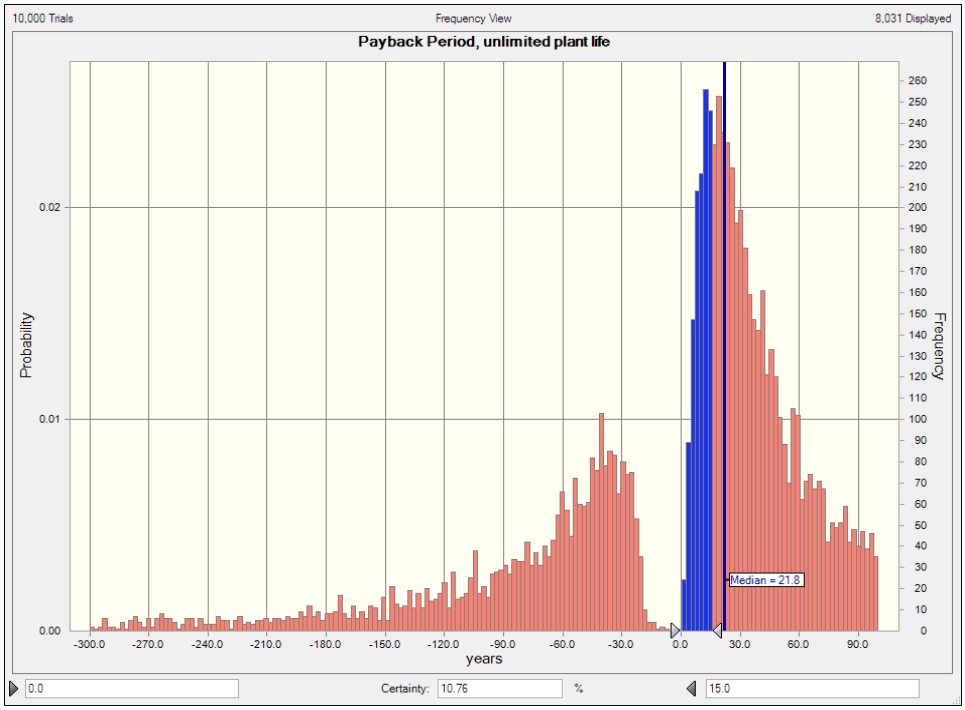

Figure F-7. Probability distribution for payback period.

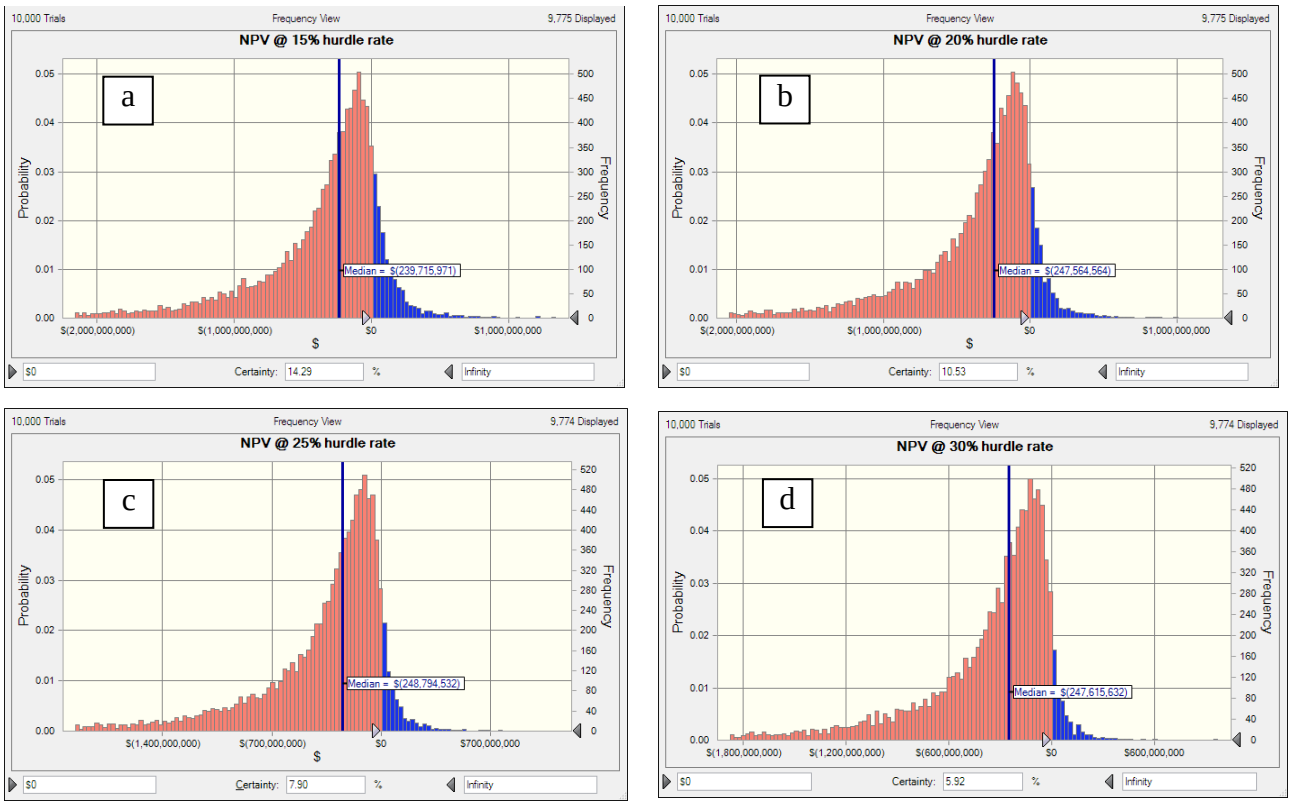

Figure F-8. Probability distribution for NPV with various hurdle rates: a) 15%, b) 20%, c) 25% and d) 30%.

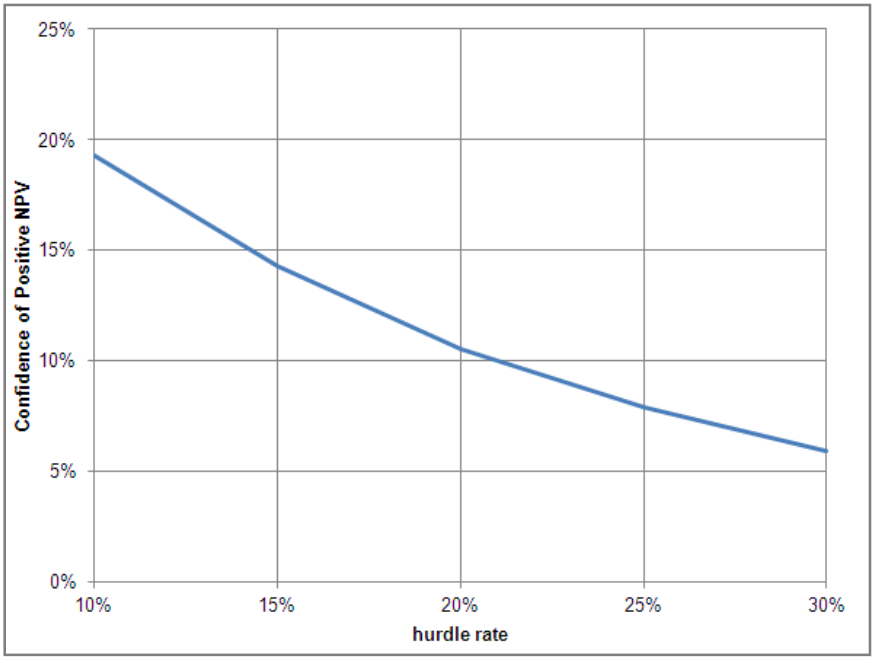

Figure F-9. Confidence of positive NPV vs. hurdle rate.